

Photometric and Spectroscopic Analysis of Cool White Dwarfs with Trigonometric Parallax Measurements¹

P. Bergeron^{2,3}

*Département de Physique, Université de Montréal, C.P. 6128, Succ. Centre-Ville, Montréal,
Québec, Canada, H3C 3J7.*

bergeron@astro.umontreal.ca

S. K. Leggett^{2,3}

UKIRT, Joint Astronomy Centre, 660 North A'ohoku Place, Hilo, HI 96720.

s.leggett@jach.hawaii.edu

and

María Teresa Ruiz^{2,3,4}

Departamento de Astronomía, Universidad de Chile, Casilla 36-D, Santiago, Chile.

mtrujiz@das.uchile.cl

ABSTRACT

A detailed photometric and spectroscopic analysis of cool ($T_{\text{eff}} \lesssim 12,000$ K) white dwarf stars is presented. The sample has been drawn from the Yale Parallax Catalog and from a proper-motion survey in the southern hemisphere. Optical $BVRI$ and infrared JHK photometry, as well as spectroscopy at $H\alpha$, have been secured for a sample of 152 white dwarfs. The discovery of seven new DA white dwarfs, two new DQ white dwarfs, one new magnetic white dwarf, and three weak magnetic white dwarf candidates, is reported. Our sample also identifies 19 known or suspected double degenerates.

¹Based partially on data obtained with the UK Infrared Telescope operated by the Joint Astronomy Centre, Hilo, HI, on behalf of the UK Particle Physics and Astronomy Research Council, and with the NASA Infrared Telescope Facility operated by the Institute for Astronomy at the University of Hawaii under contract to NASA.

²Visiting Astronomer, Cerro-Tololo Inter-American Observatory, National Optical Astronomical Observatories, which is operated by AURA, Inc., under contract with the National Science Foundation.

³Guest observer, Kitt Peak National Observatory, National Optical Astronomy Observatories, operated by the Association of Universities for Research in Astronomy, Inc., under cooperative agreement with the National Science Foundation.

⁴Visiting Astronomer at La Silla (ESO).

The photometric energy distributions, the $H\alpha$ line profiles, and the trigonometric parallax measurements are combined and compared against the predictions of model atmosphere calculations to determine the effective temperature and the radius of each object in the sample, and also to constrain the atmospheric composition. New evolutionary sequences with carbon/oxygen cores with thin and thick hydrogen layers are used to derive stellar masses and ages. The results are used to improve our understanding of the chemical evolution of cool white dwarfs.

We confirm the existence of a range in effective temperature between ~ 5000 and 6000 K where almost all white dwarfs have hydrogen-rich atmospheres. Our sample shows little evidence for mixed H/He white dwarfs, with the exception of two helium-rich DA stars, and four (possibly five) C_2H white dwarfs which have been interpreted as having mixed H/He/C atmospheres. The observed sequence of DQ stars is found to terminate abruptly near 6500 K, below which they are believed to turn into C_2H stars. True DC stars slightly above this temperature are found to exhibit hydrogen-like energy distributions despite the lack of $H\alpha$ absorption features. The mean mass of our complete sample is $0.65 M_\odot$ with a dispersion of $\sigma \sim 0.20 M_\odot$.

Attempts to interpret the chemical evolution of cool white dwarfs show the problem to be complex. Convective mixing is called upon to account for the increase of the non-DA to DA ratio below $12,000$ K, as well as the reappearance of helium-rich stars below ~ 5000 K. The possible presence of helium in cool DA stars, the existence of the non-DA gap, and the nature of the peculiar DC stars are also explained in terms of convective mixing, although our understanding of how this mechanism works needs to be revised in order to account for these observations. Given this chemical evolution uncertainty, it is not clear whether thick or thin hydrogen layer models should be used to determine cooling ages. The oldest object in our sample is ~ 7.9 Gyr or ~ 9.7 Gyr old depending on whether thin or thick hydrogen layer models are used, respectively.

Subject headings: stars: abundances, stars: atmospheres, stars: evolution, stars: fundamental parameters, white dwarfs

1. Introduction

Cool white dwarfs have recently gained attention due to the discovery of faint ($V \sim 26 - 28.5$) objects in the Hubble Deep Field Survey (see Hansen 1998, and references therein) which have been interpreted by Hansen (1998, 1999) as being cool ($T_{\text{eff}} \lesssim 3000$ K) and old ($t \gtrsim 11$ Gyr) hydrogen atmosphere white dwarfs. Hansen has shown that the location of these objects *blueward* of the white dwarf cooling sequence in the M_V vs $(V - I)$ color-magnitude diagram is the result of the extremely strong H_2 molecular absorption features which extend well into the optical regions of their energy distributions. Hence, even though hydrogen-rich white dwarfs become redder with decreasing effective temperature down to $T_{\text{eff}} \sim 4000$ K (see, e.g., Fig. 6 of Bergeron et al. 1995c),

even cooler stars actually become bluer. Note that the most recent photometric and spectroscopic analysis of cool white dwarfs in the local Galactic disk (Bergeron et al. 1997, hereafter BRL) has shown no evidence of white dwarfs cooler than 4000 K.

In addition, Hansen (1999) has also discussed the importance of using detailed stellar atmospheres as boundary conditions for calculating cooling white dwarf models. For instance, the cooling age of a $0.6 M_{\odot}$, $T_{\text{eff}} \sim 5000$ K white dwarf can differ by ~ 1.5 Gyr depending on whether the object has a hydrogen- or a helium-dominated atmosphere. Given this sensitivity, it is important to determine precisely the atmospheric composition of cool white dwarfs before any attempt to determine their age is made.

To complicate things even more, white dwarfs are not expected to preserve their hydrogen or helium atmospheric signature throughout their evolution. Indeed, there is both theoretical and observational evidence which indicates that the chemical composition of white dwarfs is likely to change many times during their lifetime due to competing mechanisms (e.g., gravitational settling, convective mixing, convective dredge-up, accretion from the interstellar medium, radiative acceleration) which may affect the composition of the outer layers of these stars as they cool (see Fontaine & Wesemael 1987, for a review on the subject). This is even more important for cool white dwarfs where convective mixing of a thin ($M_{\text{H}}/M_{\star} \lesssim 10^{-6}$) hydrogen atmosphere with the more massive convective helium envelope can turn a hydrogen-rich atmosphere into a helium-dominated atmosphere anywhere between 12,000 K and 5000 K. The exact temperature at which convective mixing occurs — or whether it will occur at all — depends on the thickness of the hydrogen layer (the thicker the hydrogen layer, the cooler the mixing temperature). Furthermore, BRL have clearly demonstrated that the chemical evolution of cool white dwarfs is even more complex than previously anticipated, and that several mechanisms — some of them still unknown — are at play to alter the chemical constituent of their atmospheres as they cool. Consequently, the age of any cool white dwarf is not only strongly dependent on its atmospheric composition, as pointed out by Hansen (1999), *but also on its chemical evolution history*. For instance, a recently mixed helium-rich atmosphere white dwarf would have an integrated cooling age of its immediate predecessor — i.e. that of a hydrogen-rich atmosphere white dwarf. Stellar ages and chemical evolution can thus not be easily disentangled. This unfortunate consequence stresses the importance of better understanding the chemical evolution of cool white dwarf stars.

For several years now, we have been pursuing our comprehensive investigation of cool white dwarf evolution. We presented in BRL photometric and spectroscopic observations of 110 cool white dwarfs, and analyzed them with model atmosphere calculations appropriate for cool white dwarfs with pure hydrogen and pure helium compositions, as well as with mixed H/He compositions. Our fitting technique consists of comparing the observed energy distributions in the optical *BVRI* and infrared *JHK* with those predicted from model atmospheres in order to determine the effective temperature of the star. When available, trigonometric parallax measurements are used to derive the radius of the star, and hence the mass through the mass-radius relation for white dwarfs. Finally, high signal-to-noise spectroscopy at $\text{H}\alpha$ is used to determine, or at least constrain, the

chemical composition of their atmospheres. The main results of the BRL analysis are summarized here together with our current understanding of the physical models which have been proposed to account for the observations.

Most cool white dwarfs have energy distributions which are consistent with either pure hydrogen or pure helium atmospheric compositions, with little evidence for objects with mixed H/He compositions. In general, the energy distributions of DA (hydrogen-line) stars are consistent with pure hydrogen atmospheres, while those of non-DA stars are consistent with pure helium atmospheres. Exceptions include a few extremely cool non-DA stars with hydrogen-dominated atmospheres which are simply too cool to exhibit any hydrogen absorption features, the so-called C₂H stars whose peculiar energy distributions and strong molecular absorption bands have been interpreted as the result of mixed H/He/C compositions with $N(\text{H})/N(\text{He}) \sim 10^{-2}$ (Schmidt et al. 1995), and a few other objects which are most likely unresolved binaries (see BRL and references therein). Note that hydrogen lines are observed in DA stars as cool as $T_{\text{eff}} \sim 4500$ K, that is, almost at the end of the observable white dwarf cooling sequence of the local Galactic disk.

BRL have also shown that the temperature distribution of DA and non-DA stars is not homogeneous. In particular, even though non-DA stars are abundant above $T_{\text{eff}} \sim 6000$ K, most white dwarfs below this temperature, down to $T_{\text{eff}} \sim 5000$ K, are of the DA type (the so-called “non-DA gap”). Moreover, BRL have identified a group of objects which lie close to, and above, $T_{\text{eff}} \sim 6000$ K whose energy distributions are better reproduced with pure hydrogen models, even though their optical spectra are completely featureless; hydrogen atmosphere white dwarfs in this particular range of temperature should exhibit strong hydrogen lines. BRL proposed an exotic model to account for both the strange nature of these objects and the existence of the non-DA gap. A warmer, pure helium atmosphere white dwarf slowly accretes hydrogen from the interstellar medium as it cools. Most atomic levels of the hydrogen accreted are quenched as a result of the high atmospheric pressures which characterize cool, helium-rich atmospheres. In particular, the bound level of H[−] is destroyed, and the corresponding bound-free H[−] opacity — the most important opacity source in hydrogen-rich atmospheres — is significantly reduced. Consequently, the accretion of hydrogen onto a helium-dominated atmosphere would have little effect on the opacity and thus on the atmospheric pressure. BRL proposed that large amounts of hydrogen could be *hidden* through this simple accretion/quenching mechanism. They also suggested that at some point, the free-free H[−] opacity would become large enough for the atmospheric pressure to drop below the threshold value at which the H[−] ion starts to recombine. The star then rapidly turns into a normal hydrogen-rich white dwarf. BRL suggested that the group of peculiar white dwarfs discussed above could represent such objects with a mixture of helium and quenched hydrogen, in the process of turning into normal DA stars, and that the non-DA gap could be accounted for by the sudden transformation of apparently helium-rich atmosphere white dwarfs into hydrogen-dominated atmospheres.

More recently, Malo et al. (1999) have explored more quantitatively the model proposed by BRL. The results of Malo et al. indicate that the accretion of even minute amounts of hydrogen onto a helium-dominated atmosphere, $\log N(\text{H})/N(\text{He}) \gtrsim 10^{-6}$, provide enough free electrons —

through the thermal ionization of hydrogen — to increase the He^- opacity significantly, which in turn, reduces the atmospheric pressure below which quenching effects on hydrogen become negligible. The presence of hydrogen therefore has an *indirect* effect on the total opacity through the free electrons it provides to the plasma. On the basis of their analysis, Malo et al. rejected the model proposed by BRL. Given these results, the nature of the peculiar objects identified by BRL and the existence of the non-DA gap remain unexplained.

Hansen (1999) provided an alternative explanation for the non-DA gap. The gap is evident in his Figure 13 even though he restricted his sample of objects to that of Liebert et al. (1988) rather than using the more complete sample studied by BRL, where the gap is even more obvious. Hansen has shown that the concentration of non-DA stars just below $T_{\text{eff}} \sim 5000$ K have nearly the same age as the concentration of DA stars around 6000 K. On the basis of this conclusion alone, Hansen suggested that the non-DA gap alluded to by BRL is only a result of the difference of cooling timescales between hydrogen-dominated and helium-dominated atmospheres. However, this interpretation cannot be correct since it neglects the fact that non-DA stars are also observed in large numbers *above* the gap at $T_{\text{eff}} \geq 6000$ K. In other words, non-DA stars are seen both above and below the gap, and the high-temperature end of the gap does not reflect a simple termination of the cooling sequence of degenerates with helium-dominated atmospheres. Unless helium-rich white dwarfs evolve more rapidly *through* the gap than above or below the gap, which is not the case, an explanation based solely on differences in cooling rates does not hold. Obviously, a chemical evolution from one spectral type to another must be invoked.

Other results from the BRL analysis support the idea that some physical mechanism, yet unidentified, is at play near the blue edge of the non-DA gap. For instance, the most widely accepted explanation for the presence of carbon in the photospheric layers of DQ stars is that carbon is convectively dredged-up from the core, as demonstrated quantitatively by Pelletier et al. (1986). These calculations show that the extent of the carbon diffusion tail is reduced at low effective temperature due to the partial recombination of carbon, and smaller carbon abundances are predicted in DQ stars with lower effective temperature, in apparent agreement with the observations (see Fig. 4 of Pelletier et al. 1986). As pointed out by BRL, however, the coolest DQ stars have the strongest observed C_2 molecular bands, and cooler objects with even smaller abundances are well within the observational limits and should be easily detectable. The BRL analysis has revealed instead the existence of an abrupt cutoff in effective temperature at $T_{\text{eff}} \sim 6500$ K below which DQ stars are no longer found. The presence of carbon in stars below this temperature threshold is in the form of what has been interpreted as C_2H molecular bands by Schmidt et al. (1995). The most obvious explanation proposed by BRL is that DQ stars turn into C_2H stars below $T_{\text{eff}} \sim 6500$ K. The mechanism proposed by BRL by which the hydrogen required to form the C_2H molecule suddenly appears in these objects relies on their composition transition model, which was later discarded by Malo et al. (1999). Hence, even though the DQ to C_2H transition remains the most likely explanation for the existence of the abrupt cutoff of the DQ star phenomenon, the physical mechanism by which this transition occurs needs further investigation.

BRL have also shown that below the non-DA gap near $T_{\text{eff}} \sim 5000$ K, non-DA stars reappear in large number. The most likely explanation for this phenomenon is the convective mixing of the relatively thin surface hydrogen layer with the deeper and more massive helium envelope. Detailed envelope calculations indicate that the bottom of the hydrogen convection layer reaches its deepest point at a certain temperature (see, e.g., Tassoul et al. 1990); white dwarfs with hydrogen layers thicker than this maximum depth point can never mix and will remain hydrogen-rich forever. The canonical value of the lowest possible mixing temperature is $T_{\text{mix}} \sim 6000$ K, which corresponds to a hydrogen layer mass of $M_{\text{H}}/M_{\star} \sim 10^{-6}$. This is ~ 1000 K hotter than the temperature required to account for the BRL observations. New envelope models discussed by BRL which include realistic model atmospheres as boundary conditions reduce the mixing temperature limit well down to 5000 K, however. Hence, convective mixing may well represent the correct interpretation for the reappearance of non-DA stars below the non-DA gap. The continued presence of DA stars requires that at least some stars have hydrogen layers thicker than $M_{\text{H}}/M_{\star} \sim 10^{-6}$.

Following the BRL analysis, Leggett et al. (1998) have gathered new photometric and spectroscopic data for the 43 cool, low-luminosity, high-proper-motion white dwarfs in the Liebert et al. (1988) sample. This sample was analyzed with the techniques developed by BRL in order to improve the determination of the cool white dwarf luminosity function and the estimate of the age of the local Galactic disk. BRL discuss at length the shortcomings of the previous estimates by Liebert et al. (1988), and in particular the lack of precise atmospheric parameter determinations as well as accurate bolometric corrections for the stars in the sample. The improved luminosity function of Leggett et al. (1998) yields an age of the local region of the Galactic disk of 8 ± 1.5 Gyr, with the uncertainty being mainly due to the core composition, the effect of separation on crystallization, and the unknown mass of the outer helium envelope. The Liebert et al. (1988) sample is being extended to a lower proper-motion limit and a new luminosity function is being determined which supports the earlier work (Liebert et al. 1999).

As mentioned in BRL, these earlier efforts represent only the first step towards a better understanding of the chemical evolution of cool white dwarfs. Even though the BRL analysis has provided us with a wealth of new observational and theoretical results, many questions have remained unanswered, and the problems to be solved have multiplied. The success of our analysis has prompted us to extend our study to a larger and more complete sample of cool white dwarfs. We thus present in this paper a detailed analysis of all cool ($T_{\text{eff}} \lesssim 12,000$ K) white dwarfs with trigonometric parallax measurements available to us. Such measurements are of particular importance to derive stellar radii, and hence stellar masses. This new sample is comprised of 152 white dwarfs for which masses can be derived. In contrast, only 67 out of the 110 white dwarfs analyzed by BRL had trigonometric parallax measurements. Furthermore, BRL concentrated their effort towards cool ($T_{\text{eff}} \lesssim 7000$ K), non-DA white dwarfs, while our new sample is distributed over a wider range of effective temperature and spectral types.

In § 2, we discuss the improvements in the model atmospheres and cooling models since our most recent analysis. In § 3, we present our new photometric and spectroscopic observations, which,

combined with our earlier observations, are analyzed in § 4. The global properties of our sample are examined in § 5. Our conclusions follow in § 6.

2. Theoretical Framework

2.1. Model Atmospheres

The model atmospheres used in this analysis are described at length in Bergeron et al. (1995b), and improvements to these models are discussed in BRL and below. These models are appropriate for cool white dwarfs with pure hydrogen or pure helium atmospheres, as well as mixed H/He compositions.

Our current model grid now includes self-consistently the He_2^+ ion in the ionization equilibrium calculations. As discussed in detail by Malo et al. (1999), the He_2^+ ion was treated as a trace element in our earlier calculations. Although this assumption is valid in terms of the number of particles, $N(\text{He}_2^+) \ll N(\text{He})$, the presence of the He_2^+ ion affects the ionization equilibrium significantly for temperatures below $T_{\text{eff}} \sim 8500$ K. In cool, pure helium (or helium-rich) models, the electron density is governed by He_2^+ , rather than He^+ (or H^- ; see Malo et al.). Hence, despite the fact that the continuous absorption opacity of He_2^+ is negligible at low temperatures, the inclusion of this ion in model atmospheres has repercussion on the He^- free-free opacity — the dominant opacity source in helium-rich models — through its effect on the electron density.

The occupation probability of Hummer & Mihalas (1988) for the calculation of the hydrogen populations has also been included more accurately in our current model grid following the work of Malo et al. (1999). This formalism allows us to calculate cool white dwarf models with arbitrarily low hydrogen abundances. Indeed, the photospheric pressures which characterize low hydrogen abundance atmospheres are so high that the hydrogen atomic levels (including that of the H^- ion) are strongly perturbed. In the most extreme cases, pressure ionization of hydrogen may even occur (we note that even though the pressure ionization model used in the Hummer-Mihalas formalism is very crude, it is sufficient for our current needs). Since the Hummer-Mihalas formalism had not been included in our earlier investigations, BRL were unable to compute cool models with $N(\text{H})/N(\text{He}) \lesssim 10^{-3}$ (see § 5.3 of BRL). We note that the nonideal effects included in the equation-of-state of our pure helium model grid (see Bergeron et al. 1995b, and references therein) are neglected in the mixed H/He models.

Our latest hydrogen (and mixed hydrogen/helium) models include the new H_2 collision-induced opacity calculations of Borysow et al. (1997), as well as the additional term discussed by Saumon & Jacobson (1999) which takes into account collisions involving three H_2 molecules. Our hydrogen model grid has also been extended to $T_{\text{eff}} = 1500$ K, the coolest models calculated by Saumon & Jacobson (1999). The non-ideal effects in the equation-of-state introduced by Saumon and Jacobson are neglected here, however. A more detailed discussion of these cooler models will be presented

elsewhere.

The hydrogen and mixed hydrogen/helium models have been calculated with the so-called $ML2/\alpha = 0.6$ parameterization of the mixing-length theory (as opposed to the ML1 calibration used in BRL), following the suggestion of Bergeron et al. (1995d) from their analysis of ZZ Ceti stars. Although this will not affect the atmospheric parameter determinations of the cooler objects in our sample ($T_{\text{eff}} \lesssim 8000$ K), the emergent energy distributions of warmer models are quite sensitive to the convective efficiency used in the calculations, as shown by Bergeron et al. (1995d). We note finally that this new model grid has not changed significantly the quality of the fits shown in BRL, or the determination of the atmospheric parameters from our previous analyses.

2.2. On the Importance of Metals in Cool, Helium-Rich Atmospheres

Recently, Jørgensen et al. (2000) have studied the importance of including metals in the atmospheres of cool, helium-rich white dwarfs. Their results indicate that the model atmospheres and predicted energy distributions are quite sensitive to the presence of additional elements. They also claim that their improved models reproduce the scatter observed in two-color diagrams better than the models used in BRL. Here, we present our own assessment of this problem. A more complete appraisal of the Jørgensen et al. results will be presented elsewhere (Bergeron 2001).

The main effect of including heavy elements in the model atmospheres of cool, helium-rich white dwarfs is to increase the number of free electrons in the plasma, which in turn affect the He^- free-free opacity considerably. As mentioned by Jørgensen et al. (2000), more than 99% of the electrons may come from metals which have a relatively low ionization potential. As an experiment, we calculated a pure helium model at $T_{\text{eff}} = 6000$ K, $\log g = 8$, but with an electron density artificially increased by a factor of 1000 (only 0.1% of the electrons come from helium directly, i.e. the value quoted by Jørgensen et al.). The temperature and pressure structures of this model are compared in Figure 1 with those of a standard pure helium model. As can be seen, the temperature structure of the upper layers has changed significantly, but that of the deeper layers where the *continuum is formed* ($\tau_R \sim 1$) has remained relatively unaffected. The gas pressure, on the other hand, has been reduced quite dramatically throughout the atmosphere as a result of the increase in the opacity ($P_g \propto \kappa^{-1}$), which in this case is dominated by the He^- free-free opacity. Perhaps of greater interest is the comparison of the predicted fluxes from these two models, displayed in Figure 2. Not surprisingly, the results indicate that the observed differences are small. The reason for this is that in the pure helium model, the He^- free-free opacity already dominates at all wavelengths where the continuum is formed. An increase in the electron density thus increases the opacity by the same factor *at all wavelengths*. Consequently, the emergent flux cannot be redistributed any differently. The small differences observed in Figure 2 can be measured more quantitatively by fitting our test model with our pure helium grid. We find that the predicted energy distribution of our test model can be fit to better than 1% at all wavelengths with our pure helium grid at $T_{\text{eff}} = 6037$ K. We thus conclude that the presence of metals in helium-rich models does not affect significantly the

atmospheric parameters derived in the BRL analysis and in this analysis. Note that the presence of metallic lines or molecular absorption features may affect the predicted broadband fluxes, but we do not believe that they can affect the model structure significantly, with the exception of the most extreme cases such as those discussed in § 3.3.

There are several reasons why the conclusions of Jørgensen et al. (2000) are different from those reached here. First they state that white dwarfs are “carbon rich”. This is simply not true as only a small fraction of cool non-DA stars exhibit carbon features. It is also a well known observational fact that the presence of carbon and metallic features are mutually exclusive (for reasons still unknown). The authors have also shown in their Figure 3 that the inclusion of molecules in their model produces a substantial heating at all layers. However, this statement is somewhat misleading since their plot shows the temperature profile as a function of gas pressure, and as these two parameters are not independent in a model atmosphere, it is not possible from such a plot to determine which of the parameters (temperature or gas pressure) has in fact changed. A more appropriate independent parameter is the Rosseland mean optical depth, as used here in Figure 1. Jørgensen et al. also claim that the new H₂-He collision-induced opacity they have calculated — and not used in our own model calculations — has a significant influence on the predicted emergent fluxes. However, their Figure 6 shows instead that the differences are actually quite small at the T_{eff} values considered here, and not pertinent to the present discussion. More importantly, they have assumed a non-zero hydrogen abundance of $N(\text{H})/N(\text{He}) = 10^{-5}$ on the basis of either old studies, or analyses of objects that do show direct or indirect traces of hydrogen (e.g., Ross 640, LHS 1126). Traces of hydrogen in these cool models produce a strong infrared flux deficiency (see their Fig. 6) which is simply not observed in cool non-DA stars studied by us (BRL and this analysis), with the glaring exception of LHS 1126 (Bergeron et al. 1994) near $T_{\text{eff}} \sim 5500$ K whose infrared flux deficiency has been attributed to the H₂-He molecular opacity. Surprisingly enough, Jørgensen et al. (2000) conclude that at this particular temperature, the H₂-He opacity has little effect. This is because they have considered hydrogen abundances which are way too small in this case — LHS 1126 has $N(\text{H})/N(\text{He}) \sim 10^{-2}$. The claim by Jørgensen et al. that the predicted energy distribution is not sensitive to the helium-to-hydrogen abundance ratio is thus also inaccurate.

Their Figures 8 and 9 show their helium-rich models, as well as some of their hydrogen-rich models, in a ($B-V$, $V-K$) two-color diagram, together with the BRL observations. Also shown for comparison are the hydrogen-rich and helium-rich models used in BRL. The authors conclude that both their hydrogen-rich and helium-rich models reproduce the observed photometric data better than the models used in BRL. However, the authors failed to distinguish the DA and non-DA stars in their Figures, as was carefully done in Figure 9 of BRL. A more careful examination of both results indicates that their helium-rich models actually fail to match the non-DA stars close to $B-V \sim 0.5$, $V-K \sim 0.9$ altogether, while our pure helium models go straight through the observed data. Their Figure 8 shows instead that their helium-rich models reproduce nicely the sequence of *DA stars* which have hydrogen-rich atmospheres. The authors also claim that at the warm end of the observed sequence, their models “follow better the tendency of a linear observed sequence

that the observations indicate, than do the BRL models which diverge toward higher values of $B-V$ ”. Again, the authors failed to realize that the warm end of the sequence in BRL is composed exclusively of non-DA stars. The fact is that DA stars *do diverge* toward higher values of $B-V$, as do the models (see our Figure 8 below). If anything, their hydrogen-rich models fail to reproduce the warm end of the observed DA sequence.

Finally and more importantly, Jørgensen et al. (2000) claim that their helium-rich models reproduce the scatter in the observational data seen at the cool end of diagram better than do the BRL models which follow an almost straight line. First of all, most of the observed scatter is due to the fact that the coolest objects include *both hydrogen-rich and helium-rich white dwarfs*. Indeed, when one considers only the helium-rich stars (the filled circles in the right panel of Fig. 9 of BRL), they do form an almost straight line, as opposed to the Jørgensen et al. models. Second, these authors show that their models can reproduce the entire cool end of the diagram by changing the C/O ratio. This is again somewhat misleading. Indeed, the observed “hook” in their predicted colors is entirely due to the H₂-He collision-induced opacity. Similar hooks can be observed in the BRL models as well, whether they are due to H₂-H₂ or H₂-He molecular opacities (see Fig. 9 of BRL). Since these collision-induced opacities are strongly dependent on the atmospheric pressure, the predicted colors will be sensitive to surface gravity (see the hydrogen sequences with various values of $\log g$ in Fig. 9 of BRL, middle panel), or to the hydrogen-to-helium abundance (see the helium-rich sequences with various values of $N(\text{He})/N(\text{H})$ in Fig. 9 of BRL, right panel). The results shown in Figure 8 of Jørgensen et al. (2000) simply reflect a change in the opacity, and thus atmospheric pressure, due to a change in the electron density for various values of C/O. More problematic is the effective temperature near 3000 K inferred from Figures 8 and 9 of Jørgensen et al. (2000) for the bulk of the coolest white dwarfs. At this temperature, the predicted energy distribution shows a strong infrared flux deficiency which is simply not observed in these objects, as discussed above. This is the danger of interpreting cool white dwarfs in two-color diagrams only, and in particular the ($B-V$, $V-K$) diagram (see § 5.2.2 of BRL), rather than fitting the entire energy distribution, which is the technique favored by BRL and in this analysis.

2.3. Evolutionary Cooling Sequences

In order to derive stellar masses from the measured radii, and to determine cooling ages, we must rely on detailed evolutionary models. In BRL, we made use of the models of Wood (1990) for the pure helium and mixed hydrogen/helium compositions, and those of Wood (1995) for the pure hydrogen models. The former models have carbon-core compositions, helium layers of $q(\text{He}) \equiv M_{\text{He}}/M_{\star} = 10^{-4}$, and no hydrogen layers, while the latter have carbon-core compositions as well, but helium layers of $q(\text{He}) = 10^{-2}$, and thick hydrogen layers of $q(\text{H}) = 10^{-4}$.

In this paper, we use instead two families of new evolutionary models kindly computed for us by G. Fontaine who used the new evolutionary code developed by P. Brassard at Université de Montréal on the basis of finite-element techniques. While details of that code will be described elsewhere

(Brassard & Fontaine 2000), a few remarks about it are worthy of interest. The code is especially designed to follow in a robust and efficient way moving discontinuities in a cooling white dwarf model, namely, the top and base of superficial convection zones, and the advancing crystallization front in the core and in the envelope. The full structure of a model, from the center to the top of the atmosphere (typically located at $\tau_R = 10^{-8}$), is included in the evolutionary calculations. Upgraded input physics, including the new model atmospheres described above, has been incorporated in the code in order to be able to compute realistic white dwarf models reaching the regime of very low effective temperatures that is of interest for discussing white dwarf populations in the halo and in old globular clusters.

The first family of evolutionary structures that we use are standard “thick envelope” stellar models with a helium mantle of $q(\text{He}) = 10^{-2}$, and an outermost hydrogen layer of $q(\text{H}) = 10^{-4}$. The core of these models consists of a uniform mixture of carbon and oxygen in equal proportions ($X_{\text{C}} = X_{\text{O}} = 0.5$). No sedimentation between carbon and oxygen upon crystallization has been taken into account in these models. Sedimentation would add a small delay to the cooling age, but would not change the mass-radius relation in any significant way. On the other hand, the effects of convective feedback on the position of the hydrogen convection zone have been taken into account in the calculations. Likewise, neutrino cooling has been included in a routine way, but this only affects the evolution in the high luminosity phases only, as is well known. No residual thermonuclear burning has been included in order to keep the same value of the fractional mass of the outer hydrogen layer in all models. Finally, 16 different masses in the range $0.2\text{--}1.3 M_{\odot}$ have been considered.

The second family of models (with again 16 different sequences) is similar to the first one, except for the assumed stratification of the envelope. This second batch of structures are now “thin envelope” stellar models with a helium mantle of $q(\text{He}) = 10^{-2}$ as before, but with an outermost hydrogen layer of only $q(\text{H}) = 10^{-10}$. No convective mixing between the hydrogen and helium layers is allowed in these models. We picked this particular stratification as representative of “thin” hydrogen envelope models. The small layer of hydrogen atop these models does not change in any significant way the mass-radius relation for the cooler models that are of interest here. From that point of view, that same mass-radius relation can thus be used for non-DA stars. Evolutionary calculations of helium-rich atmospheres can also be carried out, but the cooling times show an extreme sensitivity to the presence of even very small traces of heavy elements in the atmosphere/envelope, leading to a continuum of ages, hence we adopted the current strategy.

3. Observations

3.1. Selection of the Sample

In the BRL study, 110 genuine cool white dwarfs were selected on the basis of their spectral type classification from the catalog of McCook & Sion (1987), from a proper-motion survey in the

southern hemisphere (Ruiz et al. 1993; Ruiz & Takamiya 1995; Ruiz 1996), and from the study of Monet et al. (1992). This first sample was strongly biased against DA stars in order to determine whether true DC stars existed, and if they did, what was their atmospheric composition. Our high signal-to-noise spectroscopy actually revealed the presence of $\text{H}\alpha$ in 20 of the previously classified non-DA stars, a result which stresses the importance of large aperture telescopes for studying cool white dwarfs, as first emphasized by Greenstein (1986). Several additional DA, DQ, and DZ stars were included in the sample as well to test the validity of our model atmosphere calculations, and to improve our understanding of the chemical evolution of cool white dwarfs.

BRL found that even though the model energy distributions are somewhat sensitive to the surface gravity, it is practically impossible to determine $\log g$ from the observed photometry alone. Only for stars with available trigonometric parallax measurements is it possible to determine the stellar radius, and thus the mass through the mass-radius relation. In the BRL sample, 67 white dwarfs had trigonometric parallax measurements taken from the Yale parallax catalog (van Altena et al. 1994, hereafter YPC), and from Bergeron et al. (1992a), Ruiz et al. (1989), Ruiz et al. (1995), and Anguita et al. (1996). Stellar masses were determined for a subset of 60 white dwarfs (6 objects had unreliable parallaxes, while one DQ star had carbon bands too strong to be analyzed properly). BRL assumed a surface gravity of $\log g = 8.0$ for the remaining objects in their sample. The natural step following the comprehensive study of BRL was to gather spectroscopic and photometric data for all cool white dwarfs with measured trigonometric parallaxes available in the literature.

A total of 161 DA and non-DA white dwarfs with a temperature index ($\theta = 50,400/T_{\text{eff}}$) of 4 and cooler were thus selected from the YPC, and from Ruiz (1996). This temperature cutoff corresponds roughly to that below which convective mixing of DA stars is believed to occur. Only stars with parallax uncertainties smaller than 30% were considered; 7 objects were rejected on this basis (0145–174, 1042+593, 1639+153, 1708–147, 2139+132, 2240–017, and 2254+076). Two other objects were not considered since one is a known DC + M dwarf system (1133+358), while the other one has a known spectroscopic temperature in excess of 20,000 K (1919+145). Hence, 152 white dwarf candidates were retained for photometric and spectroscopic observations. Among this sample, 67 objects are in common with BRL, and new photometric and spectroscopic data are presented in this paper for 85 white dwarfs.

Since this new sample is based on trigonometric parallax measurements, it should contain no bias against any specific spectral type, in contrast with the BRL analysis which favored non-DA white dwarfs. The number of DA and non-DA stars as a function of T_{eff} for our trigonometric parallax sample is displayed in Figure 3. Also shown is the subset of objects in the BRL sample whose stellar masses could be determined from trigonometric parallax measurements — $M(\pi)$. The temperature estimates are obtained from the detailed fits to the photometric energy distributions (§ 5 of BRL and § 5.1 below; 60 stars in the BRL sample and 150 stars in this analysis), while the spectral types are determined from our high signal-to-noise spectroscopic observations. The comparison indicates that our new sample has significantly increased the number of DA stars above $T_{\text{eff}} = 5000$ K and the number of non-DA stars at all temperatures with respect to the BRL sample.

Also apparent from this figure is the paucity of non-DA stars in the 5000–6000 K temperature range. Note that the coolest bin of the non-DA panel may contain a significant number of hydrogen-rich white dwarfs that are simply too cool to exhibit an $H\alpha$ feature.

3.2. Optical Spectroscopy

High signal-to-noise spectroscopy has been obtained for all 152 objects in our sample, 15 of which have been secured by Greenstein (1986). Some of the spectroscopic observations have already been presented in BRL and in Leggett et al. (1998). The new spectra reported here have been obtained during several observing runs using the KPNO and CTIO 4 m telescopes equipped with the RC spectrograph (1996, 1998; where the years indicate the period the observations were obtained), and the ESO 3.6 m telescope equipped with the EFOSC (1996, 1998). The spectral resolution varies between 5 and 15 Å (18 Å for the Greenstein spectra). Details of our observing procedure and data reduction are provided in Bergeron et al. (1992a). The spectral coverage varies according to the detector used although all spectra cover at least the $H\alpha$ region.

The new spectra — not already shown in BRL — which show $H\alpha$ are displayed in Figure 4 in order of decreasing equivalent widths. The names of the 7 newly identified DA stars are italicized in Figure 4. We note that the coolest DA stars in our sample are all new DA identifications, a result which stresses once again the importance of large aperture telescopes for the spectral classification of cool white dwarfs (BRL, Greenstein 1986).

Objects of particular interest in Figure 4 include two magnetic white dwarfs with discernible Zeeman splitting: GD 175 (1503–070) discovered in this survey, and G128–72 (2329+267) first identified by Moran et al. (1998). There are also two objects with particularly broad and shallow profiles: the DZA stars Ross 640 (1626+368) and the DZQA star L745–46A (0738–172). Both of these objects have helium-dominated atmospheres (Liebert 1977; Koester & Allard 1996; Koester & Wolff 2000, this analysis), with their $H\alpha$ line profile broadened by van der Waals interactions with neutral helium; we note that such objects are rare in our sample. The $H\alpha$ line profile of the G107–70A/B system (0727+482A/B) is also broad and shallow with respect to other cool objects. In this case, however, since the A and B components of the system are not resolved, it is more likely that we are dealing with a normal DA star whose line profile is diluted by a featureless white dwarf companion (see § 4.2.6, however). The central component of the Zeeman triplet in emission is also clearly visible in the spectrum of GD 356 (1639+537; see also Greenstein & McCarthy 1985), while the π components are outside the wavelength range displayed here. Finally, the coolest DA star shown in Figure 4 is G227–28 (1820+609) with an effective temperature of 4780 K. This is still 500 K hotter than the coolest DA star in our complete sample, LHS 239 (0747+073B), with $T_{\text{eff}} = 4210$ K (see BRL and § 5.1 below).

Our non-DA spectra — not already shown in BRL — are displayed in Figure 5. As noted in BRL, a featureless white dwarf spectrum does not necessarily imply a helium-rich atmosphere

since a hydrogen-rich white dwarf may be too cool to show an $\text{H}\alpha$ absorption feature, and a full analysis of the energy distribution is required to establish properly the atmospheric composition of these objects.

The subset of DQ stars with blue spectral coverage is displayed in Figure 6 in order of decreasing effective temperature (as determined in § 5.1). These are all well known DQ stars with the exception of two new identifications, LHS 2392 (1115–029) and G184–12 (1831+197). As discussed in BRL and above, the convective dredge-up model of Pelletier et al. (1986) predicts a continuous decrease of carbon abundances with decreasing effective temperature. As seen from Figure 6, however, the coolest DQ stars have the strongest carbon features, and therefore, the sudden disappearance of the DQ phenomenon at even cooler temperatures needs to be attributed to an additional effect.

3.3. Optical and Infrared Photometry

Optical $BVRI$ and infrared JHK photometry has been secured for 150 and 148 program objects, respectively, out of our complete sample of 152 white dwarfs. Since some optical photometry is required for fitting the energy distribution, BV photometry for the 2 missing objects 0326–273 and 0839–327 has been taken from McCook & Sion (1999).

Most of the data for the 67 objects in common with BRL were acquired between 1991 August and 1996 February, but we have supplemented that data with some newer photometry. Additional $BVRI$ photometry presented here has been obtained with the 0.9 m telescopes at KPNO (1996, 1998) and CTIO (1995), while the new JHK photometry has been obtained with the CTIO Blanco 4 m telescope using CIRIM (1995), the NSFCAM camera on the NASA IRTF (1996), the IRCAM on UKIRT (1996, 1998), and UKIRT service time (1997 to 1999). Details of our observing procedure and data reduction are provided in Bergeron et al. (1992a).

The $BVRI$ and JHK photometry is presented in Table 1 together with the number of independent observations (N). Also given in Table 1 are the WD number and the name of each object, the measured trigonometric parallax and uncertainty, and the $\text{H}\alpha$ equivalent width (W). A value of $W = 0$ implies a featureless spectrum near the $\text{H}\alpha$ region; for the magnetic DA stars, the equivalent width is taken as the sum of the three Zeeman components. The photometric uncertainties are typically 3% at V , R , and I , and 5% elsewhere, with the exception of the data marked “:” which indicates a 10% uncertainty. The optical and infrared photometry is on the Cousins system (Bessell & Weis 1987) and the CIT system (Elias et al. 1982), respectively.

The optical and infrared photometry of the A and B components of the G107–70 (0727+482) system is based on our combined optical photometry and the $\Delta V = 0.30$ mag difference reported by Liebert et al. (1988) and references therein, as well as on our own magnitude difference measurement of 0.3 ± 0.1 mag at J , H , and K . Note that the spectrum of G107–70A/B displayed in Figure 4 is the *combined* spectrum of both components.

The M_V vs $(V-I)$ color-magnitude diagram is displayed in Figure 7 for 149 stars; 3 objects in Table 1 have no $(V-I)$ measurement. The left panel shows all objects together with the error measurements associated with the trigonometric parallax measurements. In the middle and right panels, the same objects are distinguished in terms of their DA or non-DA spectral types. The pure hydrogen and pure helium cooling sequences, calculated as in Bergeron et al. (1995c) but with our latest model grid and cooling models discussed in § 2, are superimposed on the observed data.

DA and non-DA stars form well-defined narrow sequences in this diagram, although not as narrow as the USNO data set of Monet et al. (1992), also shown in Bergeron et al. (1995c), which is a much more homogeneous parallax sample than the one studied here. Interestingly, all overluminous stars with apparent masses below $0.4 M_\odot$ are of the DA spectral type, with the exception of LP 31–40 (0324+738) which is probably too cool to show $H\alpha$ anyway. As discussed in BRL, most, if not all, of these objects are unresolved binaries (e.g. L870–2, Saffer et al. 1988) and their luminosity is the contribution of two white dwarfs with probably normal masses. The color-magnitude diagram presented in Figure 7 indicates that such systems are mostly composed of DA white dwarfs, a result which suggests a particular evolutionary path. We will come back to this point below (see § 5.3).

A particularly interesting object in Figure 7 is the non-DA star ESO 439–26 (1136–286) analyzed in detail by Ruiz et al. (1995). This object with its absolute visual magnitude of $M_V = 17.4$ was first interpreted as an extremely old — and thus cool — white dwarf. However, the Ruiz et al. analysis convincingly demonstrated that the low luminosity of this object could be attributed to its small radius (or high mass). The most recent parameters derived for this object come from the BRL analysis, $T_{\text{eff}} = 4490$ K and $M = 1.20 M_\odot$. However, as first demonstrated by Hansen (1998), white dwarfs with $T_{\text{eff}} \lesssim 4000$ K become increasingly *bluer*. An inspection of Figure 7 now suggests an alternate interpretation for ESO 439–26, namely that this star could be a $T_{\text{eff}} \sim 3200$ K, $\sim 0.8 M_\odot$ white dwarf; such a low temperature would imply an age of roughly 13 Gyr, i.e. twice as old as the age determined by BRL for this object. The detailed analysis of the entire energy distribution presented below will show that the infrared J magnitude is totally inconsistent with this last interpretation, and that the earlier conclusions reached by Ruiz et al. (1995) are still valid.

If the overluminous DA stars and ESO 439–26 are excluded, all objects in Figure 7 have masses in the range $0.4 \lesssim M/M_\odot \lesssim 1.0$. If we assume that most DA stars have hydrogen-rich atmospheres, as demonstrated by BRL, their mean mass inferred from Figure 7 is somewhere around $0.7 M_\odot$. Similarly, if we assume that most non-DA stars have helium-rich atmospheres (with the exception of the hydrogen-rich white dwarfs which are too cool to show $H\alpha$), their mean mass inferred from Figure 7 is also somewhere near $0.7 M_\odot$. Both of these average masses are about $0.1 M_\odot$ higher than those inferred from the spectroscopic analyses of warmer DA and DB stars (Bergeron et al. 1992b, 1995d; Beauchamp et al. 1996).

Under similar assumptions, the coolest DA and non-DA stars in Figure 7 have temperatures near $T_{\text{eff}} \sim 4500$ K based on their location in this diagram with respect to the pure hydrogen and pure helium cooling sequences, respectively. As mentioned above, however, the coolest non-DA

stars may well have a hydrogen-rich atmospheric composition, and only a complete analysis of the combined energy distribution will yield reliable temperature estimates. As can be seen from Figure 7, such an uncertainty in the atmospheric composition could easily result in a ~ 500 K temperature uncertainty for the coolest non-DA white dwarfs in our sample.

The $(B-V, V-K)$ two-color diagram is displayed in Figure 8 for 145 objects; 2 objects in Table 1 have no $(B-V)$ measurement while 5 have no K measurement. DA and non-DA stars form two distinct sequences which overlap near $(V-K) \sim 0.4$. This behavior is observed in the model sequences as well. We note in particular that both the observed and predicted DA sequences tend to diverge toward higher values of $B-V$ for $V-K < 0.4$, in contrast with the models of Jørgensen et al. (2000) which follow instead the non-DA sequence in this range of $V-K$. Even though the observed DA sequence is well reproduced by the $0.6 M_{\odot}$ pure hydrogen models at the hot end of the sample, an increasing departure is observed above $(V-K) \sim 1.3$. In these regions the cool observed DA sequence is better reproduced by the pure helium models! BRL proposed an explanation for this departure in terms of a missing opacity source near the B filter in the pure hydrogen models, most likely due to a pseudocontinuum opacity originating from the Lyman edge (see § 5.2.2 of BRL for a complete description). Figure 13 of BRL shows indeed how the agreement between the observations and the model predictions could be improved by including, even approximately, such an opacity in the model calculations. However, the lack of a more precise theoretical framework precludes us from including this opacity in our current model grid, and until this can be accomplished, we must refrain from interpreting such $(B-V, V-K)$ diagrams for DA stars any further.

On the other hand, the non-DA observed sequence in Figure 8 and the pure helium models are in much better agreement. Non-DA stars, most of which have helium-rich atmospheres, are characterized by more transparent atmospheres than hydrogen-rich atmospheres, and as a result, their broadband colors are particularly sensitive to the presence of strong metallic lines or molecular bands. Consequently, several non-DA stars in Figure 8 lie well outside the “mean” observed sequence. This is the case for LP 701–29 (2251–070) whose spectrum exhibits a strong drop in the flux shortward of ~ 4400 Å attributed to Ca I and II lines (Kapranidis & Liebert 1986), LHS 1126 (0038–226) which shows a strong infrared flux deficiency attributed to H₂-He collision-induced absorptions (Bergeron et al. 1994), G165–7 (1328+307) a heavily blanketed white dwarf with strong metallic lines (Wehrse & Liebert 1980), G240–72 (1748+708) whose spectrum is characterized by a “yellow sag” $\sim 15\%$ deep and ~ 2000 Å wide (see, e.g., Fig. 19 of Wesemael et al. 1993), and the strong DQ star BPM 27606 (2154–512) whose spectrum is displayed in Figure 6.

Because of the theoretical problems outlined above with the pure hydrogen models, BRL preferred to rely on the $(V-I, V-K)$ two-color diagram in which a much better agreement between theory and observation could be achieved. Such a diagram is displayed in Figure 9 for 144 objects; 3 objects in Table 1 have no $(B-V)$ measurement while 5 have no K measurement. The results show that both DA and non-DA stars form narrow cooling sequences, but that they are offset by ~ 0.1 mag. The outliers are all of the non-DA type, some of which have been identified in the right panel and already discussed above. G148-B4B (1215+323) has most likely its I magnitude contaminated

by the close M dwarf companion, while G195–19 (0912+536) is a ~ 100 MG magnetic white dwarf with some undetermined spectroscopic features (Schmidt & Smith 1994). The non-DA stars LP 131–66 (1247+550) and ER 8 (1310–472) actually have hydrogen-rich atmospheres (see BRL and the detailed analysis below).

Also shown in the DA and non-DA panels are the model sequences for pure hydrogen, pure helium, and mixed He/H atmospheres. The departure of the pure hydrogen and mixed He/H models from the pure helium models is due to the collision-induced absorption by molecular hydrogen due to collisions with H₂ and neutral helium, respectively. Because of these strong infrared absorption features, the ($V-I$, $V-K$) two-color diagram is particularly useful for detecting extremely cool hydrogen-rich white dwarfs, as well as cool white dwarfs with mixed hydrogen and helium atmospheres. As can be seen from Figure 9, such objects are extremely rare, with the glaring exception of LHS 1126 which has already been analyzed in BRL ($T_{\text{eff}} = 5390$ K, $N(\text{He})/N(\text{H}) \sim 70$; see their Fig. 31).

Finally, the existence of a non-DA gap in the 5000–6000 K temperature range is already obvious in this diagram, especially when the non-DA sequence is contrasted with the DA sequence. The only two objects inside the gap are LHS 2710 (1313–198) and ESO 292–43 (2345–447) which have already been analyzed by BRL and identified as being peculiar (see § 6.3.1 of BRL for more details). It is again unlikely that the explanation proposed by Hansen (1999), namely that different evolutionary timescales of hydrogen-rich and helium-rich atmosphere white dwarfs, can account for the *observational* fact shown in the right panel of Figure 9, unless non-DA stars evolve more rapidly within the gap than outside the gap.

4. Detailed Analysis

4.1. Fitting Technique

Our fitting technique is described at length in BRL. Briefly, magnitudes are converted into observed fluxes, and the resulting energy distributions are fitted with those predicted from our model atmosphere calculations using a nonlinear least-squares method. Only T_{eff} and the solid angle $(R/D)^2$ are considered free parameters. The distance D is obtained from the trigonometric parallax measurement, and the stellar radius R is converted into mass using the new cooling sequences described in § 2 with thin hydrogen layers for the pure helium and mixed hydrogen/helium compositions, and those with thick hydrogen layers for the pure hydrogen models; masses derived from thin hydrogen layer are about $0.03 M_{\odot}$ smaller than those obtained from thick hydrogen models (Bergeron et al. 1995d).

As discussed in § 3.3, there is a significant UV flux deficiency in hydrogen-rich stars, most likely due to a pseudocontinuum opacity originating from the Lyman edge. As such, the B magnitude has been omitted in the fits of hydrogen-rich stars cooler than $T_{\text{eff}} \sim 5500$ K. For identical reasons, it

has also been omitted in the fits of strong DZ stars such as vMa 2 (0046+051), G165–7 (1328+307), LP 701–29 (2251–070), etc.

Some objects in our sample possess strong molecular absorption features which are not taken into account in our model flux calculations. Such objects include the DQ stars, the C₂H stars — LHS 1126 (0038–226), LHS 290 (1043–188), and G225–68 (1633+572), as well as G240–72 (1748+708) whose spectrum is characterized by the yellow sag discussed above. BRL have shown that the fits to the energy distribution of DQ stars are not affected significantly by the presence of the C₂ Swan bands, with the glaring exception of BPM 27606 (2154–512), the strongest DQ star known. For some of the strongest C₂H stars and for G240–72, the molecular absorption features are so important that the quality of the fits is poor. In these cases, we rely on a technique used in BRL where the optical spectrum of the star is normalized to a continuum set to unity, and folded with the grid of model spectra. The presence of the strong molecular bands is thus taken into account, at least in first order, in the calculations of the emergent flux distributions. This approximate procedure improves the quality of our fits markedly.

4.2. Sample Fits

Several fits to cool white dwarfs with various effective temperatures, surface gravities, and chemical compositions have already been displayed in BRL. In particular, their §§ 5.3 and 5.4 show how the combined photometric energy distributions together with the high signal-to-noise spectra at H α could be used to determine, or at least constrain, the chemical composition of cool degenerates. The most important discriminant between the hydrogen-rich and helium-rich energy distributions lies near the infrared *H* bandpass where hydrogen-dominated atmospheres exhibit a local maximum in their emergent flux due to the bound-free H $^{-}$ opacity threshold at 1.6 μ m. This bump in the emergent flux distribution is of course not observed in pure helium atmospheres. The chemical composition effects on our fits will not be repeated here, and we simply refer the reader to Figures 15 and 16 of BRL where several illustrative examples are displayed. Here we present instead typical fits to hydrogen-rich stars, helium-rich stars, stars with mixed compositions, confirmed or suspected double degenerates, as well as other objects of astrophysical interest. We attempt as much as possible to present fits for objects which have not already been analyzed in BRL. In the following plots, the observed fluxes and corresponding uncertainties are represented by error bars while the model fluxes are shown as filled circles. The atmospheric parameters of each fit are indicated in each panel.

4.2.1. Hydrogen-rich Atmosphere White Dwarfs

Sample fits for DA stars covering the effective temperature range of interest are displayed in Figure 10; sample fits for hydrogen-rich non-DA white dwarfs too cool to exhibit H α have already

been shown in Figure 26 of BRL. The values of T_{eff} and $\log g$ given in each panel are obtained from fits with pure hydrogen atmospheric compositions. The effects of using models with small traces of helium are discussed in detail in § 5.3 of BRL. The spectroscopic observations at $\text{H}\alpha$ are not used directly in the fitting procedure, but they serve as an internal check of our photometric solutions. The theoretical line profiles are simply interpolated at the values of T_{eff} and $\log g$ obtained from the energy distribution fits and compared with the observed line profiles. As can be seen from Figure 10, the observed energy distributions are well reproduced by our theoretical models throughout the temperature range of interest, and the predicted line profiles are in excellent agreement with the solution derived from the photometric observations.

LTT 4816 (1236–495; top object in Fig. 10) is a known ZZ Ceti star for which Bergeron et al. (1995d) obtained a spectroscopic solution of $T_{\text{eff}} = 11,730 \pm 350$ K and $\log g = 8.81 \pm 0.05$, in good agreement with the parameters derived here $T_{\text{eff}} = 11,550 \pm 470$ K and $\log g = 8.63 \pm 0.18$. It is worth emphasizing that the atmospheric parameter determination of both analyses is based on completely different techniques. In the former case, Bergeron et al. (1995d) used fits to the Balmer line profiles ($\text{H}\beta$ to $\text{H}8$), while here we rely on T_{eff} and $\log g$ estimates based on photometric observations and trigonometric parallax measurements. Note that both analyses use the same calibration of the mixing-length theory in the model calculations, namely the so-called $\text{ML2}/\alpha = 0.6$ parameterization. Interestingly enough, our photometric fit to LTT 4816 based on $\text{ML2}/\alpha = 1.0$ models yields $T_{\text{eff}} = 11,410$ K and $\log g = 8.64$ (with the same uncertainties as above), while the spectroscopic fit to the Balmer lines based on the same models yields $T_{\text{eff}} = 12,670$ K and $\log g = 8.66$ (see Table 2 of Bergeron et al. 1995d). Hence, even though the photometric solution is not very sensitive to the value of α (i.e. the ratio of the mixing length to the pressure scale height), the spectroscopic solution differs by 940 K in T_{eff} and 0.15 dex in $\log g$. Moreover, the internal consistency between the spectroscopic and photometric solutions is much better with $\text{ML2}/\alpha = 0.6$ than with $\text{ML2}/\alpha = 1.0$ models. A similar conclusion was reached by Bergeron et al. (1995d) based on a comparison of the atmospheric parameters of 22 ZZ Ceti stars obtained from fits to the ultraviolet energy distributions and fits to the Balmer line profiles. Our result thus brings additional support to the conclusion that the $\text{ML2}/\alpha = 0.6$ calibration of the mixing-length theory provides an excellent internal consistency between atmospheric parameters determined with various techniques over a wide range of wavelengths, which now extends from the ultraviolet to the infrared.

A similar example is G74–7 (0208+396; middle panel of Fig. 10), a well-studied DAZ white dwarf which has been re-analyzed recently by Billères et al. (1997) who presented an analysis of optical and ultraviolet spectroscopic observations. Their spectroscopic fit to the Balmer lines (see their Fig. 4) yields $T_{\text{eff}} = 7260 \pm 40$ K and $\log g = 8.03 \pm 0.07$, in excellent agreement with our photometric solution $T_{\text{eff}} = 7310 \pm 180$ K and $\log g = 8.01 \pm 0.09$. More comparisons between photometric and spectroscopic solutions are provided in § 5.2.

The coolest object in Figure 10 is LHS 1801 (0551+468) with $T_{\text{eff}} = 5380$ K. The fit to its energy distribution suffers from the pathological problem discussed above for the coolest hydrogen-rich stars in our sample in which some unknown pseudocontinuum opacity unaccounted for in our

model calculations affect the emergent flux near the B bandpass. Note that this problem does not occur for LHS 2522 (1208+576; also shown in Fig. 10), a DA star which is only 500 K hotter than LHS 1801. Hence, the phenomenon begins to manifest itself in the intermediate temperature regime near $T_{\text{eff}} \sim 5500$ K. As discussed in § 4.1, the B filter has been dropped in all fits to hydrogen-rich stars below this temperature threshold. As shown in Figure 10, the internal consistency achieved in this manner of the fit to the energy distribution and the $\text{H}\alpha$ line profile is more than satisfactory.

4.2.2. Helium-rich Atmosphere White Dwarfs

Sample fits for helium-rich, non-DA stars covering the effective temperature range of interest are displayed in Figure 11. The values of T_{eff} and $\log g$ given in each panel are obtained from fits with pure helium atmospheric compositions. The spectroscopic fits are of course not shown here since all objects are featureless near the $\text{H}\alpha$ region (see Figure 5). Pure helium models provide excellent fits to the energy distributions of all of these objects in the T_{eff} range considered in this analysis, with the exception of G24–9 (2011+065) which is discussed below. In particular, at low effective temperatures (see, e.g., LHS 542), the problem observed in hydrogen-rich stars at the blue end of the energy distribution is not observed in helium-rich stars. This supports our conclusion that some unaccounted UV opacity from hydrogen is at the origin of this problem.

The first object in Figure 11 is LP 257–28 (0802+386), a hot DZ star with a blue spectrum showing strong H and K lines (Sion et al. 1990). LHS 43 (1142–645) is a weak DQ star (see Figure 6). BRL have discussed at length the validity of the pure helium models to analyze DZ and DQ stars despite the presence of strong metallic lines or carbon bands. LHS 2333 (1055–072) is classified as a DA white dwarf in McCook & Sion (1999), although a note added in their catalog reports the star to be featureless according to Schmidt & Smith (1995). Our own spectroscopic observation which covers the range 4600 – 7300 Å confirms the results of Schmidt & Smith that LHS 2333 has a featureless spectrum — a true DC star. BRL have shown that DC stars in this temperature range ($8000 \gtrsim T_{\text{eff}} \gtrsim 6000$ K) usually belong to a group of peculiar objects whose energy distributions are better reproduced with pure hydrogen models rather than with pure helium models (for reasons still unknown). A good example of such a peculiar white dwarf is the next object shown in Figure 11, G24–9 (2011+065), where the fits with both pure helium and pure hydrogen models are displayed. LHS 2333 seems to be an exception to the rule, unless there is something even more peculiar with this particular object. It is tempting to suggest that LHS 2333 may have recently changed spectral type from DA to DC. However, despite the three DA spectral classifications of this object in the catalog of McCook & Sion (1999), only that of Eggen & Greenstein (1965) is an actual spectroscopic observation (the other two references in the catalog do not report any new observation). Given that this classification relies on old photographic plates, it is difficult to claim that the spectral type of this object has actually changed over the 30 year or so period.

Finally, the last object in Figure 11, LHS 542 (2316–064), is a cool DC white dwarf according to our own spectrum which reveals no significant absorption feature in the range ~ 3780 – 6890 Å.

4.2.3. Mixed H/He Atmosphere White Dwarfs

There is little evidence for a large population of cool white dwarfs with mixed hydrogen and helium atmospheres, as first demonstrated by BRL. Such stars would show up easily in $(B-V, V-K)$ or $(V-I, V-K)$ two-color diagrams due to the H_2 –He collision induced opacity which produces a strong infrared flux deficiency. The C₂H stars also have energy distributions characterized by such an infrared flux deficiency, the most striking example of which is LHS 1126 labeled in the right panel of Figure 9. As mentioned above, such stars have been interpreted as having mixed H/He/C atmospheres with $N(H)/N(He) \sim 10^{-2}$ (Schmidt et al. 1995). Jørgensen et al. (2000) have recently cast some doubt on the Schmidt et al. interpretation based of their own analysis of the chemical abundance equilibrium of a mixture of H/He/C/O and heavier elements. However they have explored atmospheric parameters which do not match those inferred for C2H stars: hydrogen abundances about three orders of magnitude too small and effective temperatures much cooler ($T_{\text{eff}} = 4300$ K) than the narrow range of $T_{\text{eff}} \sim 5400 - 6200$ K where such stars are found.

The presence of trace amounts of hydrogen can be deduced from the presence of a broad and shallow H α absorption feature in an otherwise helium-rich atmosphere due to the van der Waals broadening of the hydrogen lines by neutral helium. This is the case for Ross 640 (1626+368) and L745–46A (0738–172) whose fits are displayed in Figure 12. Also shown in this Figure is the fit to LHS 290 (1043–188), a C₂H star whose optical spectrum is shown in Figure 30 of BRL but for which we had not obtained any photometry at the time of writing the BRL analysis (see Fig. 31 of BRL for fits to additional C₂H stars). In Figure 12, the effective temperature and surface gravity of each object is derived from the fits to the energy distribution, while the hydrogen-to-helium abundance ratio is determined from fits to the H α line profile; only a limit to the abundance can be obtained in the case of LHS 290. The effective temperatures and abundances we derive for Ross 640 and L745–46A are in excellent agreement with those determined by Koester & Wolff (2000) and references therein.

4.2.4. Unresolved Double Degenerates

Overluminous objects in the M_V vs $(V-I)$ color-magnitude diagram displayed in Figure 7 are most likely unresolved binaries composed of two normal white dwarfs. The masses inferred for these objects in a color-magnitude diagram are well below $0.4 M_{\odot}$; note that two unresolved $0.6 M_{\odot}$ white dwarfs would appear in such a diagram as a single $\sim 0.3 M_{\odot}$ white dwarf. Alternatively, it is also possible that the overluminous objects in Figure 7 correspond to single low-mass ($M < 0.4 M_{\odot}$) white dwarf stars.

Sample fits for five of those overluminous objects are displayed in Figure 13. As mentioned above, all of these are of the DA spectral type, and the surface gravities determined by fitting the solid angle are well below the average for normal DA stars. Otherwise, the fits to the energy distributions do not reveal any additional peculiarity, and in particular, they are all consistent

with single white dwarfs. If we were dealing with double degenerates with much different effective temperatures and luminosities, one could expect the combined energy distribution to be somewhat distorted. The results of Figure 13 suggest that either these are single low-mass white dwarfs, or double degenerates with comparable atmospheric parameters.

The evidence that we are actually dealing with unresolved double degenerates stems from the fits to the $H\alpha$ line profiles also shown in Figure 13. In the case of a single low-mass star, the fit to the $H\alpha$ line profile would not show any discrepancy. Those shown here, however, are certainly at odds with the atmospheric parameters obtained from the energy distributions (contrast the fits shown in Figure 13 with those shown in Figure 10). The only marginal case for which the theoretical line profile provides a satisfactory fit is L870–2 (0135–052), a well-known double degenerate system discovered by Saffer et al. (1988)! Bergeron et al. (1990) have actually determined that the effective temperatures of both components of the L870–2 system differ by only 500 K ($T_{\text{eff}} = 6920$ and 7470 K), a result which explains why the combined $H\alpha$ line profile can be reproduced by a single spectrum with an intermediate effective temperature. For the other stars in Figure 13, the line profile fit discrepancies are much more obvious. G21–15 (1824+040) is also a known double degenerate with a period of 6.266 days (Saffer et al. 1998; Maxted & Marsh 1999). Maxted & Marsh (1999) have reported a null result for G1–45 (0101+048) in their radial velocity survey, however. Nothing is known about the two remaining objects in Figure 13.

4.2.5. Magnetic White Dwarfs

Our sample includes magnetic white dwarfs, several of which have been discovered and analyzed in the course of our survey (see BRL and references therein). Here we present additional fits to magnetic white dwarfs as well as magnetic candidates.

Figure 14 shows our best fits to the magnetic white dwarfs G128–72 (2329+267) and GD 175 (1503–070), both of which exhibit Zeeman splitting at $H\alpha$. As discussed above, the magnetic nature of G128–72 has been reported by Moran et al. (1998) while GD 175 represents a new discovery. Here the effective temperatures and surface gravities have been taken from our best fits to the energy distributions. The synthetic magnetic spectra are calculated using offset dipole models following the prescription outlined in Bergeron et al. (1992a). Both the value of the dipole field strength, B_d , and the dipole offset, a_z , are considered free parameters, while the viewing angle i between the dipole axis and the line of sight is determined from a visual inspection of the fits. For G128–72, our best fit is achieved with $B_d = 2.2$ MG, $a_z = 0.1$, and $i = 50^\circ$, in good agreement with the values derived by Moran et al. (1998), $B_d = 2.31 \pm 0.59$ MG and $i = 60 \pm 5^\circ$, under the assumption of a centered dipole model. Note that the shape of the shifted Zeeman components are particularly useful to determine the viewing angle, as shown for instance in Figure 4 of Bergeron et al. (1992a).

GD 175 is an obvious case of an unresolved double degenerate binary containing a magnetic DA

component and a featureless DC component, similar to the G62–46 system analyzed by Bergeron et al. (1993, see also the case of LHS 2273 shown in Fig. 33 of BRL). In such systems, the $\text{H}\alpha$ line profile predicted under the assumption of a single magnetic DA star is much stronger than the observed line profile, as shown in Figure 14 for GD 175 (dotted line). The simplest explanation for this discrepancy is that GD 175 is an unresolved double degenerate binary system composed of a magnetic DA star whose emergent flux is diluted by the presence of a featureless DC companion. The thick solid line in the bottom panel represents our best solution with the assumption that this DC white dwarf contributes equally to the total continuum flux near $\text{H}\alpha$. We do not attempt here to derive the atmospheric parameters for the individual components of the system, as carried out for G62–46 by Bergeron et al. (1993). Instead we note that if two identical — but different chemical compositions — white dwarfs are contributing to the total flux, the mass of the magnetic DA component is near $1 M_\odot$, as opposed to $M \sim 0.7 M_\odot$ when a single star is assumed.

Cool DA white dwarfs with much weaker magnetic fields will not show any Zeeman splitting, at least not at the spectroscopic resolution used here. A good example of such an object is the ~ 35 kG white dwarf LHS 1038 (0009+501) reported by Schmidt & Smith (1994) and analyzed photometrically by BRL (see their Fig. 33). The spectroscopic fit at $\text{H}\alpha$ using non-magnetic models is reproduced in Figure 15. For all objects in this figure, the atmospheric parameters are those obtained from the energy distributions. As mentioned in BRL, the theoretical line profile for LHS 1038 is predicted somewhat too deep, as a result of the magnetic splitting of the $\text{H}\alpha$ line core into its unresolved Zeeman components. A similar object has also been reported by BRL (see their Fig. 30), LHS 5064 (0257+080), and its fit at $\text{H}\alpha$ is reproduced in Figure 15 as well. BRL made the suggestion that LHS 5064 was also a weakly magnetic ($\lesssim 100$ kG) DA star. Recently, Schmidt (1998) observed this object using the technique of Zeeman spectropolarimetry and indeed detected a weak (~ 30 kG) magnetic field at $\text{H}\alpha$. Three additional objects in our survey exhibit similar features — LHS 2800 (1344+106), G138–47 (1635+137), and G156–64 (2253–081), and the fits at $\text{H}\alpha$ are also shown in Figure 15. Schmidt (1998) has reported a null result on all three of these objects, however. It is always possible that an unfortunate orientation of the magnetic axis prevents the detection of circular polarization. Given the resemblance of these fits, it would be worth observing these stars at high spectral resolution to detect any weak Zeeman splitting. Alternative explanations for these three peculiar fits to the $\text{H}\alpha$ line profile include the presence of helium in their atmosphere. Experiments with mixed H/He models, not shown here, indicate that by the time the predicted depth of the $\text{H}\alpha$ line *core* agrees with the observed profile, the line *wings* are predicted much too broad. Another possibility is the presence of an unresolved DC white dwarf which would dilute the absorption profile of the DA star. However, the trigonometric parallax measurements of these objects make them subluminous in an absolute magnitude-color diagram, implying larger than average masses, and inconsistent with these stars being unresolved degenerate binaries as they would then be superluminous. Finally, the remaining object displayed in Figure 15 is LHS 3501 (1953–011) recently reported to be magnetic by Maxted et al. (2000a, and references therein), with a field strength of ~ 500 kG although the Zeeman triplet at $\text{H}\alpha$ indicates a field strength of only ~ 100 kG. The line profile is also found to be variable over a time-scale of a day

or less. Our line fit shown here appears to be consistent with a non-magnetic DA star, however. It is possible that our spectroscopic observation was secured during a rotational phase when Zeeman splitting was the least apparent.

Figure 16 shows our best fit to the energy distribution of the magnetic white dwarf G227–35 (1829+547). This star has been analyzed in detail by Putney & Jordan (1995) who convincingly demonstrated that this object is a strongly magnetic ~ 117 MG *hydrogen-rich* white dwarf. Their spectrum shows a prominent feature in circular polarization with a weak corresponding absorption feature which corresponds to the $2p\text{-}1\text{-}3d\text{-}2$ transition of $\text{H}\alpha$. However, as shown in Figure 16, the observed energy distribution is reproduced much better with a pure helium atmosphere rather than a pure hydrogen atmosphere! The most likely explanation in this case is that the H^- continuum opacity in pure hydrogen magnetic models is sufficiently disrupted in the presence of such a high magnetic field that the corresponding energy distribution resembles instead that of a pure helium model.

4.2.6. Additional Objects of Astrophysical Interest

ESO 439–26.—As discussed in § 3.3, with the recent result that extremely cool, hydrogen atmosphere white dwarfs become bluer, there are now two possible interpretations for the location of the non-DA star ESO 439–26 (1136–286) in the M_V vs $(V\text{-}I)$ color-magnitude diagram displayed in Figure 7. The first one is that the object is a massive ($M \sim 1.20 M_\odot$), pure helium atmosphere white dwarf, i.e. the interpretation proposed by Ruiz et al. (1995). The second one is that the object is a much cooler ($T_{\text{eff}} < 4000$ K), and thus older, lower mass white dwarf. Our best fit to the complete energy distribution using our pure helium model grid is displayed in Figure 17. Our solution, $T_{\text{eff}} = 4490$ K and $\log g = 9.02$, which corresponds to $M = 1.19 M_\odot$, is consistent with the location of ESO 439–26 in the right panel of Figure 7 (i.e. the pure helium sequences). Also shown in Figure 17 is our best fit to the V and I measurements using our pure hydrogen model grid. This time our solution, $T_{\text{eff}} = 3150$ K and $\log g = 8.29$, which corresponds to $M \sim 0.76 M_\odot$, is consistent with the location of ESO 439–26 in the middle panel of Figure 7 (i.e. the pure hydrogen sequences). However, the predicted flux at J is clearly inconsistent with the observed flux, and the pure hydrogen solution must be rejected. This result stresses the importance of obtaining infrared photometry for such cool white dwarfs before drawing any conclusion about their temperature and especially their age.

G107–70A/B.—G107–70A/B (0727+482A/B) is a partially resolved pair of cool degenerate stars with an orbital period of 20.5 yr (Strand et al. 1976; Harrington et al. 1981). This system has long been thought to be composed of two DC white dwarfs, but our new combined spectrum shown in Figure 4 clearly shows a weak $\text{H}\alpha$ absorption feature, a result which indicates that at least one of the two components of the system has some hydrogen in its atmosphere. A visual inspection of the spectra of the coolest DA stars in Figure 4 shows that the $\text{H}\alpha$ profile of G107–70A/B is much broader and shallower than the other DA spectra with similar line strengths. This suggests that

the system may be composed of a normal DA star whose $H\alpha$ absorption line profile is diluted by the contribution of a featureless white dwarf component. In the following we attempt to determine the atmospheric parameters of the individual components of the G107–70A/B system. The magnitude difference between both white dwarfs of the G107–70A/B system has been measured to be 0.3 mag at V , J , H , and K ; we assume the same difference at B , R , and I . We have obtained fits to the A and B components under the assumption that one star has a pure hydrogen atmosphere, while the other one has either a pure hydrogen or pure helium atmosphere (for a total of three possible combinations). Then the theoretical combined spectrum is calculated as the sum of both interpolated spectra, properly weighted by the luminosity of each star. Our results indicate that acceptable fits to the energy distributions can always be achieved, no matter what atmospheric composition is assumed. On the other hand, the $H\alpha$ line profile is always predicted much weaker and sharper than the observed line profile. The dilution of the $H\alpha$ line profile by the DC component does not alter significantly enough the *shape* of the combined line profile. Our best solution shown in Figure 18 is obtained with two pure hydrogen atmosphere white dwarfs. The discrepancy at $H\alpha$ cannot be attributed to an inadequacy with the models since we are able to fit single DA stars in the same range of effective temperature (see, e.g., LHS 1801 in Figure 10). We have also tried to restrict our analysis to only V and the infrared where the magnitude difference has actually been measured, but without improvement. Experiments with mixed H/He atmospheres have not been successful either. Perhaps the $H\alpha$ absorption feature of one of the DA component, or both, is broadened by a weak magnetic field. It is even possible that the G107–70 system is composed of three degenerate components; after all, such systems are now known to exist (Maxted et al. 2000b). We note finally that the combined mass of the pair with our adopted solution is $M \sim 1.19 M_\odot$, in excellent agreement with the astrometric value of $1.29 M_\odot$ derived by Borgman & Lippincott (1983).

5. Global Properties of the Sample

5.1. Adopted Atmospheric Parameters

Among the 152 white dwarfs listed in Table 1, 150 have been analyzed with the techniques described in this paper. The stars omitted are L481–60 (1544–377) which has a bright star nearby that contaminates the photometric observations, and BPM 27606 (2154–512) whose C_2 Swan bands are so strong that the color indices are significantly affected and cannot be modeled within the present theoretical framework.

As opposed to the BRL analysis, all white dwarfs analyzed here have trigonometric parallax measurements which allow us to determine their radii, and hence their masses and surface gravities through the mass-radius relation. The results of our analysis are reported in Table 2. For each white dwarf we give the effective temperature, the surface gravity, the dominant atmospheric constituent, the stellar mass, the absolute visual magnitude, the total luminosity, and the white dwarf cooling

age (not including the main sequence lifetime). The bolometric magnitudes can be derived from the simple expression, $M_{\text{bol}} = -2.5 \log L/L_{\odot} + 4.75$. The numbers in parentheses in Table 2 correspond to the uncertainties of each parameter. The error of T_{eff} is derived directly from the fits to the energy distributions, while the errors of $\log g$ and other quantities have been derived by propagating the error of the trigonometric parallax uncertainty. We have also assumed single stars for all objects in Table 2, even for the suspected or known unresolved degenerate binaries, and a note mentioning the binary nature of these systems has been added.

As discussed in § 4.1, new C/O core evolutionary models with thin and thick hydrogen layers have been used for the helium- and hydrogen-dominated atmospheres, respectively. We have assumed pure hydrogen and pure helium compositions for the hydrogen- and helium-rich white dwarfs, respectively, with the exception of the C₂H stars, as well as Ross 640 and L745–46A displayed in Figure 12, for which the helium abundances have been determined individually. Pure helium compositions were also assumed for the group of peculiar hot ($T_{\text{eff}} > 6000$ K) non-DA white dwarfs whose energy distributions are consistent with pure hydrogen models (see BRL); a note in Table 2 identifies these objects. For the magnetic white dwarf G227–35 shown in Figure 16, we adopt the pure helium solution since its energy distribution is better reproduced by the pure helium model rather than the pure hydrogen model, despite the fact it has a hydrogen-rich composition according to Putney & Jordan (1995).

5.2. Comparison with Spectroscopic Determinations for DA Stars

Additional blue spectroscopic observations which cover the high Balmer lines from H β to H9 are also available to us for a subset of 24 cool DA white dwarfs in our sample. These observations can be used to obtain independent estimates of T_{eff} and $\log g$ using the spectroscopic technique (see, e.g., Bergeron et al. 1992b) which consists of fitting all the hydrogen line profiles observed in each star simultaneously. The value of $\log g$ can be converted into mass using an appropriate mass-radius relation for white dwarfs. These independent determinations can be compared against the values derived here using optical/infrared photometry and trigonometric parallaxes.

The comparison of effective temperature and mass determinations for the 24 white dwarfs in common with our sample is displayed in Figure 19. Seven objects discussed further below are numbered in this figure in order of increasing right ascension. The effective temperatures agree well within the uncertainties of both techniques throughout the entire temperature range considered in this analysis, with the exception of the four stars labeled in the bottom panel of Figure 19. Of these, L587–77A (0326–273; labeled 2) and Case 2 (1606+422; labeled 3) are both low-mass ($M < 0.4 M_{\odot}$) white dwarfs, and they are most likely unresolved degenerate binaries with individual components having much different effective temperatures, while G21–15 (1824+040; labeled 6) is a known double degenerate (Saffer et al. 1998; Maxted & Marsh 1999, see our fit in Fig. 13). This comparison indicates that photometry combined with spectroscopy can be used to identify unresolved degenerate binary candidates. The last object, G128–72 (2329+267; labeled 7), is

a magnetic white dwarf with our best fit at $\text{H}\alpha$ already shown in Figure 14. In this case, the spectroscopic temperature is overestimated since the blue spectrum of this star has been fit with non-magnetic models, and magnetic line broadening can be compensated, to some extent, by an increase in effective temperature (and $\log g$, see below).

The agreement between the photometric masses and the spectroscopic masses for this sample of 24 DA stars, shown in the top panel of Figure 19, is not as good as that between the effective temperatures, even within the mass uncertainties. In general, the spectroscopic masses are larger than those obtained from trigonometric parallax measurements. There are a few exceptions, however, and these are labeled in the top panel of Figure 19. First, G19–20 (1716+020; labeled 5) has a photometric mass of $0.67 \pm 0.08 M_{\odot}$ and a spectroscopic mass of $0.49 \pm 0.03 M_{\odot}$. An independent mass estimate for this white dwarf star comes from the gravitational redshift measurement which yields a value of $0.48 \pm 0.05 M_{\odot}$ (Bergeron et al. 1995a), a result which suggests that the trigonometric parallax measurement is probably in error for this particular object. Second, G31–35 (0011+000; labeled 1), has a fairly large mass uncertainty ($M = 0.85 \pm 0.12 M_{\odot}$) due to a $\sim 15\%$ error in the trigonometric parallax measurement, and the difference from the spectroscopic mass of $M = 0.70 \pm 0.04 M_{\odot}$ is not significant. The objects whose spectroscopic masses are larger than the photometric masses include the three low-mass white dwarfs (objects labeled 2, 3, and 6) already identified as binaries or binary candidates in the bottom panel of Figure 19, and G128–72 (2329+267; labeled 7) the magnetic white dwarf discussed above. For the three binaries, the photometric masses are underestimated since the total flux received from the system is assumed to originate from a single object, while the spectroscopic masses are intermediate values of the masses of the individual components, as demonstrated by Liebert et al. (1991). If we assume instead that two identical white dwarfs contribute to the total flux received at Earth, we obtain the photometric masses indicated by the three vectors in Figure 19, and these agree perfectly with the spectroscopic masses for two of these objects, while the third object is probably composed of two white dwarfs with different luminosities.

As discussed in § 4.2.1, there are DA stars for which the agreement between the photometric and spectroscopic solutions is excellent, the best example of which is G74–7 (0208+396) displayed in Figure 10. Why then are there several DA white dwarfs whose spectroscopic masses are significantly larger than the photometric masses? What is the missing parameter, if any? Bergeron et al. (1989) has suggested that the convective mixing of a thin hydrogen atmosphere with the deeper and more massive helium envelope, which is believed to occur in hydrogen-rich white dwarfs cooler than $T_{\text{eff}} \sim 12,000$ K, could result in atmospheres which are only moderately enriched with helium rather than in helium-dominated atmospheres. Since helium is spectroscopically invisible at these temperatures, the mixed H/He white dwarfs would still appear as normal DA stars. Bergeron et al. (1989, see also Bergeron et al. 1991) has also demonstrated that normal gravity, helium-enriched atmospheres are totally equivalent, *from a spectroscopic point of view*, to pure hydrogen atmospheres but with large surface gravities (and hence masses). Hydrogen line profiles at a given temperature are affected by atmospheric pressure, which in turn is sensitive to changes in the surface gravity

and in the helium abundance, and both effects cannot be disentangled from spectroscopy alone. In contrast, the photometric technique provides a direct measure of the star radius — which is not very sensitive to the presence of helium. Hence, the mass discrepancies observed in Figure 19 could well be the result of helium enrichment in some of the white dwarfs in our sample.

We illustrate the effect of adding small amounts of helium to the atmospheres of cool DA white dwarfs in Figure 20 for LHS 3254 (1655+215), the most discrepant case in Figure 19 (labeled 4 in the top panel). The top panels show our best photometric fit (left panel) and our best spectroscopic fit (right panel) using our pure hydrogen model grid. Even though the effective temperatures agree within ~ 200 K, the surface gravity determined from spectroscopy, $\log g = 8.20$ (or $M = 0.73 M_{\odot}$), is much larger than that obtained from the photometric solution, $\log g = 7.87$ (or $M = 0.53 M_{\odot}$). By allowing a small amount of helium in the model grid, in this case $\log N(\text{He})/N(\text{H}) = -0.20$, we achieve the solutions displayed in the bottom panels of Figure 20. First, the photometric fit has changed little, both qualitatively and quantitatively, a result which implies that the overall results of our analysis remain unaffected by this new parameter. Second, the spectroscopic fit has not changed qualitatively, but the surface gravity has decreased significantly, and most importantly, the photometric and spectroscopic $\log g$ values (and hence masses) are now in perfect agreement. The effective temperatures are also in better agreement. Hence, our results reinforce the conclusions of Bergeron et al. (1989) that several — but probably not all — cool DA stars have helium-enriched atmospheres, with helium abundances as high as $N(\text{He})/N(\text{H}) \sim 1$. We note that (see the following section) the spectroscopically determined masses for hot DB stars can also be brought into better agreement with our photometrically determined values if very small amounts of hydrogen are added to the pure helium model grid. At least trace amounts of both hydrogen and helium are therefore likely to exist in many cool white dwarf atmospheres.

5.3. Mass Distributions

The mass of all white dwarfs in our sample is shown as a function of effective temperature in Figure 21. Each object is represented by a different symbol indicating its atmospheric composition and/or spectral type. Filled and open symbols represent hydrogen-rich and helium-rich atmospheric compositions, respectively. The more specific symbols are discussed in the next section. A comparison of this Figure with Figure 35 of BRL indicates that our new sample has increased in size considerably, especially above $T_{\text{eff}} \sim 7000$ K where the BRL sample contains only a few objects. Furthermore, it is possible here to determine stellar masses for all white dwarfs in our sample, in contrast with BRL who could only determine masses for about 50% of their sample.

While massive white dwarfs are found with both hydrogen and helium atmospheres, low mass white dwarfs have mostly hydrogen-rich atmospheres, with the exceptions of the DQ star G184–12 (1831+197) at $T_{\text{eff}} = 7590$ K, and LP 31–40 (0324+738) at $T_{\text{eff}} = 4650$ K. The mass of the former object could be as large as $0.56 M_{\odot}$ due to the large parallax uncertainty, while the latter object lacks the crucial JHK photometry which would allow us to determine its atmospheric constituent

more precisely, and this object may well have a hydrogen-rich atmosphere. Consequently, it is probable that all low-mass white dwarfs possess hydrogen-rich atmospheres. This conclusion is supported by the spectroscopic analyses of hotter ($T_{\text{eff}} \gtrsim 12,000$ K) DA and DB stars (Bergeron et al. 1991; Beauchamp et al. 1996) which revealed the existence of a low mass tail in the mass distribution of DA stars which is not observed in the DB sample. These results are illustrated in Figure 22 where we compare the mass distributions of the hydrogen- and helium-rich atmosphere white dwarfs in our sample (top panel) and in the hotter spectroscopic samples (bottom panel); note that the photometric and spectroscopic samples do not overlap in effective temperature. Since common envelope evolution is required to produce degenerates with mass $\lesssim 0.5 M_{\odot}$ — the Galaxy being too young to have produced them from single star evolution — we must conclude that this particular evolutionary channel does not produce helium-rich atmosphere white dwarfs, presumably because the objects which go through this close-binary phase end up with hydrogen layers too massive to allow the DA to DB conversion near $T_{\text{eff}} \sim 30,000$ K (Beauchamp et al. 1996), or any possible convective mixing below 12,000 K. The fraction of low-mass, hydrogen-rich atmosphere white dwarfs is larger in the parallax sample ($\sim 20\%$) than in the spectroscopic sample ($\sim 10\%$). This is due to the fact that in the parallax sample, unresolved double degenerate systems composed of two normal $0.6 M_{\odot}$ white dwarfs, for example, will appear as a single overluminous low-mass $\sim 0.3 M_{\odot}$ star, while it will still appear as a single $0.6 M_{\odot}$ object when analyzed spectroscopically.

There are significant differences at high masses as well where the trigonometric parallax sample contains more massive stars ($M \gtrsim 1.0 M_{\odot}$) than the spectroscopic sample. Since the former sample is composed of older objects, it is possible that it contains several cases of mergers which would result in a single white dwarf with higher than average mass (Iben 1990). Note that the most massive star in our sample with $M \sim 1.2 M_{\odot}$ is ESO 439–26 (1136–286), discussed at length above.

The mean mass of the hydrogen-rich parallax subsample is $\langle M \rangle = 0.61 M_{\odot}$ with a dispersion of $\sigma(M) = 0.20 M_{\odot}$, while we find for the helium-rich subsample a mean mass of $\langle M \rangle = 0.72 M_{\odot}$ with a dispersion of $\sigma(M) = 0.17 M_{\odot}$; the combined sample yields $\langle M \rangle = 0.65 M_{\odot}$, $\sigma(M) = 0.20 M_{\odot}$. The lower mean value of the hydrogen-rich set is entirely due to the existence of the low-mass tail component. These numbers can be compared with the values derived for the spectroscopic analyses of hotter DA stars, $\langle M \rangle = 0.59 M_{\odot}$ and $\sigma(M) = 0.13 M_{\odot}$ (Bergeron et al. 1991, 1995d), and of DB stars, $\langle M \rangle = 0.59 M_{\odot}$ and $\sigma(M) = 0.06 M_{\odot}$ (Beauchamp et al. 1996). Note that the dispersions of the spectroscopic mass distributions are considerably smaller due to the increased sensitivity to $\log g$ of the spectroscopic technique over the trigonometric parallax method. While the mean masses obtained for the cool hydrogen atmospheres and warmer DA stars agree well, those of the helium atmospheres and DB stars differ by $\sim 0.13 M_{\odot}$. As discussed in BRL, these results can be somewhat reconciled if small amounts of undetectable hydrogen is present in the cool helium-rich atmospheres. Quantitative results not shown here indicate that the masses derived from the pure helium models could be reduced by $\sim 0.07 M_{\odot}$ were they analyzed with a $N(\text{H})/N(\text{He}) = 10^{-4} - 10^{-3}$ model grid.

It is worth mentioning that the spectroscopic analyses of DA and DB stars discussed above

are not sensitive to the presence of unknown traces of hydrogen or helium. Indeed, DA stars in these studies are restricted to a range of temperature above 15,000 K where the assumption of pure hydrogen atmospheres is most certainly valid due to the gravitational settling of helium (Bergeron et al. 1991). Similarly, DB (and DBA) stars have temperatures in excess of 12,000 K where the hydrogen abundance is well determined, or at least constrained (Beauchamp et al. 1996). Hence, the spectroscopic mass distributions displayed in Figure 22 are not sensitive to unknown abundances of trace elements, unlike the results for cool ($T_{\text{eff}} \lesssim 12,000$ K) DA stars discussed in § 5.2 and shown in Figure 19, in which the presence of spectroscopically invisible helium could overestimate the spectroscopic masses.

5.4. Spectral Evolution

Out of the 150 objects plotted in Figure 21, 96 have a hydrogen-rich atmosphere while 54 have a helium-rich atmosphere. Hence 36% of all white dwarfs in our sample have helium-rich atmospheres, a ratio which is significantly larger than the canonical value of 20% for hotter white dwarfs (Fontaine & Wesemael 1987). The ratio determined here, however, is not constant over the temperature range considered in this analysis. Figure 23 shows the number of hydrogen-rich and helium-rich stars as a function of effective temperature in 1000 K bins using the results presented in Table 2; the corresponding hydrogen- to helium-rich ratio is also shown. The \sim 5000-6000 K bin shows a marked increase in the number of white dwarfs with hydrogen-rich atmospheres, and a marked drop in the number with helium-rich atmospheres. This is the non-DA gap first identified by BRL. Our new results, with a much larger sample and with no overt spectroscopic classification bias, confirms the reality of this gap. Note also that there is no particular concentration of non-DA stars below $T_{\text{eff}} \sim 5000$ K, nor is there any particular concentration of DA stars around 6000 K, contrary to the claim of Hansen (1999). Quite the opposite, hydrogen- and helium-rich white dwarfs in Figure 21 are more or less homogeneously distributed in effective temperature, with the exception of the non-DA gap itself.

We thus reaffirm our earlier conclusion that some as yet unidentified physical mechanism is responsible for turning helium-rich atmosphere white dwarfs into hydrogen-dominated atmospheres near $T_{\text{eff}} \sim 6000$ K. The fact that the cooling timescales of these white dwarfs may depend on their atmospheric composition, as observed by Hansen (1999), has nothing to do with the conclusions reached here. Indeed, if the existence of this gap is the result of the spectral evolution of helium-rich into hydrogen-rich white dwarfs, the only important factor is the mass-dependency of the mechanism through which this transition occurs. If this mechanism — still unknown — is only weakly mass-dependent, then helium-rich white dwarfs will turn into DA stars near 6000 K, no matter what their cooling age might be.

An alternative explanation for the non-DA gap could be that the blue end of the gap at 6000 K represents the end of the cooling sequence for helium-rich white dwarfs, and that all non-DA stars observed below the red end of the gap are the result of convectively mixed DA stars at 5000 K.

However, the cooling age of helium-rich white dwarfs near 6000 K is only around 4 Gyr, and since much older DA stars exist, older and cooler helium-rich white dwarfs should exist as well.

The spectroscopic behavior seen in our sample around the gap is also of interest. To summarize, Figure 21 shows that: hydrogen-rich white dwarfs are seen at all effective temperatures; DQ stars are seen at $T_{\text{eff}} \gtrsim 6500$ K; DZ at $T_{\text{eff}} \gtrsim 6500$ K and 4500–5500 K; helium-rich DA’s at 8000–9000 K; C₂H stars at 5500–6500 K; and the peculiar group whose featureless energy distributions are better fit with pure hydrogen models at 6000–7500 K.

At temperatures just above and near the non-DA gap, non-DA white dwarfs that are neither DQ nor DZ belong to the peculiar group of white dwarfs whose featureless energy distributions are better fit with pure hydrogen models. One exception directly above the gap is the DC star G125–3 (1917+386) with $T_{\text{eff}} = 6390$ K. According to Greenstein & Liebert (1990), this object could have barely visible, heavily broadened C₂ bands. Their spectrum which is available to us reveals three weak and broad absorption features which actually match those of C₂H stars, and it is possible that this object belongs to this spectral type, although better spectroscopic observations are required before this result is confirmed. Near 7500 K, there are three additional DC stars. The coolest object is Stein 2051B (0426+588) with $T_{\text{eff}} = 7120$ K, a true DC star according to Wegner & Yackovich (1982) who reported featureless optical as well as ultraviolet spectroscopic observations. The second DC star is G195–19 (0912+536, $T_{\text{eff}} = 7160$ K), a polarized ~ 100 MG magnetic white dwarf (Schmidt & Smith 1995), and the last one is LHS 2333 (1055–072, $T_{\text{eff}} = 7420$ K) whose fit has already been discussed in §4.2.2 and displayed in Figure 11. Another helium-rich object with only a slightly higher effective temperature is GD 356 (1639+537, $T_{\text{eff}} = 7510$ K), a DAE white dwarf whose spectrum exhibits a hydrogen Zeeman triplet in emission (Greenstein & McCarthy 1985).

Most non-DA white dwarfs within the non-DA gap are C₂H stars. G240–72 (1748+708) is considered in this spectral class as well, following the interpretation of BRL that the observed 15% deep yellow sag near 5000 Å is the result of C₂H molecular absorption features in the ~ 200 MG magnetic field which characterizes this star. Near the red edge of the gap are LHS 2710 (1313–198) and ESO 292–43 (2345–447) which have already been identified by BRL as being peculiar in that the energy distributions cannot be matched by our models (see their Figure 37 and the accompanying discussion). Most importantly, *our new larger sample has not added any new non-DA star within the gap*. During the course of our observational survey, every time a previously classified non-DA star was found inside the gap, subsequent high signal-to-noise spectroscopy would systematically reveal the presence of H α . Note that the new magnetic candidate C₂H star LHS 2229 recently reported by Schmidt et al. (1999) has an effective temperature of $T_{\text{eff}} \sim 4400$ K when analyzed with our fitting technique (assuming $\log g = 8.0$). If this interpretation is correct, C₂H stars may exist well below the red edge of the non-DA gap.

The results shown in Figure 21 reveal that DQ and C₂H stars do not overlap in effective temperature. Indeed, there are no DQ stars observed below $T_{\text{eff}} = 6400$ K, while C₂H stars are

found only below this temperature. This suggests that DQ stars probably turn into C₂H stars, and that the existence of the non-DA gap and the nature of the C₂H white dwarfs are somehow related. Since C₂H stars have been interpreted by Schmidt et al. (1995) as the result of mixed H/He/C compositions, it is the additional presence of hydrogen in a supposedly helium and carbon mixture that would turn DQ stars into C₂H stars when they cool off below 6400 K. The origin of the hydrogen source remains a mystery, however, since the exotic model proposed by BRL has been discarded by Malo et al. (1999) based on detailed model simulations. We just note that the same source of hydrogen, once identified, could be also responsible for turning the remaining non-DA stars above ~ 6000 K (DZ and peculiar) into DA stars below this temperature.

Peculiar white dwarfs whose energy distributions are better reproduced with hydrogen models despite the absence of H α are found over a range of effective temperature of 6200–7600 K, i.e. all above the non-DA gap. The hottest of these stars is LP 434–97 (1154+186) at $T_{\text{eff}} = 7630$ K. Interestingly, immediately above this temperature are the two helium-rich DA stars in our sample, L745–46A (0738–172) at $T_{\text{eff}} = 7710$ K, and Ross 640 (1626+368) at $T_{\text{eff}} = 8640$ K. Given that there are no other such helium-rich DA stars known, it is tempting to suggest that an evolutionary link exists between these objects and the peculiar white dwarfs. Above 8000 K, most non-DA stars are of the DQ type, although some are reported to be featureless in the literature. The number of stars in this temperature range is still too small, however, to draw meaningful conclusions about any spectral evolution from one type to another.

The reappearance of non-DA stars below the gap has been interpreted by BRL as the result of the convective mixing of the hydrogen atmosphere with the deeper helium envelope, turning DA stars into non-DA stars. The calculations reported by BRL showed indeed that envelope models which include realistic model atmospheres as boundary conditions could reduce the mixing temperature limit from the canonical value of $T_{\text{eff}} \sim 6000$ K down to 5000 K, which occurs for a hydrogen layer mass of $M_{\text{H}}/M_{\star} \sim 10^{-6}$. Obviously, some DA stars have thicker hydrogen layers since they did not mix, in particular the (apparent or true) low-mass white dwarfs which are either unresolved binaries, or the result of common envelope evolution. We note that the coolest non-DA stars in our sample have hydrogen-rich atmospheres despite the lack of any detectable hydrogen absorption features. While H α can be detected almost to the end of the disk cooling sequence, it will certainly not be detected in any cooler white dwarfs discovered in the Galactic halo.

Our sample contains a higher ratio of non-DA to DA stars than is seen in the temperature range 12,000–30,000 K, where the ratio is around 25% (Fontaine & Wesemael 1987). This increase can certainly be interpreted as the result of convective mixing over a still unknown temperature range. Since the 10,000–11,000 K bin in Figure 23 already shows a ratio near unity, and since the reappearance of non-DA stars in large number below the non-DA gap has also been interpreted as the result of convective mixing, we can conclude that the convective mixing mechanism operate from $T_{\text{eff}} \sim 11,000$ K, all the way down to the coolest possible mixing temperature near 5000 K. This implies that DA stars must possess a large range of possible hydrogen layer thicknesses, including very thick hydrogen layers above $q(\text{H}) = 10^{-6}$.

Out of the 13 magnetic white dwarfs in our sample — 8 with hydrogen-rich and 5 with helium-rich atmospheres, 12 are located in a narrow range of effective temperature between $T_{\text{eff}} = 5300$ and 8000 K; the exception is GW+70 8247 (1900+705) at $T_{\text{eff}} = 12,070$ K. It is possible that the lower boundary represents only a selection effect since Zeeman splitting would make the detection of H α more difficult in cool magnetic DA stars than in non-magnetic white dwarfs. However, the spectrum of the coolest magnetic star in our sample, LHS 1734 (0503–174), still exhibits strong H α absorption features (see the spectrum in Fig. 5 of BRL), and the detection of even weaker features is well within the detection limit of our spectroscopic observations. Furthermore, while there are no magnetic white dwarfs in the three dozen or so objects included in our sample between $T_{\text{eff}} \sim 8000$ and 12,000 K, a few magnetic stars in this particular range of effective temperature are known to exist (Schmidt & Smith 1995).

All the features of the chemical distribution shown in Figure 21 cannot be accounted for by convective mixing alone, however, or by any simple theoretical model. Hence we are left with very few possible explanations, despite the abundance of observational clues unveiled in BRL and in this analysis. Given these results, it is worth repeating and developing an alternative explanation proposed by BRL who questioned the stability of convectively mixed hydrogen and helium convection zones. Consider a 0.6 M_{\odot} , pure helium atmosphere white dwarf which accretes $\sim 10^{-8} M_{\odot}$ of hydrogen by the time it reaches 6000 K. This value is totally plausible if one allows a low accretion rate from the interstellar medium of $10^{-17} M_{\odot} \text{ yr}^{-1}$ over a period of ~ 1 Gyr or so. Since the mass of the helium convection zone is almost constant below $T_{\text{eff}} \sim 12,000$ K ($M_{\text{He-conv}} \sim 10^{-6} M_{\odot}$), the resulting abundance of $N(\text{H})/N(\text{He}) \sim 10^{-2}$ would make the star appear as a non-DA white dwarf at 6000 K, H α being wiped out by van der Waals broadening with neutral helium. It is reasonable to wonder whether such a mixed hydrogen and helium convection zone would remain convectively stable as the results shown in Figure 40 of BRL indicate that a DA star with a hydrogen layer mass of $\sim 10^{-8} M_{\odot}$ or slightly larger, would not have mixed in the first place, at least not at $T_{\text{eff}} \sim 6000$ K. It is possible that convectively mixed hydrogen and helium atmospheres return to a well separated hydrogen-dominated atmosphere with a helium-rich envelope. Note that the chemical separation needs to be complete only in the photospheric layers for the atmosphere to appear hydrogen-rich. Such “born again” DA stars cannot retain a DA signature for long, however. As the star cools from $T_{\text{eff}} \sim 6000$ K down to 5000 K, the bottom of the hydrogen atmosphere further plunges from $q(\text{H}) = 10^{-8}$ to 10^{-6} (depending on the mass of the star, see Fig. 4 of BRL), leading to another episode of convective mixing, and supporting the trends seen in Figure 21.

If the separation of hydrogen and helium layers does occur, we can speculate about what the energy distribution of these stars might look like at the moment just before the separation occurs. Obviously, the hydrogen and helium abundance profiles throughout the atmosphere will be very inhomogeneous, even over the disk surface. Perhaps this would explain why BRL (see also Malo et al. 1999) were unable to fit the energy distributions of those peculiar white dwarfs above 6000 K with pure hydrogen, pure helium, or *homogeneously mixed* hydrogen and helium compositions. Models with inhomogeneous abundance profiles could hold the key to these peculiar stars.

We note finally that if the total mass of hydrogen is small, the convectively mixed hydrogen and helium layer is stable. This can certainly be the case for the C₂H stars with mixed atmospheres of hydrogen, helium, and carbon, as well as Ross 640 and L745–46A, which are simply too hot and thus too young to have accreted enough hydrogen (these objects have $N(\text{H})/N(\text{He}) \lesssim 10^{-3}$).

5.5. White Dwarf Cosmochronology

The isochrones for our C/O core evolutionary models with thin and thick hydrogen layers are shown in Figures 24 and 25, respectively. In these plots, we no longer distinguish between objects with hydrogen- and helium-rich atmospheres since the atmospheric composition of these stars may have changed several times over their lifetime, and as such, it is not a trivial task to associate a cooling age to a single object, as discussed in the Introduction. Also shown are the corresponding isochrones but with the main sequence lifetime added to the white dwarf cooling age; here we simply assume (Leggett et al. 1998) $t_{\text{MS}} = 10(M_{\text{MS}}/M_{\odot})^{-2.5}$ Gyr and $M_{\text{MS}}/M_{\odot} = 8 \ln[(M_{\text{WD}}/M_{\odot})/0.4]$. As can be seen from these results, white dwarfs with $M \lesssim 0.48 M_{\odot}$ cannot have C/O cores, and yet have been formed from single star evolution within the lifetime of this Galaxy. As discussed above, some of these low-mass objects must be either unresolved double degenerates, or single white dwarfs with helium cores. In the former case, the stellar masses inferred from these figures are underestimated — especially if the unresolved components have comparable luminosities, and the corresponding cooling ages derived here become meaningless. While some of these low-mass white dwarfs may still be interpreted as having C/O cores when the masses are corrected to allow for two objects in the system, the lowest mass objects in our sample would still yield “corrected” masses too low to be C/O-core degenerates. The second possibility corresponds to single (or binary) helium-core degenerates whose core mass was truncated by Case B mass transfer before helium ignition was reached. Such low-mass white dwarfs would be best described with helium-core evolutionary models. However, since it is impossible to distinguish between the two possibilities discussed above for most of the low-mass stars in our sample, we refrain from interpreting these objects any further.

In this temperature regime, low-mass (i.e. large-radius) white dwarfs evolve faster than their more massive counterparts, with the exception of the most massive objects ($M \gtrsim 1.0 M_{\odot}$) in which the onset of crystallization reduces the cooling timescales considerably. These begin to cool off much more rapidly than the lower mass stars to produce the observed parabola-shaped isochrones. With decreasing effective temperature, crystallization gradually occurs in lower mass models, and the turning point of these parabolas moves slowly towards lower masses. Consequently, the inferred stellar ages are strongly mass-dependent, a result which stresses the importance of determining reliable masses through precise trigonometric parallax measurements. The best example is provided by ESO 439–26 (1136–286), the most massive object in our sample, which could have an inferred cooling age anywhere between 5 and 7.5 Gyr if its mass was not known (assuming thin hydrogen layer models).

The effect of using different thicknesses for the outer hydrogen layer varies as a function of the mass of the star as well. For instance, the coolest white dwarfs near $0.6 M_{\odot}$ have cooling ages of roughly 8 Gyr with the thin hydrogen layer models, and 1 Gyr *older* with the thick models. Out of the three oldest objects in our sample, two have hydrogen-rich atmospheres, the coolest of which is ER 8 (1310–472) with $T_{\text{eff}} = 4220$ K and mass near $0.6 M_{\odot}$. If we make the assumption that this star has a thick hydrogen envelope, the corresponding white dwarf cooling age is $t_{\text{WD}} = 9.3$ Gyr ($t_{\text{WD+MS}} \sim 9.7$ Gyr). The oldest object in Figure 25, LP 701–29 (2251–070) with $T_{\text{eff}} = 4580$ K, has a helium-rich atmosphere and it thus cannot have had a thick outer hydrogen layer, otherwise it would have remained hydrogen-rich. Its more probable age derived from Figure 24 is actually much shorter, $t_{\text{WD}} = 7.8$ Gyr ($t_{\text{WD+MS}} \sim 7.9$ Gyr). There are two objects in our sample cooler than ER 8 with hydrogen-rich atmospheres with apparently low masses of $\sim 0.4 M_{\odot}$, LHS 239 (0747+073B, $T_{\text{eff}} = 4210$ K) and LP 131–66 (1247+550, 4050 K). If these objects are in fact an unresolved pair of normal mass white dwarfs then the total age of these systems is around 10 Gyr.

6. Summary and Conclusions

A detailed photometric and spectroscopic analysis of 152 cool white dwarfs with trigonometric parallax measurements was presented. Optical and infrared photometry were combined and compared with an improved grid of model atmosphere calculations to determine the effective temperatures and the solid angles for all objects, which combined with the measured parallaxes yielded the stellar radii. The latter were then converted into stellar masses through the mass-radius relations obtained from new evolutionary models which best characterize cool white dwarfs. These have carbon/oxygen cores, with both thin $M_{\text{H}}/M_{\star} = q(\text{H}) = 10^{-10}$ and thick $q(\text{H}) = 10^{-4}$ hydrogen layers. This parallax sample more than doubles the number of cool white dwarfs with known masses compared to the sample presented in BRL. Furthermore, this new sample is more representative of the population of cool white dwarf stars as it contains, presumably, no bias in favor of any particular spectral type, as opposed to the BRL sample which favored non-DA stars.

One of the main results of our analysis is the confirmation of the existence of a range in effective temperature between roughly 5000 and 6000 K in which almost all white dwarfs have hydrogen-rich atmospheres. The only non-DA stars in this range of effective temperature are the so-called C₂H stars which are believed to represent the cooler stage of the DQ sequence, found only above the gap. Clearly, the existence of this gap holds the key to our understanding of the chemical evolution of cool white dwarfs. Unfortunately, our understanding of the physical mechanisms that could alter the atmospheric composition of cool white dwarfs as they evolve are at best sketchy. After the “phase transition” model proposed in BRL was convincingly discarded by Malo et al. (1999), very few alternatives exist.

It has become clear from our analysis, however, that convection plays an important role, but that our understanding of what to expect from the result of convective mixing needs to be revised. It is generally believed that when the bottom of the thin hydrogen convection zone deepens and

reaches the underlying and more massive convective helium envelope, convective mixing will occur, and that the resulting atmospheric composition will simply be governed by the mass ratio of the hydrogen and helium convection zones. Such arguments lead to predicted abundances after convective mixing of $N(\text{H})/N(\text{He}) = 10^{-4}$, 10^{-3} , 10^{-2} , and 10^{-1} , for mixing temperatures of $T_{\text{mix}} \sim 11,000$, $10,000$, 8500 , and 6500 K, respectively, the mixing temperature depending on the exact thickness of the hydrogen layer. Our analysis has demonstrated that such objects do not exist, at least in our sample. Even the objects which possess mixed hydrogen and helium atmospheres, and in particular Ross 640 and L745–46A, have abundances that do not fit this simple convective mixing picture. On the other hand, the definite increase of the ratio of non-DA to DA stars in the temperature range considered in this analysis with respect to that of hotter white dwarfs cannot easily be explained in terms other than convective mixing. Also, convective mixing has been called upon to explain the reappearance of non-DA stars below the non-DA gap near 5000 K.

A different picture is now starting to emerge from our findings, and those of other analyses, in which convective mixing *processes* may lead to predicted chemical abundances that differ from the standard model. First, our comparison of atmospheric parameters determined from photometry and spectroscopy reveals that a mass discrepancy exists in several DA stars, and that this discrepancy can be resolved if we allow some amount of helium to be present in their atmospheres. The required abundances close to $N(\text{He})/N(\text{H}) = 1$ are clearly at odds with the standard convective mixing model predictions, as noted also by Bergeron et al. (1990). Note that helium is spectroscopically invisible in the temperature regime considered here and cannot be detected directly. It is possible to conceive that helium is being brought to the surface not by convective mixing, but perhaps by convective overshooting of the helium convection zone into the hydrogen layer. The bottom of the hydrogen convection zone would then carry some of this helium to the surface, in a very similar fashion to the way carbon is being brought to the photosphere of DQ stars, with the exception that ordinary diffusion is responsible in this case for polluting the bottom of the helium layer with carbon.

A variance of the convective model that could account for the existence of the non-DA gap has also been proposed. The question arises when one considers a helium-rich atmosphere on top of which indefinite amounts of hydrogen are accumulated, presumably from interstellar accretion. It is clear that the hydrogen abundance ratio will gradually increase until some point where the homogeneously mixed hydrogen and helium convection zone can no longer be sustained. A stable chemical separation between the hydrogen and the helium layers could then occur, leading to the predominance of DA stars below $T_{\text{eff}} \sim 6000$ K. The implication of this proposed model is that cool white dwarfs must accrete reasonable amounts of hydrogen from the interstellar medium for this mechanism to work. Also, it was proposed that the chemical separation could occur in a non-homogeneous fashion, leading to chemically inhomogeneous atmospheres, similar to the hotter DAB stars (see Koester et al. 1994; Beauchamp et al. 1993). Such inhomogeneous atmospheres could perhaps account for the peculiar objects identified in our sample whose energy distributions share both characteristics of hydrogen and helium atmospheres.

Given the complexity of the chemical evolution of cool white dwarf atmospheres revealed in our analysis, it is not clear what evolutionary models should be used to derive cooling ages. Thin and thick hydrogen layer models yield cooling ages which differ by 2 Gyr in some cases. Non-DA stars are probably better characterized by thin hydrogen models; even if they were once DA stars, they probably had thin hydrogen layers anyway in order to eventually mix. But cool DA stars may have thin or thick hydrogen layers. Thick hydrogen layer white dwarfs remain DA forever, but the fraction of such stars is still unknown. The problem becomes even more complex when one attempts to determine the age of the Galactic disk using the luminosity function of cool white dwarfs. The theoretical luminosity functions should in fact reflect the actual population of cool white dwarfs, and should be a combination of thin and thick hydrogen layer models. The problems are greatly simplified for hotter DA, DB, or DO stars. From the results presented here, the oldest white dwarfs in our sample have a minimum stellar age of 8.5 Gyr, but are more likely characterized by models with thick hydrogen layers which yield an age around 9.5 Gyr.

We feel at this point that we have pushed both the observational and theoretical aspects of this cool white dwarf study to their limits, and that more work now needs to be done on the theoretical front to explain the various features discovered in this analysis. Several avenues of investigation have been proposed, most of which are related to our poor understanding of convective mixing.

We wish to acknowledge G. Fontaine for calculating the cooling models used in our analysis, P. Brassard for making his evolutionary code available to us, and G. D. Schmidt for his spectropolarimetric observations of the magnetic white dwarf candidates. We are deeply grateful to the various observatories for awarding us so many nights for this project and to all the staff at the observatories who were extremely helpful. We also wish to thank the referee for pointing us out the results of Jorgensen et al. of which we were unaware. This work was supported in part by the NSERC Canada and by the Fund FCAR (Québec). MTR received partial support from Fondecyt grant 1980659 and Catedra Presidencial en Ciencias.

REFERENCES

Anguita, C., Loyola, P., & Ruiz, M. T. 1996, private communication

Beauchamp, A., Wesemael, F., Bergeron, P., Liebert, J., & Saffer, R. A. 1996, in ASP Conf. Ser. Vol. 96, Hydrogen-Deficient Stars, ed. S. Jeffery & U. Heber (San Francisco: ASP), 295

Beauchamp, A., Wesemael, F., Fontaine, G., & Bergeron, P. 1993, in White Dwarfs: Advances in Observation and Theory, ed. M. Barstow (Dordrecht: Kluwer), 281

Bergeron, P. 2001, in preparation

Bergeron, P., Liebert, J., & Fulbright, M. S. 1995a, *ApJ*, 444, 810

Bergeron, P., Ruiz, M. T., & Leggett, S. K. 1992a, *ApJ*, 400, 315

Bergeron, P., Ruiz, M. T., & Leggett, S. K. 1993, *ApJ*, 407, 733

Bergeron, P., Ruiz, M. T., & Leggett, S. K. 1997, *ApJS*, 108, 339 (BRL)

Bergeron, P., Ruiz, M. T., Leggett, S. K., Saumon, D., & Wesemael, F. 1994, *ApJ*, 423, 456

Bergeron, P., Saffer, R. A., & Liebert, J. 1991, in 7th European Workshop on White Dwarfs, NATO ASI Series, ed. G. Vauclair & E. M. Sion (Dordrecht: Kluwer Academic Publishers), 75

Bergeron, P., Saffer, R. A., & Liebert, J. 1992b, *ApJ*, 394, 228

Bergeron, P., Saumon, D., & Wesemael, F. 1995b, *ApJ*, 443, 764

Bergeron, P., Wesemael, F., & Beauchamp, A. 1995c, *PASP*, 107, 1047

Bergeron, P., Wesemael, F., Fontaine, G., & Liebert, J. 1990, *ApJ*, 351, L21

Bergeron, P., Wesemael, F., Lamontagne, R., Fontaine, G., Saffer, R. A., & Allard, N. F. 1995d, *ApJ*, 449, 258

Bergeron, P., Wesemael, F., Liebert, J., & Fontaine, G. 1989, *ApJ*, 345, L91

Bessell, M. S., & Weis, E. W. 1987, *PASP*, 99, 642

Billères, M., Wesemael, F., Bergeron, P., & Beauchamp, A. 1997, *ApJ*, 488, 368

Borgman, E. R., & Lippincott, S. L. 1983, *AJ*, 88, 120

Borysow, A., Jørgensen, U. G., & Zheng C. 1997, *A&A*, 324, 185

Brassard, G., & Fontaine, G. 2000, in preparation

Eggen, O. J., & Greenstein, J. L. 1965, *ApJ*, 141, 83

Elias, J. H., Frogel, J. A., Matthews, K., & Neugebauer, G. 1982, AJ, 87, 1029

Fontaine, G., & Wesemael, F. 1987, in IAU Colloquium 95, The Second Conference on Faint Blue Stars, eds. A. G. D. Philip, D. S. Hayes & J. Liebert (Schenectady: L. Davis Press), 319

Greenstein, J. L. 1986, ApJ, 304, 334

Greenstein, J. L., & Liebert, J. W. 1990, ApJ, 360, 662

Greenstein, J. L., & McCarthy, J. K. 1985, ApJ, 289, 732

Hansen, B. M. S. 1998, Nature, 394, 860

Hansen, B. M. S. 1999, ApJ, 520, 680

Harrington, R. S., Christy, J. W., & Strand, K. Aa. 1981, AJ, 86, 909

Hummer, D. G., & Mihalas, D. 1988, ApJ, 331, 794

Iben, I., Jr. 1990, ApJ, 353, 215

Jørgensen, U. G., Hammer, D., Borysow, A., & Falkesgaard, J. 2000, A&A, 361, 283

Kapranidis, S., & Liebert, J. 1986, ApJ, 305, 863

Koester, D., & Allard, N. F. 1996, in ASP Conf. Ser. Vol. 96, Hydrogen-Deficient Stars, ed. S. Jeffery & U. Heber (San Francisco: ASP), 324

Koester, D., Liebert, J., & Saffer, R. A. 1994, ApJ, 422, 783

Koester, D., & Wolff, B. 2000, A&A, 357, 587

Leggett, S. K., Ruiz, M. T., & Bergeron, P. 1998, ApJ, 497, 294

Liebert, J. 1977, A&A, 60, 101

Liebert, J., Bergeron, P., & Saffer, R.A. 1991, in 7th European Workshop on White Dwarfs, NATO ASI Series, ed. G. Vauclair & E. M. Sion (Dordrecht: Kluwer Academic Publishers), 409

Liebert, J., Dahn, C. C., Harris, H. C. & Leggett, S. K. 1999, in ASP Conf. Ser. Vol. 169, 11th European Workshop on White Dwarfs, ed. S.-E. Solheim & E. G. Meištas (San Francisco: ASP), 51

Liebert, J., Dahn, C. C., & Monet, D. G. 1988, ApJ, 332, 891

Malo, A., Wesemael, F., & Bergeron P. 1999, ApJ, 517, 901

Maxted, P. F. L., Ferrario, L., Marsh, T. R., & Wickramasinghe, D. T. 2000a, MNRAS, 315, 41

Maxted, P. F. L., & Marsh, T. R. 1999, MNRAS, 307, 122

Maxted, P. F. L., Marsh, T. R., Moran, C. K. J., & Han, Z. 2000b, MNRAS, 314, 334

McCook, G. P., & Sion, E. M. 1987, ApJS, 65, 603

McCook, G. P., & Sion, E. M. 1999, ApJS, 121, 1

Monet, D. G., Dahn, C. C., Vrba, F. J., Harris, H. C., Pier, J. R., Luginbuhl, C. B., & Ables, H. D. 1992, AJ, 103, 638

Moran, C., Marsh, T. R., & Dhillon, V. S. 1998, MNRAS, 299, 218

Pelletier, C., Fontaine, G., Wesemael, F., Michaud, G., & Wegner, G. 1986, ApJ, 307, 242

Putney, A., & Jordan, S. 1995, ApJ, 449, 863

Ruiz, M. T. 1996, AJ, 111, 1267

Ruiz, M. T., Anguita, C., & Maza, J. 1989 in IAU Colloquium 114, White Dwarfs, ed. G. Wegner (New York: Springer), 122

Ruiz, M. T., Bergeron, P., Leggett, S. K., & Anguita, C. 1995, ApJ, 455, L159

Ruiz, M. T., & Takamiya, M. Y. 1995, AJ, 109, 2817

Ruiz, M. T., Takamiya, M. Y., Mendez, R. A., Maza, J., & Wischnjewsky, M. 1993, AJ, 106, 2575

Saffer, R. A., Liebert, J., & Olszewski, E. M. 1988, ApJ, 334, 947

Saffer, R. A., Livio, M., & Yungelson, L. R. 1998, ApJ, 502, 394

Saumon, D., & Jacobson, S. B. 1999, ApJ, 511, L107

Schmidt, G. D. 1998, private communication

Schmidt, G. D., Bergeron, P., & Fegley, B., Jr. 1995, ApJ, 443, 274

Schmidt, G. D., Liebert, J., Harris, H. C., Dahn, C. C., & Leggett, S. K. 1999, ApJ, 512, 916

Schmidt, G. D., & Smith, P. S. 1994, ApJ, 423, L63

Schmidt, G. D., & Smith, P. S. 1995, ApJ, 448, 305

Sion, E. M., Kenyon, S. J., & Aannestad, P. A. 1990, ApJ, 72, 707

Strand, K. Aa., Dahn, C. C., & Liebert, J. 1976, BAAS, 8, 506

Tassoul, M., Fontaine, G., & Winget, D. E. 1990, ApJS, 72, 335

van Altena, W. F., Lee, J. T., & Hoffleit, E. D. 1994, The General Catalogue of Trigonometric Parallaxes (New Haven: Yale University Observatory)

Wegner, G., & Yackovich, F. H. 1982, AJ, 87, 155

Wehrse, R., & Liebert, J. 1980, A&A, 83, 184

Wesemael, F., Greenstein, J. L., Liebert, J., Lamontagne, R., Fontaine, G., Bergeron, P., & Glaspey, J. W. 1993, PASP, 105, 761

Wood, M. A. 1990, Ph. D. thesis, Univ. of Texas at Austin

Wood, M. A. 1995, in 9th European Workshop on White Dwarfs, NATO ASI Series, ed. D. Koester & K. Werner (Berlin: Springer), 41

Table 1. Observational Results

| WD | Name | π (mas) | σ_π (mas) | W (Å) | V | $B - V$ | $V - R$ | $V - I$ | N (BVRI) | J | $J - H$ | $H - K$ | N (JHK) | Notes |
|----------------|-------------|----------------|-----------------------|------------|-------|---------|---------|---------|-------------|--------|---------|---------|------------|------------|
| 0000-345 | LHS 1008 | 75.7 | 9.0 | 0.0 | 15.02 | +0.44 | +0.30 | +0.57 | 1 | 14.17 | +0.15 | +0.15 | 1 | 1, 2 |
| 0009+501 | LHS 1038 | 90.6 | 3.7 | 8.91 | 14.36 | +0.45 | +0.28 | +0.59 | 1 | 13.41 | +0.15 | +0.05 | 1 | 1, 2, 3, 4 |
| 0011+000 | G31-35 | 32.9 | 4.8 | 34.8 | 15.35 | +0.20 | +0.08 | +0.18 | 1 | 15.21 | +0.08 | +0.01 | 1 | 2 |
| 0011-134 | LHS 1044 | 51.3 | 3.8 | 7.15 | 15.89 | +0.63 | +0.33 | +0.67 | 1 | 14.85 | +0.23 | +0.10 | 1 | 1, 2, 4, 5 |
| 0029-032 | LHS 1093 | 42.6 | 1.0 | 0.0 | 17.32 | +1.12 | +0.61 | +1.14 | 1 | 15.56 | +0.19 | +0.02 | 4 | 1, 2 |
| 0033+016 | G1-7 | 30.4 | 4.0 | 44.2 | 15.61 | +0.18 | +0.02 | +0.08 | 1 | 15.63 | +0.03 | -0.03 | 1 | 2 |
| 0038-226 | LHS 1126 | 101.2 | 10.4 | 0.0 | 14.50 | +0.70 | +0.42 | +0.79 | 2 | 13.32 | -0.15 | -0.24 | 2 | 1, 2 |
| 0038+555 | G218-8 | 43.4 | 2.0 | 0.0 | 14.05 | +0.05 | +0.04 | +0.12 | 1 | 13.97: | -0.11: | -0.05: | 1 | 2, 6 |
| 0046+051 | vMa 2 | 232.5 | 1.9 | 0.0 | 12.39 | +0.52 | +0.26 | +0.49 | 2 | 11.69 | +0.08 | +0.09 | 1 | 1, 2, 5 |
| 0101+048 | G1-45 | 46.9 | 3.8 | 18.0 | 14.00 | +0.26 | +0.17 | +0.34 | 1 | 13.51 | +0.12 | +0.01 | 1 | 2 |
| 0115+159 | LHS 1227 | 64.9 | 3.0 | 0.0 | 13.85 | +0.10 | +0.11 | +0.20 | 1 | 13.72 | +0.00 | -0.02 | 1 | 1, 2 |
| 0117-145 | LHS 1233 | 34.8 | 1.2 | 1.05 | 16.96 | +0.89 | +0.51 | +0.98 | 1 | 15.47 | +0.30 | +0.09 | 1 | 2, 7 |
| 0121+401 | G133-8 | 32.1 | 5.5 | 4.17 | 17.12 | +0.79 | +0.45 | +0.90 | 1 | 15.64 | +0.21 | +0.02 | 2 | 2, 7 |
| 0126+101 | G2-40 | 28.4 | 3.1 | 15.9 | 14.40 | +0.24 | +0.12 | +0.28 | 1 | 14.05 | +0.13 | -0.02 | 1 | 2, 6 |
| 0135-052 | L870-2 | 81.0 | 2.8 | 11.5 | 12.86 | +0.33 | +0.23 | +0.48 | 1 | 12.12 | +0.18 | +0.02 | 1 | 1, 2 |
| 0142+312 | G72-31 | 28.2 | 4.3 | 28.0 | 14.78 | +0.22 | +0.11 | +0.26 | 1 | 14.38 | +0.05 | -0.05 | 1 | 2 |
| 0208+396 | G74-7 | 59.8 | 3.5 | 12.2 | 14.51 | +0.33 | +0.25 | +0.47 | 1 | 13.80 | +0.15 | +0.02 | 1 | 1, 2, 5 |
| 0213+427 | LHS 153 | 50.2 | 4.1 | 3.64 | 16.22 | +0.73 | +0.45 | +0.85 | 1 | 14.98 | +0.25: | +0.21: | 2 | 2, 5, 6 |
| 0222+648 | LHS 1405 | 31.4 | 0.8 | 0.0 | 18.29 | +1.30 | +0.71 | +1.34 | 1 | 16.35 | +0.29 | +0.08 | 2 | 1, 2 |
| 0230-144 | LHS 1415 | 64.0 | 3.9 | 3.20 | 15.77 | +0.69 | +0.43 | +0.84 | 1 | 14.43 | +0.26 | +0.06 | 1 | 1, 2 |
| 0243-026 | LHS 1442 | 47.1 | 5.0 | 10.2 | 15.54 | +0.40 | +0.26 | +0.53 | 2 | 14.71 | +0.22 | -0.02 | 2 | 1, 2 |
| 0245+541 | LHS 1446 | 96.6 | 3.1 | 0.73 | 15.36 | +0.92 | +0.52 | +1.00 | 1 | 13.89 | +0.23 | +0.06 | 2 | 1, 2, 6 |
| 0257+080 | LHS 5064 | 35.9 | 3.5 | 7.09 | 15.90 | +0.43 | +0.28 | +0.58 | 1 | 15.01 | +0.17 | +0.04 | 1 | 1, 2, 4 |
| 0324+738 | LP 31-40 | 25.0 | 3.8 | 0.0 | 17.68 | +1.27 | +0.77 | +1.39 | 1 | ... | ... | ... | 0 | 2 |
| 0326-273 | L587-77A | 57.6 | 13.6 | 25.3 | 14.00 | ... | ... | ... | 1 | 13.27 | +0.15 | +0.04 | 1 | 2, 8 |
| 0341+182 | Wolf 219 | 52.6 | 3.0 | 0.0 | 15.19 | +0.33 | +0.28 | +0.54 | 1 | 14.56 | +0.21 | -0.05 | 1 | 1, 2, 5 |
| 0357+081 | LHS 1617 | 56.1 | 3.7 | 5.97 | 15.92 | +0.70 | +0.41 | +0.83 | 1 | 14.59 | +0.26 | +0.07 | 2 | 1, 2 |
| 0426+588 | Stein 2051B | 180.6 | 0.8 | 0.0 | 12.43 | +0.30 | +0.26 | +0.57 | 1 | 11.84 | +0.11 | +0.05 | 1 | 2, 5, 6 |
| 0433+270 | G39-27 | 60.2 | 2.9 | 4.02 | 15.81 | +0.67 | +0.41 | +0.80 | 1 | 14.61 | +0.29 | +0.10 | 1 | 1, 2 |
| 0435-088 | L879-14 | 105.2 | 2.6 | 0.0 | 13.75 | +0.33 | +0.32 | +0.57 | 2 | 13.00 | +0.15 | +0.06 | 1 | 1, 2, 5 |

Table 1—Continued

| WD | Name | π (mas) | σ_π (mas) | W (Å) | V | $B - V$ | $V - R$ | $V - I$ | N (<i>BVRI</i>) | J | $J - H$ | $H - K$ | N (<i>JHK</i>) | Notes |
|----------------|------------|----------------|-----------------------|------------|-------|---------|---------|---------|----------------------|-------|---------|---------|---------------------|------------|
| 0440+510 | G175-46 | 21.6 | 5.2 | 19.0 | 15.95 | +0.24 | +0.13 | +0.26 | 1 | 15.60 | +0.10 | -0.03 | 1 | 2 |
| 0503-174 | LHS 1734 | 45.6 | 4.0 | 3.82 | 16.01 | +0.72 | +0.44 | +0.90 | 1 | 14.55 | +0.22 | +0.10 | 2 | 1, 2, 4 |
| 0518+333 | G86-B1B | 15.3 | 2.2 | 20.1 | 16.06 | +0.22 | +0.19 | +0.41 | 1 | 15.52 | +0.19 | -0.01 | 1 | 2 |
| 0548-001 | G99-37 | 90.3 | 2.8 | 0.0 | 14.56 | +0.52 | +0.34 | +0.61 | 1 | 13.73 | +0.10 | +0.00 | 2 | 1, 2, 4 |
| 0551+468 | LHS 1801 | 32.3 | 1.5 | 2.18 | 17.23 | +0.84 | +0.47 | +0.94 | 1 | 15.84 | +0.29 | +0.02 | 2 | 2, 7 |
| 0552-041 | LP 658-2 | 155.0 | 2.1 | 0.0 | 14.47 | +1.01 | +0.50 | +0.98 | 2 | 13.02 | +0.12 | +0.08 | 2 | 1, 2, 5 |
| 0553+053 | G99-47 | 125.0 | 3.6 | 8.23 | 14.16 | +0.62 | +0.38 | +0.75 | 2 | 12.96 | +0.19 | +0.11 | 2 | 1, 2, 4, 5 |
| 0618+067 | LHS 1838 | 44.2 | 4.2 | 5.52 | 16.41 | +0.56 | +0.36 | +0.74 | 2 | 15.29 | +0.24 | +0.05 | 2 | 1, 2 |
| 0644+025 | G108-26 | 54.2 | 5.5 | 15.3 | 15.71 | +0.35 | +0.23 | +0.46 | 2 | 15.00 | +0.15 | -0.08 | 2 | 1, 2 |
| 0648+641 | LP 58-53 | 30.0 | 5.2 | 6.24 | 16.65 | +0.56 | +0.36 | +0.74 | 1 | 15.46 | +0.27 | +0.07 | 1 | 2 |
| 0651-479 | ESO 207-21 | 16.1 | 1.6 | 0.0 | 19.54 | +1.21 | +0.65 | +1.24 | 3 | 17.70 | +0.23 | +0.02 | 2 | 1, 9 |
| 0654+027 | G108-42 | 26.0 | 3.7 | 0.0 | 16.17 | +0.12 | +0.15 | +0.20 | 1 | 15.98 | +0.00 | +0.00 | 1 | 2 |
| 0657+320 | LHS 1889 | 53.5 | 0.9 | 1.60 | 16.62 | +1.02 | +0.53 | +1.01 | 1 | 14.99 | +0.22 | +0.08 | 5 | 1, 2 |
| 0659-064 | LHS 1892 | 81.0 | 24.2 | 8.31 | 15.43 | +0.43 | +0.30 | +0.60 | 1 | 14.58 | +0.29 | +0.05 | 1 | 2, 5 |
| 0706+377 | G87-29 | 41.2 | 2.4 | 0.0 | 15.64 | +0.30 | +0.26 | +0.48 | 1 | 15.00 | +0.12 | +0.06 | 1 | 1, 2 |
| 0727+482A..... | G107-70A | 90.0 | 1.0 | 1.41 | 15.26 | +0.98 | +0.53 | +1.02 | 1 | 13.66 | +0.24 | +0.09 | 3 | 1, 2, 5, 7 |
| 0727+482B..... | G107-70B | 90.0 | 1.0 | 1.41 | 15.56 | +0.98 | +0.53 | +1.02 | 1 | 13.96 | +0.24 | +0.09 | 3 | 1, 2, 5, 7 |
| 0738-172 | L745-46A | 112.4 | 2.7 | 4.88 | 13.06 | +0.24 | +0.18 | +0.34 | 1 | 12.65 | +0.04 | +0.09 | 3 | 2, 5 |
| 0743-340 | vB 3 | 57.5 | 3.1 | 0.0 | 16.60 | +1.21 | +0.64 | +1.21 | 2 | 14.85 | +0.14 | +0.16 | 2 | 1, 10 |
| 0747+073A..... | LHS 240 | 54.7 | 0.7 | 0.41 | 16.63 | +1.06 | +0.58 | +1.08 | 2 | 14.96 | +0.23 | +0.01 | 2 | 1, 2, 5 |
| 0747+073B..... | LHS 239 | 54.7 | 0.7 | 0.0 | 16.96 | +1.21 | +0.65 | +1.26 | 2 | 15.05 | +0.15 | +0.04 | 2 | 1, 2, 5 |
| 0751+578 | G193-78 | 28.4 | 3.8 | 0.0 | 15.08 | +0.09 | +0.08 | +0.17 | 1 | 14.94 | +0.00 | -0.02 | 1 | 2 |
| 0752-676 | BPM 4729 | 141.2 | 8.4 | 4.70 | 13.95 | +0.65 | +0.37 | +0.75 | 1 | 12.79 | +0.27 | +0.09 | 2 | 1, 2 |
| 0752+365 | G90-28 | 29.5 | 4.3 | 13.2 | 16.09 | +0.29 | +0.18 | +0.40 | 1 | 15.50 | +0.15 | +0.00 | 1 | 2 |
| 0802+386 | LP 257-28 | 24.0 | 3.0 | 0.0 | 15.56 | +0.04 | +0.05 | +0.08 | 1 | 15.60 | +0.02 | -0.06 | 1 | 2 |
| 0816+387 | G111-71 | 25.2 | 2.5 | 13.1 | 16.51 | +0.30 | +0.22 | +0.44 | 1 | 15.87 | +0.15 | -0.01 | 1 | 2 |
| 0827+328 | LHS 2022 | 44.9 | 3.8 | 13.4 | 15.73 | +0.32 | +0.22 | +0.47 | 1 | 15.01 | +0.16 | +0.01 | 1 | 2 |
| 0839-327 | L532-81 | 112.7 | 9.7 | 26.7 | 11.90 | +0.25 | ... | ... | 0 | 11.59 | +0.04 | +0.00 | 1 | 2, 8 |
| 0856+331 | G47-18 | 48.8 | 3.4 | 0.0 | 15.16 | +0.03 | +0.13 | +0.19 | 1 | 15.12 | +0.03 | -0.02 | 1 | 1, 2 |
| 0912+536 | G195-19 | 97.3 | 1.9 | 0.0 | 13.84 | +0.35 | +0.20 | +0.33 | 2 | 13.22 | +0.07 | +0.06 | 1 | 1, 2, 4, 5 |

Table 1—Continued

| WD | Name | π (mas) | σ_π (mas) | W (Å) | V | $B - V$ | $V - R$ | $V - I$ | N ($BVRI$) | J | $J - H$ | $H - K$ | N (JHK) | Notes |
|----------------|------------|----------------|-----------------------|------------|-------|---------|---------|---------|-----------------|-------|---------|---------|----------------|---------|
| 0913+442 | G116-16 | 34.6 | 4.0 | 22.0 | 15.37 | +0.22 | +0.15 | +0.30 | 1 | 14.96 | +0.12 | -0.03 | 1 | 2 |
| 0930+294 | G117-25 | 31.2 | 4.6 | 21.2 | 15.98 | +0.24 | +0.15 | +0.32 | 1 | 15.51 | +0.11 | -0.05 | 1 | 2 |
| 0946+534 | G195-42 | 43.5 | 3.5 | 0.0 | 15.18 | +0.17 | +0.13 | +0.28 | 1 | 14.90 | +0.03 | -0.01 | 2 | 1, 2 |
| 0955+247 | G49-33 | 40.9 | 4.5 | 20.1 | 15.06 | +0.24 | +0.12 | +0.32 | 1 | 14.66 | +0.07 | -0.06 | 1 | 2 |
| 1012+083 | G43-38 | 34.5 | 3.9 | 8.68 | 16.03 | +0.41 | +0.27 | +0.57 | 1 | 15.20 | +0.21 | +0.05 | 1 | 2 |
| 1019+637 | LP 62-147 | 61.2 | 3.6 | 11.5 | 14.70 | +0.38 | +0.25 | +0.53 | 1 | 13.83 | +0.20 | -0.02 | 1 | 2 |
| 1039+145 | G44-32 | 22.2 | 3.5 | 0.0 | 16.51 | +0.28 | +0.22 | +0.41 | 1 | 15.93 | +0.07 | +0.08 | 2 | 1, 2 |
| 1043-188 | LHS 290 | 56.9 | 6.5 | 0.0 | 15.52 | +0.57 | +0.49 | ... | 1 | 14.62 | +0.21 | +0.05 | 1 | 2, 5 |
| 1055-072 | LHS 2333 | 82.3 | 3.5 | 0.0 | 14.33 | +0.30 | +0.20 | +0.42 | 1 | 13.81 | +0.10 | +0.02 | 1 | 2, 5 |
| 1108+207 | LHS 2364 | 38.3 | 2.7 | 0.0 | 17.70 | +0.97 | +0.53 | +1.07 | 2 | 15.91 | +0.22 | +0.07 | 2 | 1, 2, 5 |
| 1115-029 | LHS 2392 | 26.3 | 5.1 | 0.0 | 15.34 | +0.08 | +0.09 | +0.17 | 1 | 15.23 | -0.04: | -0.02: | 1 | 2 |
| 1121+216 | Ross 627 | 74.4 | 2.8 | 14.0 | 14.21 | +0.31 | +0.20 | +0.45 | 1 | 13.58 | +0.18 | +0.00 | 1 | 2, 5 |
| 1124-296 | ESO 439-80 | 16.4 | 1.7 | 29.3 | 15.02 | ... | +0.07 | +0.26 | 1 | 14.90 | +0.02 | +0.08 | 1 | 1, 9 |
| 1136-286 | ESO 439-26 | 24.5 | 1.0 | 0.0 | 20.52 | +1.03 | +0.64 | +1.14 | 3 | 18.64 | ... | ... | 1 | 1, 11 |
| 1142-645 | LHS 43 | 218.3 | 6.7 | 0.0 | 11.49 | +0.17 | +0.16 | +0.29 | 1 | 11.19 | +0.07 | +0.03 | 1 | 2 |
| 1147+255 | LP 375-51 | 19.5 | 2.9 | 43.9 | 15.66 | +0.15 | +0.06 | +0.13 | 1 | 15.53 | +0.04 | -0.02 | 1 | 2 |
| 1154+186 | LP 434-97 | 33.5 | 3.5 | 0.0 | 15.61 | +0.26 | +0.18 | +0.37 | 1 | 15.15 | +0.12 | +0.01 | 1 | 2 |
| 1208+576 | LHS 2522 | 48.9 | 4.6 | 4.87 | 15.78 | +0.57 | +0.37 | +0.74 | 1 | 14.64 | +0.25 | +0.07 | 1 | 2 |
| 1215+323 | G148-B4B | 32.2 | 3.6 | 0.0 | 17.00 | +0.33 | +0.23 | +0.60 | 2 | 16.39 | +0.15 | -0.13: | 1 | 2 |
| 1236-495 | LT 4816 | 61.0 | 9.4 | 45.5 | 13.80 | +0.18 | -0.02 | -0.03 | 1 | 13.92 | +0.02 | -0.08 | 1 | 2 |
| 1244+149 | G61-17 | 15.7 | 4.2 | 39.6 | 15.89 | +0.17 | +0.03 | +0.06 | 1 | 15.84 | -0.02 | +0.02 | 1 | 2 |
| 1247+550 | LP 131-66 | 39.6 | 0.7 | 0.0 | 17.79 | +1.44 | +0.76 | +1.45 | 1 | 15.72 | +0.05 | +0.04 | 2 | 1, 2, 5 |
| 1257+037 | LHS 2661 | 60.3 | 3.8 | 5.07 | 15.84 | +0.66 | +0.38 | +0.76 | 2 | 14.56 | +0.23 | +0.08 | 2 | 1, 2, 5 |
| 1257+278 | G149-28 | 28.9 | 4.1 | 20.4 | 15.41 | +0.23 | +0.15 | +0.28 | 1 | 14.99 | +0.08 | +0.00: | 1 | 2 |
| 1300+263 | LHS 2673 | 28.4 | 3.3 | 0.0 | 18.77 | +1.24 | +0.68 | +1.28 | 2 | 16.89 | +0.18 | +0.01 | 2 | 5, 12 |
| 1310-472 | ER 8 | 66.5 | 2.4 | 0.0 | 17.13 | +1.39 | +0.72 | +1.41 | 2 | 15.21 | +0.10 | +0.08 | 1 | 1, 2 |
| 1313-198 | LHS 2710 | 40.6 | 1.8 | 0.0 | 17.14 | +0.95 | +0.43 | +0.82 | 2 | 15.87 | +0.17 | +0.14 | 4 | 1, 9 |
| 1325+581 | G199-71 | 27.0 | 5.5 | 9.74 | 16.70 | +0.40 | +0.28 | +0.54 | 1 | 15.82 | +0.14 | +0.03 | 1 | 2 |
| 1328+307 | G165-7 | 33.4 | 5.3 | 0.0 | 16.03 | +0.70 | +0.29 | +0.43 | 1 | 15.50 | +0.14 | +0.02 | 1 | 2 |
| 1334+039 | Wolf 489 | 121.4 | 3.4 | 1.19 | 14.63 | +0.95 | +0.51 | +1.01 | 1 | 13.06 | +0.26 | +0.10 | 2 | 1, 2, 5 |

Table 1—Continued

| WD | Name | π (mas) | σ_π (mas) | W (Å) | V | $B - V$ | $V - R$ | $V - I$ | N (BVRI) | J | $J - H$ | $H - K$ | N (JHK) | Notes |
|-----------------|-----------|----------------|-----------------------|------------|--------|---------|---------|---------|-------------|--------|---------|---------|------------|------------|
| 1344+106 | LHS 2800 | 49.9 | 3.6 | 11.6 | 15.12 | +0.38 | +0.22 | +0.48 | 1 | 14.38 | +0.18 | +0.01 | 1 | 2, 5 |
| 1345+238 | LP 380-5 | 82.9 | 2.2 | 0.46 | 15.71 | +1.15 | +0.59 | +1.13 | 2 | 13.92 | +0.25 | +0.08 | 2 | 1, 2, 5 |
| 1418-088 | G124-26 | 24.6 | 3.8 | 17.9 | 15.38 | +0.28 | +0.17 | +0.38 | 1 | 14.81 | +0.12 | +0.00 | 1 | 2 |
| 1444-174 | LHS 378 | 69.0 | 4.0 | 0.0 | 16.44 | +1.03 | +0.49 | +1.01 | 1 | 14.94 | +0.15 | +0.11 | 2 | 1, 2, 5 |
| 1455+298 | LHS 3007 | 28.9 | 4.1 | 13.0 | 15.60 | +0.31 | +0.22 | +0.42 | 1 | 14.86 | +0.13 | +0.01 | 1 | 2 |
| 1503-070 | GD 175 | 38.5 | 5.5 | 9.08 | 15.88 | +0.40 | +0.28 | +0.55 | 1 | 15.07 | +0.14 | +0.02 | 1 | 2, 4 |
| 1544-377 | L481-60 | 74.6 | 10.1 | 33.8 | 12.97: | +0.18: | +0.22: | +0.60: | 1 | ... | ... | ... | 0 | 2, 13 |
| 1606+422 | Case 2 | 22.2 | 3.5 | 48.8 | 13.82 | +0.11 | -0.03 | -0.06 | 1 | 13.92 | +0.00 | -0.09 | 1 | 2 |
| 1609+135 | LHS 3163 | 54.5 | 4.7 | 25.9 | 15.11 | +0.20 | +0.10 | +0.24 | 1 | 14.77 | +0.01 | +0.01 | 1 | 2 |
| 1625+093 | G138-31 | 42.8 | 3.7 | 10.8 | 16.14 | +0.34 | +0.27 | +0.52 | 3 | 15.34 | +0.22 | +0.06 | 3 | 1, 2 |
| 1626+368 | Ross 640 | 62.7 | 2.0 | 8.99 | 13.83 | +0.19 | +0.08 | +0.17 | 2 | 13.58 | +0.01 | -0.01 | 1 | 2 |
| 1633+433 | G180-63 | 66.2 | 3.0 | 9.11 | 14.84 | +0.43 | +0.27 | +0.56 | 1 | 13.95 | +0.19 | +0.03 | 1 | 2 |
| 1633+572 | G225-68 | 69.2 | 2.5 | 0.0 | 14.99 | +0.50 | +0.31 | +0.61 | 1 | 14.03 | +0.06 | -0.02 | 2 | 1, 2, 5 |
| 1635+137 | G138-47 | 25.5 | 4.6 | 11.1 | 16.94 | +0.38 | +0.27 | +0.47 | 2 | 16.11 | +0.15 | -0.02: | 1 | 2, 7 |
| 1637+335 | G180-65 | 35.0 | 3.2 | 34.3 | 14.65 | +0.18 | +0.06 | +0.14 | 1 | 14.56 | +0.06 | -0.04 | 1 | 2 |
| 1639+537 | GD 356 | 47.4 | 3.5 | -4.85 | 15.05 | +0.29 | +0.21 | +0.39 | 2 | 14.54 | +0.08 | +0.04 | 1 | 2, 4 |
| 1655+215 | LHS 3254 | 43.0 | 3.1 | 26.4 | 14.13 | +0.21 | +0.10 | +0.21 | 1 | 13.89 | +0.09 | -0.05 | 1 | 2 |
| 1656-062 | LP 686-32 | 30.7 | 0.9 | 4.21 | 17.14 | +0.79 | +0.34 | +0.72 | 2 | 15.89 | +0.25 | +0.08 | 1 | 1, 9 |
| 1705+030 | G139-13 | 57.0 | 5.4 | 0.0 | 15.20 | +0.43 | +0.24 | +0.46 | 1 | 14.62 | +0.12 | +0.02 | 1 | 2 |
| 1716+020 | G19-20 | 28.1 | 2.6 | 60.2 | 14.36 | +0.12 | -0.04 | -0.04 | 1 | 14.68 | +0.03 | -0.06: | 1 | 2 |
| 1733-544 | L270-137 | 45.6 | 0.8 | 7.35 | 15.70 | +0.46 | +0.29 | +0.53 | 2 | 14.89 | +0.34 | +0.09 | 1 | 1, 9 |
| 1736+052 | G140-2 | 23.4 | 3.9 | 38.8 | 15.92 | +0.23 | +0.12 | +0.26 | 1 | 15.62 | +0.06 | +0.07 | 1 | 2 |
| 1748+708 | G240-72 | 164.7 | 2.4 | 0.0 | 14.13 | +0.48 | +0.53 | +1.05 | 1 | 12.77 | +0.07 | +0.20 | 1 | 1, 2, 4, 5 |
| 1756+827 | LHS 56 | 63.9 | 2.9 | 12.1 | 14.34 | +0.35 | +0.22 | +0.47 | 2 | ... | ... | ... | 0 | 2, 5 |
| 1811+327A | G206-17 | 19.5 | 4.3 | 10.7 | 16.40 | +0.30 | +0.20 | +0.41 | 1 | 15.71 | +0.15 | +0.02 | 1 | 2 |
| 1811+327B | G206-18 | 19.5 | 4.3 | 6.82 | 17.07 | +0.44 | +0.28 | +0.59 | 1 | 16.08 | +0.14 | +0.12: | 1 | 2, 6 |
| 1818+126 | G141-2 | 24.5 | 5.5 | 5.08 | 16.09 | +0.51 | +0.33 | +0.67 | 1 | 15.07 | +0.17 | +0.03 | 1 | 1, 2 |
| 1820+609 | G227-28 | 78.2 | 4.1 | 0.82 | 15.69 | +0.98 | +0.54 | +1.05 | 1 | 13.96 | +0.23 | +0.08 | 2 | 2, 7 |
| 1824+040 | G21-15 | 18.2 | 2.3 | 33.8 | 13.89 | +0.09 | -0.05 | -0.07 | 1 | 14.07 | -0.07 | +0.00 | 1 | 2, 6 |
| 1826-045 | G21-16 | 34.9 | 3.8 | 23.8 | 14.58 | +0.21 | +0.11 | +0.26 | 1 | 14.44: | +0.00: | +0.05: | 1 | 2, 6 |

Table 1—Continued

| WD | Name | π (mas) | σ_π (mas) | W (Å) | V | $B - V$ | $V - R$ | $V - I$ | N (BVRI) | J | $J - H$ | $H - K$ | N (JHK) | Notes |
|----------------|------------|----------------|-----------------------|------------|-------|---------|---------|---------|-------------|--------|---------|---------|------------|------------|
| 1829+547 | G227-35 | 66.8 | 5.6 | 0.0 | 15.57 | +0.49 | +0.29 | +0.60 | 1 | 14.76 | +0.15 | +0.11 | 1 | 2, 4 |
| 1831+197 | G184-12 | 17.9 | 4.8 | 0.0 | 16.41 | +0.29 | +0.23 | +0.37 | 3 | 15.93 | +0.11 | +0.01 | 1 | 2 |
| 1840+042 | GD 215 | 40.2 | 3.4 | 24.3 | 14.79 | +0.22 | +0.13 | +0.27 | 1 | 14.53: | +0.07: | -0.04: | 1 | 2 |
| 1855+338 | G207-9 | 30.5 | 4.4 | 54.8 | 14.64 | +0.17 | +0.01 | -0.02 | 1 | 14.74 | +0.02 | -0.05 | 1 | 2 |
| 1900+705 | GW+70 8247 | 77.0 | 2.3 | 0.0 | 13.25 | +0.06 | +0.01 | +0.02 | 1 | ... | ... | ... | 0 | 2, 4 |
| 1917+386 | G125-3 | 85.5 | 3.4 | 0.0 | 14.61 | +0.45 | +0.30 | +0.57 | 1 | 13.77 | +0.08 | +0.10 | 1 | 1, 2 |
| 1953-011 | LHS 3501 | 87.8 | 2.9 | 13.8 | 13.69 | +0.28 | +0.19 | +0.38 | 2 | 13.12 | +0.10 | +0.00 | 1 | 2, 4 |
| 2002-110 | LHS 483 | 57.7 | 0.8 | 0.0 | 16.95 | +1.16 | +0.59 | +1.09 | 2 | 15.32 | +0.21 | +0.02 | 2 | 1, 2, 5, 6 |
| 2011+065 | G24-9 | 44.7 | 1.9 | 0.0 | 15.78 | +0.38 | +0.27 | +0.53 | 2 | 14.94 | +0.15 | +0.04 | 2 | 1, 2 |
| 2048+263 | G187-8 | 49.8 | 3.4 | 1.80 | 15.63 | +0.92 | +0.52 | +1.00 | 1 | 14.12 | +0.29 | +0.04 | 2 | 1, 2 |
| 2054-050 | vB 11 | 64.6 | 5.1 | 0.0 | 16.69 | +1.20 | +0.66 | +1.32 | 1 | 14.82 | +0.21 | +0.07 | 1 | 1, 2, 5 |
| 2059+190 | G144-51 | 26.1 | 4.4 | 7.91 | 16.36 | +0.43 | +0.26 | +0.54 | 1 | 15.52 | +0.16 | +0.02 | 2 | 1, 2 |
| 2059+247 | G187-16 | 36.1 | 4.2 | 7.75 | 16.57 | +0.59 | +0.31 | +0.64 | 1 | 15.45 | +0.16 | +0.03 | 1 | 2, 7 |
| 2059+316 | G187-15 | 29.0 | 3.5 | 0.0 | 15.04 | +0.11 | +0.07 | +0.14 | 1 | 14.94 | -0.03 | -0.01 | 1 | 2 |
| 2105-820 | L24-52 | 58.6 | 8.8 | 35.5 | 13.61 | +0.21 | +0.05 | +0.14 | 1 | 13.52 | -0.01 | -0.05 | 1 | 2 |
| 2107-216 | LHS 3636 | 42.2 | 1.5 | 6.45 | 16.80 | +0.59 | +0.35 | +0.77 | 1 | 15.63 | +0.18: | +0.05: | 2 | 1, 9 |
| 2111+261 | G187-32 | 31.4 | 3.7 | 18.2 | 14.68 | +0.24 | +0.16 | +0.32 | 1 | 14.15 | +0.07 | -0.01 | 1 | 2, 6 |
| 2136+229 | G126-18 | 23.8 | 3.1 | 31.9 | 15.25 | +0.17 | +0.06 | +0.14 | 1 | 15.04 | +0.08 | -0.13 | 1 | 2, 6 |
| 2140+207 | LHS 3703 | 79.9 | 3.2 | 0.0 | 13.24 | +0.13 | +0.14 | +0.26 | 1 | 12.95 | +0.02 | -0.02 | 1 | 2, 6 |
| 2154-512 | BPM 27606 | 68.5 | 10.6 | 0.0 | 14.74 | +0.19 | +0.44 | +0.61 | 1 | 13.47 | +0.00 | +0.18 | 1 | 1, 2, 13 |
| 2207+142 | G18-34 | 39.2 | 4.4 | 12.8 | 15.60 | +0.29 | +0.20 | +0.42 | 1 | 14.99 | +0.18 | -0.03 | 1 | 2, 6 |
| 2246+223 | G67-23 | 52.5 | 4.1 | 49.2 | 14.39 | +0.17 | +0.05 | +0.14 | 1 | 14.28 | -0.03 | -0.06 | 1 | 2 |
| 2248+293 | G128-7 | 47.8 | 4.2 | 4.70 | 15.54 | +0.66 | +0.40 | +0.79 | 1 | 14.24 | +0.23 | +0.07 | 2 | 1, 2, 5 |
| 2251-070 | LP 701-29 | 123.7 | 4.3 | 0.0 | 15.71 | +1.84 | +0.61 | +1.15 | 2 | 13.86 | +0.23 | +0.16 | 2 | 1, 2, 5 |
| 2253-081 | G156-64 | 36.7 | 5.3 | 8.45 | 16.48 | +0.40 | +0.27 | +0.56 | 1 | 15.59 | +0.12 | +0.11: | 2 | 2 |
| 2311-068 | G157-34 | 39.8 | 4.7 | 0.0 | 15.40 | +0.23 | +0.18 | +0.35 | 1 | 14.98 | +0.05 | +0.03 | 2 | 2, 6 |
| 2312-024 | LHS 3917 | 37.5 | 5.9 | 0.0 | 16.31 | +0.51 | +0.26 | +0.49 | 1 | 15.70 | +0.17 | -0.05 | 1 | 1, 2 |
| 2316-064 | LHS 542 | 32.2 | 3.7 | 0.0 | 18.15 | +1.08 | +0.62 | +1.16 | 1 | 16.38 | +0.24 | +0.04 | 2 | 5, 12 |
| 2329+267 | G128-72 | 25.9 | 4.7 | 32.4 | 15.33 | +0.27 | +0.06 | +0.17 | 2 | 15.13 | +0.10 | -0.15 | 1 | 2 |
| 2345-447 | ESO 292-43 | 38.1 | 2.2 | 0.0 | 17.87 | +0.79 | +0.42 | +0.84 | 1 | 16.66 | +0.07 | +0.26 | 2 | 1, 9 |

Table 1—Continued

| WD | Name | π (mas) | σ_π (mas) | W (Å) | V | $B - V$ | $V - R$ | $V - I$ | N (<i>BVRI</i>) | J | $J - H$ | $H - K$ | N (<i>JHK</i>) | Notes |
|----------------|----------|----------------|-----------------------|------------|-------|---------|---------|---------|----------------------|-------|---------|---------|---------------------|---------|
| 2347+292 | LHS 4019 | 46.5 | 4.1 | 4.12 | 15.76 | +0.59 | +0.35 | +0.72 | 1 | 14.59 | +0.24 | +0.11 | 1 | 1, 2, 6 |
| 2352+401 | G171-27 | 38.7 | 5.6 | 0.0 | 14.94 | +0.19 | +0.19 | +0.32 | 1 | 14.57 | +0.05 | +0.02 | 1 | 1, 2 |

Note. — (1) In common with Bergeron et al. (1997); (2) π from Yale Parallax Catalog; (3) Spectrum from Schmidt & Smith (1994); (4) Magnetic; (5) In common with Leggett et al. (1998); (6) Spectrum from Greenstein (1986); (7) Newly identified DA white dwarf; (8) V and $B - V$ from McCook & Sion (1999); (9) π from Ruiz (1996); (10) π from Ruiz et al. (1989); (11) π from Ruiz et al. (1995); (12) π from Liebert et al. (1988); (13) Not analyzed (see text).

Table 2. Atmospheric Parameters of Cool White Dwarfs

| WD | T_{eff} (K) | $\log g$ | Comp | M/M_{\odot} | M_V | $\log L/L_{\odot}$ | Age ^a (Gyr) | Notes |
|---------------|-------------------------|-------------|------|---------------|--------------|--------------------|---------------------------|-------|
| 0000-345..... | 6240 (140) | 8.31 (0.16) | He | 0.77 (0.11) | 14.41 (0.26) | -3.85 (0.11) | 4.18 (0.89) | 1 |
| 0009+501..... | 6540 (150) | 8.23 (0.06) | H | 0.74 (0.04) | 14.15 (0.09) | -3.71 (0.03) | 2.97 (0.38) | 2 |
| 0011+000..... | 9610 (260) | 8.40 (0.19) | H | 0.85 (0.12) | 12.94 (0.32) | -3.15 (0.12) | 1.29 (0.52) | |
| 0011-134..... | 6010 (120) | 8.20 (0.11) | H | 0.71 (0.07) | 14.44 (0.16) | -3.84 (0.07) | 3.65 (0.79) | 2 |
| 0029-032..... | 4770 (50) | 8.07 (0.04) | He | 0.61 (0.02) | 15.47 (0.05) | -4.17 (0.02) | 7.07 (0.18) | |
| 0033+016..... | 10700 (350) | 8.66 (0.16) | H | 1.02 (0.09) | 13.02 (0.29) | -3.14 (0.12) | 1.67 (0.45) | |
| 0038-226..... | 5400 (170) | 7.91 (0.17) | He | 0.52 (0.10) | 14.53 (0.22) | -3.87 (0.09) | 3.51 (1.21) | 3 |
| 0038+555..... | 10900 (630) | 8.14 (0.07) | He | 0.67 (0.04) | 12.24 (0.10) | -2.77 (0.04) | 0.62 (0.05) | 4 |
| 0046+051..... | 6770 (200) | 8.40 (0.01) | He | 0.83 (0.01) | 14.22 (0.02) | -3.77 (0.01) | 3.67 (0.04) | 5 |
| 0101+048..... | 8080 (200) | 7.55 (0.14) | H | 0.37 (0.05) | 12.36 (0.18) | -2.96 (0.07) | 0.63 (0.07) | 6 |
| 0115+159..... | 9800 (360) | 8.38 (0.06) | He | 0.82 (0.04) | 12.91 (0.10) | -3.10 (0.04) | 1.17 (0.16) | 4 |
| 0117-145..... | 5150 (110) | 7.75 (0.06) | H | 0.44 (0.03) | 14.67 (0.07) | -3.86 (0.03) | 2.63 (0.27) | |
| 0121+401..... | 5340 (120) | 7.90 (0.29) | H | 0.52 (0.16) | 14.65 (0.38) | -3.88 (0.15) | 2.93 (1.87) | |
| 0126+101..... | 8500 (200) | 7.20 (0.17) | H | 0.25 (0.04) | 11.67 (0.24) | -2.68 (0.10) | 0.43 (0.06) | 6 |
| 0135-052..... | 7140 (160) | 7.19 (0.06) | H | 0.25 (0.01) | 12.40 (0.07) | -3.00 (0.03) | 0.66 (0.03) | 6 |
| 0142+312..... | 8660 (210) | 7.51 (0.25) | H | 0.35 (0.10) | 12.03 (0.33) | -2.82 (0.13) | 0.52 (0.11) | 6 |
| 0208+396..... | 7310 (180) | 8.01 (0.09) | H | 0.60 (0.05) | 13.39 (0.13) | -3.38 (0.05) | 1.38 (0.17) | |
| 0213+427..... | 5600 (160) | 8.12 (0.12) | H | 0.66 (0.08) | 14.72 (0.18) | -3.91 (0.07) | 3.89 (1.09) | |
| 0222+648..... | 4520 (40) | 8.00 (0.05) | He | 0.57 (0.03) | 15.77 (0.06) | -4.23 (0.02) | 7.08 (0.46) | |
| 0230-144..... | 5480 (120) | 8.11 (0.09) | H | 0.65 (0.06) | 14.80 (0.13) | -3.95 (0.05) | 4.28 (0.94) | |
| 0243-026..... | 6820 (160) | 8.18 (0.15) | H | 0.70 (0.10) | 13.90 (0.23) | -3.61 (0.09) | 2.27 (0.78) | |
| 0245+541..... | 5280 (120) | 8.28 (0.05) | H | 0.76 (0.03) | 15.28 (0.07) | -4.11 (0.03) | 6.93 (0.30) | |
| 0257+080..... | 6680 (150) | 7.96 (0.16) | H | 0.57 (0.09) | 13.68 (0.21) | -3.51 (0.08) | 1.60 (0.38) | 2 |
| 0324+738..... | 4650 (50) | 7.10 (0.42) | He | 0.19 (0.10) | 14.67 (0.33) | -3.77 (0.14) | 1.97 (0.74) | 6 |
| 0326-273..... | 7200 (200) | 7.53 (0.40) | H | 0.35 (0.15) | 12.80 (0.52) | -3.15 (0.21) | 0.82 (0.30) | 6 |
| 0341+182..... | 6900 (170) | 8.16 (0.09) | He | 0.67 (0.05) | 13.80 (0.12) | -3.58 (0.05) | 2.24 (0.35) | 4 |
| 0357+081..... | 5490 (130) | 8.02 (0.11) | H | 0.60 (0.06) | 14.66 (0.14) | -3.90 (0.06) | 3.40 (0.87) | |
| 0426+588..... | 7120 (180) | 8.17 (0.01) | He | 0.68 (0.00) | 13.71 (0.01) | -3.54 (0.01) | 2.08 (0.02) | |
| 0433+270..... | 5620 (110) | 8.14 (0.07) | H | 0.67 (0.05) | 14.71 (0.10) | -3.92 (0.04) | 4.07 (0.69) | |
| 0435-088..... | 6620 (160) | 8.08 (0.04) | He | 0.62 (0.02) | 13.86 (0.05) | -3.61 (0.02) | 2.22 (0.17) | 4 |
| 0440+510..... | 8710 (220) | 7.96 (0.38) | H | 0.57 (0.21) | 12.62 (0.53) | -3.05 (0.22) | 0.82 (0.39) | |
| 0503-174..... | 5300 (120) | 7.60 (0.16) | H | 0.37 (0.07) | 14.31 (0.19) | -3.74 (0.07) | 1.86 (0.33) | 2 |
| 0518+333..... | 7780 (180) | 7.14 (0.24) | H | 0.24 (0.06) | 11.98 (0.31) | -2.81 (0.12) | 0.52 (0.09) | 6 |
| 0548-001..... | 6400 (140) | 8.32 (0.04) | He | 0.78 (0.03) | 14.34 (0.07) | -3.81 (0.02) | 3.90 (0.22) | 2, 4 |
| 0551+468..... | 5380 (120) | 8.01 (0.08) | H | 0.59 (0.04) | 14.78 (0.10) | -3.92 (0.04) | 3.75 (0.73) | |

Table 2—Continued

| WD | T_{eff} (K) | $\log g$ | Comp | M/M_{\odot} | M_V | $\log L/L_{\odot}$ | Age ^a (Gyr) | Notes |
|---------------|-------------------------|-------------|------|---------------|--------------|--------------------|---------------------------|-------|
| 0552–041..... | 5060 (60) | 8.31 (0.02) | He | 0.77 (0.01) | 15.42 (0.03) | –4.21 (0.02) | 6.92 (0.05) | 5 |
| 0553+053..... | 5790 (110) | 8.20 (0.05) | H | 0.71 (0.03) | 14.65 (0.06) | –3.90 (0.02) | 4.11 (0.35) | 2 |
| 0618+067..... | 5940 (120) | 8.27 (0.14) | H | 0.76 (0.09) | 14.64 (0.21) | –3.90 (0.09) | 4.27 (0.90) | |
| 0644+025..... | 7410 (180) | 8.66 (0.12) | H | 1.01 (0.07) | 14.38 (0.22) | –3.78 (0.08) | 3.79 (0.23) | |
| 0648+641..... | 5780 (120) | 7.75 (0.30) | H | 0.45 (0.14) | 14.04 (0.38) | –3.66 (0.15) | 1.74 (0.65) | |
| 0651–479..... | 4660 (40) | 8.02 (0.16) | He | 0.58 (0.10) | 15.57 (0.22) | –4.19 (0.09) | 7.00 (1.24) | |
| 0654+027..... | 9450 (340) | 8.51 (0.18) | He | 0.91 (0.12) | 13.24 (0.31) | –3.26 (0.12) | 1.79 (0.56) | |
| 0657+320..... | 4990 (130) | 8.07 (0.03) | H | 0.62 (0.02) | 15.26 (0.04) | –4.09 (0.02) | 6.55 (0.27) | |
| 0659–064..... | 6520 (150) | 8.71 (0.36) | H | 1.04 (0.22) | 14.97 (0.67) | –4.04 (0.27) | 4.81 (0.60) | |
| 0706+377..... | 6990 (180) | 8.14 (0.09) | He | 0.66 (0.05) | 13.71 (0.13) | –3.55 (0.05) | 2.09 (0.32) | 4 |
| 0727+482A.... | 5020 (120) | 7.92 (0.02) | H | 0.53 (0.01) | 15.03 (0.02) | –4.00 (0.01) | 4.60 (0.22) | 6 |
| 0727+482B.... | 5000 (130) | 8.12 (0.02) | H | 0.66 (0.01) | 15.33 (0.02) | –4.12 (0.01) | 7.02 (0.14) | 6 |
| 0738–172..... | 7710 (220) | 8.09 (0.03) | He | 0.63 (0.02) | 13.31 (0.05) | –3.35 (0.02) | 1.45 (0.05) | |
| 0743–340..... | 4740 (50) | 7.97 (0.09) | He | 0.55 (0.05) | 15.40 (0.12) | –4.14 (0.04) | 6.36 (0.96) | |
| 0747+073A.... | 4850 (50) | 8.04 (0.02) | He | 0.59 (0.01) | 15.32 (0.03) | –4.13 (0.01) | 6.71 (0.15) | |
| 0747+073B.... | 4210 (90) | 7.69 (0.03) | H | 0.40 (0.01) | 15.65 (0.03) | –4.19 (0.01) | 5.27 (0.23) | |
| 0751+578..... | 9770 (360) | 8.01 (0.21) | He | 0.58 (0.12) | 12.35 (0.29) | –2.89 (0.12) | 0.71 (0.20) | |
| 0752–676..... | 5730 (110) | 8.21 (0.09) | H | 0.72 (0.06) | 14.70 (0.13) | –3.93 (0.06) | 4.36 (0.70) | |
| 0752+365..... | 7700 (190) | 8.19 (0.21) | H | 0.71 (0.13) | 13.44 (0.32) | –3.40 (0.13) | 1.60 (0.69) | |
| 0802+386..... | 11070 (480) | 8.31 (0.18) | He | 0.78 (0.11) | 12.46 (0.27) | –2.85 (0.11) | 0.76 (0.18) | 5 |
| 0816+387..... | 7570 (190) | 8.19 (0.14) | H | 0.71 (0.09) | 13.52 (0.22) | –3.43 (0.09) | 1.67 (0.51) | |
| 0827+328..... | 7270 (180) | 8.39 (0.11) | H | 0.85 (0.07) | 13.99 (0.18) | –3.63 (0.08) | 3.06 (0.58) | |
| 0839–327..... | 8930 (230) | 7.70 (0.14) | H | 0.44 (0.07) | 12.16 (0.19) | –2.86 (0.07) | 0.57 (0.08) | 6 |
| 0856+331..... | 10390 (410) | 8.84 (0.07) | He | 1.11 (0.04) | 13.60 (0.15) | –3.33 (0.06) | 2.07 (0.08) | 4 |
| 0912+536..... | 7160 (190) | 8.28 (0.03) | He | 0.75 (0.02) | 13.78 (0.04) | –3.59 (0.02) | 2.54 (0.16) | 2 |
| 0913+442..... | 8490 (220) | 8.19 (0.17) | H | 0.71 (0.11) | 13.06 (0.25) | –3.23 (0.10) | 1.22 (0.34) | |
| 0930+294..... | 8330 (220) | 8.38 (0.20) | H | 0.84 (0.13) | 13.45 (0.32) | –3.38 (0.12) | 1.94 (0.74) | |
| 0946+534..... | 8760 (290) | 8.45 (0.11) | He | 0.87 (0.07) | 13.37 (0.18) | –3.35 (0.07) | 1.97 (0.41) | 4 |
| 0955+247..... | 8670 (220) | 8.27 (0.15) | H | 0.77 (0.10) | 13.12 (0.24) | –3.24 (0.09) | 1.31 (0.40) | |
| 1012+083..... | 6750 (150) | 8.02 (0.18) | H | 0.60 (0.10) | 13.72 (0.25) | –3.53 (0.09) | 1.72 (0.52) | |
| 1019+637..... | 6780 (160) | 7.98 (0.09) | H | 0.58 (0.05) | 13.63 (0.13) | –3.50 (0.05) | 1.59 (0.22) | |
| 1039+145..... | 7280 (200) | 7.93 (0.26) | He | 0.53 (0.14) | 13.24 (0.35) | –3.36 (0.14) | 1.32 (0.47) | 1 |
| 1043–188..... | 6190 (200) | 8.09 (0.17) | He | 0.63 (0.11) | 14.30 (0.25) | –3.74 (0.10) | 2.85 (1.03) | 3 |
| 1055–072..... | 7420 (200) | 8.42 (0.06) | He | 0.85 (0.04) | 13.91 (0.09) | –3.62 (0.04) | 3.01 (0.22) | |
| 1108+207..... | 4650 (160) | 8.07 (0.11) | H | 0.62 (0.07) | 15.62 (0.15) | –4.21 (0.06) | 7.71 (0.98) | |

Table 2—Continued

| WD | T_{eff} (K) | $\log g$ | Comp | M/M_{\odot} | M_V | $\log L/L_{\odot}$ | Age ^a (Gyr) | Notes |
|---------------|-------------------------|-------------|------|---------------|--------------|--------------------|---------------------------|-------|
| 1115–029..... | 10120 (490) | 8.13 (0.30) | He | 0.66 (0.18) | 12.44 (0.43) | −2.90 (0.17) | 0.76 (0.31) | 4 |
| 1121+216..... | 7490 (180) | 8.20 (0.05) | H | 0.72 (0.03) | 13.57 (0.08) | −3.45 (0.03) | 1.76 (0.22) | |
| 1124–296..... | 9440 (250) | 7.10 (0.15) | H | 0.23 (0.03) | 11.09 (0.23) | −2.43 (0.10) | 0.30 (0.04) | 6 |
| 1136–286..... | 4490 (80) | 9.02 (0.05) | He | 1.19 (0.02) | 17.47 (0.09) | −4.94 (0.03) | 4.96 (0.27) | |
| 1142–645..... | 8490 (270) | 8.27 (0.05) | He | 0.75 (0.03) | 13.19 (0.07) | −3.28 (0.02) | 1.44 (0.13) | 4 |
| 1147+255..... | 9790 (270) | 7.92 (0.23) | H | 0.55 (0.13) | 12.11 (0.33) | −2.82 (0.13) | 0.57 (0.17) | |
| 1154+186..... | 7630 (220) | 8.06 (0.16) | He | 0.61 (0.10) | 13.23 (0.23) | −3.35 (0.09) | 1.44 (0.32) | 1 |
| 1208+576..... | 5880 (120) | 7.95 (0.15) | H | 0.56 (0.09) | 14.23 (0.20) | −3.73 (0.08) | 2.18 (0.60) | |
| 1215+323..... | 7100 (210) | 8.68 (0.13) | He | 1.02 (0.08) | 14.54 (0.24) | −3.88 (0.10) | 3.91 (0.10) | 1 |
| 1236–495..... | 11550 (470) | 8.63 (0.18) | H | 1.00 (0.11) | 12.73 (0.34) | −2.98 (0.13) | 1.24 (0.44) | 7 |
| 1244+149..... | 10280 (310) | 7.88 (0.42) | H | 0.53 (0.21) | 11.87 (0.60) | −2.71 (0.24) | 0.48 (0.24) | |
| 1247+550..... | 4050 (70) | 7.57 (0.03) | H | 0.35 (0.01) | 15.78 (0.04) | −4.20 (0.01) | 4.63 (0.31) | |
| 1257+037..... | 5590 (110) | 8.16 (0.09) | H | 0.68 (0.06) | 14.74 (0.14) | −3.94 (0.05) | 4.32 (0.88) | |
| 1257+278..... | 8540 (240) | 7.97 (0.22) | H | 0.58 (0.13) | 12.71 (0.31) | −3.09 (0.12) | 0.87 (0.26) | |
| 1300+263..... | 4320 (100) | 8.07 (0.18) | H | 0.62 (0.12) | 16.04 (0.25) | −4.34 (0.11) | 8.73 (1.47) | |
| 1310–472..... | 4220 (80) | 8.12 (0.05) | H | 0.65 (0.04) | 16.24 (0.08) | −4.41 (0.03) | 9.34 (0.34) | |
| 1313–198..... | 5330 (100) | 8.33 (0.06) | He | 0.79 (0.04) | 15.18 (0.10) | −4.14 (0.04) | 6.47 (0.19) | |
| 1325+581..... | 6810 (160) | 8.14 (0.31) | H | 0.68 (0.19) | 13.86 (0.45) | −3.58 (0.17) | 2.08 (1.21) | |
| 1328+307..... | 7320 (230) | 8.21 (0.24) | He | 0.71 (0.15) | 13.65 (0.35) | −3.51 (0.14) | 2.02 (0.87) | 5 |
| 1334+039..... | 5030 (120) | 7.95 (0.05) | H | 0.55 (0.03) | 15.05 (0.06) | −4.01 (0.02) | 4.90 (0.57) | |
| 1344+106..... | 7110 (170) | 8.10 (0.11) | H | 0.65 (0.07) | 13.61 (0.16) | −3.48 (0.06) | 1.67 (0.31) | |
| 1345+238..... | 4590 (150) | 7.76 (0.05) | H | 0.44 (0.02) | 15.30 (0.06) | −4.07 (0.02) | 4.57 (0.51) | |
| 1418–088..... | 7810 (190) | 7.43 (0.26) | H | 0.32 (0.09) | 12.34 (0.34) | −2.96 (0.13) | 0.63 (0.12) | 6 |
| 1444–174..... | 4960 (60) | 8.37 (0.08) | He | 0.81 (0.05) | 15.63 (0.13) | −4.29 (0.05) | 7.19 (0.07) | |
| 1455+298..... | 7310 (170) | 7.66 (0.23) | H | 0.41 (0.11) | 12.90 (0.31) | −3.19 (0.12) | 0.89 (0.21) | 6 |
| 1503–070..... | 6990 (160) | 8.17 (0.21) | H | 0.70 (0.13) | 13.81 (0.31) | −3.56 (0.12) | 2.02 (0.91) | 2 |
| 1606+422..... | 11320 (570) | 7.12 (0.23) | H | 0.25 (0.05) | 10.55 (0.35) | −2.11 (0.13) | 0.18 (0.04) | 6 |
| 1609+135..... | 9080 (250) | 8.75 (0.10) | H | 1.07 (0.06) | 13.79 (0.19) | −3.50 (0.07) | 2.71 (0.17) | |
| 1625+093..... | 6870 (170) | 8.44 (0.12) | H | 0.88 (0.07) | 14.30 (0.19) | −3.76 (0.07) | 3.74 (0.48) | |
| 1626+368..... | 8640 (280) | 8.03 (0.05) | He | 0.60 (0.03) | 12.82 (0.07) | −3.12 (0.03) | 1.02 (0.07) | |
| 1633+433..... | 6650 (150) | 8.14 (0.07) | H | 0.68 (0.04) | 13.94 (0.10) | −3.63 (0.04) | 2.28 (0.34) | |
| 1633+572..... | 6180 (240) | 8.09 (0.06) | He | 0.63 (0.03) | 14.19 (0.08) | −3.74 (0.03) | 2.84 (0.37) | 3 |
| 1635+137..... | 6990 (190) | 8.29 (0.26) | H | 0.78 (0.16) | 13.97 (0.40) | −3.63 (0.15) | 2.77 (1.15) | |
| 1637+335..... | 9940 (280) | 8.13 (0.13) | H | 0.68 (0.08) | 12.37 (0.20) | −2.91 (0.08) | 0.74 (0.14) | |
| 1639+537..... | 7510 (210) | 8.14 (0.11) | He | 0.67 (0.07) | 13.43 (0.16) | −3.42 (0.07) | 1.64 (0.27) | 2 |

Table 2—Continued

| WD | T_{eff} (K) | $\log g$ | Comp | M/M_{\odot} | M_V | $\log L/L_{\odot}$ | Age ^a (Gyr) | Notes |
|---------------|-------------------------|-------------|------|---------------|--------------|--------------------|---------------------------|-------|
| 1655+215..... | 9180 (230) | 7.87 (0.12) | H | 0.53 (0.06) | 12.30 (0.16) | -2.91 (0.07) | 0.64 (0.09) | |
| 1656-062..... | 5520 (100) | 8.03 (0.04) | H | 0.60 (0.03) | 14.58 (0.06) | -3.89 (0.03) | 3.34 (0.38) | |
| 1705+030..... | 7050 (180) | 8.35 (0.13) | He | 0.80 (0.09) | 13.98 (0.21) | -3.66 (0.08) | 3.11 (0.62) | 5 |
| 1716+020..... | 13470 (900) | 8.11 (0.13) | H | 0.67 (0.08) | 11.60 (0.20) | -2.37 (0.09) | 0.32 (0.06) | |
| 1733-544..... | 6520 (150) | 8.13 (0.03) | H | 0.67 (0.02) | 13.99 (0.04) | -3.65 (0.01) | 2.37 (0.14) | |
| 1736+052..... | 8890 (230) | 8.11 (0.25) | H | 0.67 (0.15) | 12.77 (0.37) | -3.10 (0.14) | 0.97 (0.35) | |
| 1748+708..... | 5590 (90) | 8.36 (0.02) | He | 0.81 (0.01) | 15.21 (0.03) | -4.07 (0.02) | 5.86 (0.06) | 2, 3? |
| 1756+827..... | 7270 (330) | 7.98 (0.07) | H | 0.58 (0.04) | 13.37 (0.10) | -3.38 (0.04) | 1.35 (0.13) | |
| 1811+327A.... | 7380 (180) | 7.65 (0.37) | H | 0.41 (0.16) | 12.85 (0.49) | -3.17 (0.19) | 0.86 (0.33) | |
| 1811+327B.... | 6480 (160) | 7.75 (0.37) | H | 0.45 (0.18) | 13.52 (0.49) | -3.45 (0.20) | 1.32 (0.60) | |
| 1818+126..... | 6340 (130) | 7.28 (0.41) | H | 0.26 (0.12) | 13.04 (0.50) | -3.26 (0.20) | 0.93 (0.26) | 6 |
| 1820+609..... | 4780 (140) | 7.83 (0.09) | H | 0.48 (0.05) | 15.16 (0.11) | -4.03 (0.04) | 4.68 (0.95) | |
| 1824+040..... | 12240 (680) | 7.00 (0.16) | H | 0.23 (0.03) | 10.19 (0.28) | -1.89 (0.11) | 0.12 (0.03) | 6 |
| 1826-045..... | 9480 (350) | 7.94 (0.17) | H | 0.57 (0.09) | 12.29 (0.24) | -2.89 (0.10) | 0.64 (0.14) | |
| 1829+547..... | 6280 (140) | 8.50 (0.11) | H | 0.90 (0.07) | 14.69 (0.18) | -3.96 (0.08) | 4.76 (0.24) | 2, 8 |
| 1831+197..... | 7590 (210) | 7.61 (0.48) | He | 0.37 (0.19) | 12.67 (0.60) | -3.12 (0.24) | 0.80 (0.40) | 4 |
| 1840+042..... | 9090 (340) | 8.19 (0.12) | H | 0.71 (0.08) | 12.81 (0.18) | -3.11 (0.08) | 1.02 (0.18) | |
| 1855+338..... | 11240 (430) | 8.19 (0.20) | H | 0.72 (0.13) | 12.06 (0.32) | -2.73 (0.12) | 0.58 (0.18) | 7 |
| 1900+705..... | 12070 (990) | 8.58 (0.03) | He | 0.95 (0.02) | 12.68 (0.06) | -2.88 (0.03) | 0.94 (0.09) | 2 |
| 1917+386..... | 6390 (140) | 8.28 (0.05) | He | 0.75 (0.04) | 14.27 (0.09) | -3.79 (0.03) | 3.68 (0.32) | 3? |
| 1953-011..... | 7920 (200) | 8.23 (0.05) | H | 0.74 (0.03) | 13.41 (0.07) | -3.38 (0.03) | 1.63 (0.16) | 2 |
| 2002-110..... | 4800 (50) | 8.31 (0.02) | He | 0.77 (0.01) | 15.76 (0.03) | -4.31 (0.01) | 7.35 (0.04) | |
| 2011+065..... | 6400 (150) | 8.13 (0.06) | He | 0.65 (0.04) | 14.03 (0.09) | -3.69 (0.03) | 2.73 (0.38) | 1 |
| 2048+263..... | 5200 (110) | 7.31 (0.12) | H | 0.26 (0.04) | 14.12 (0.15) | -3.64 (0.06) | 1.53 (0.15) | 6 |
| 2054-050..... | 4620 (40) | 8.09 (0.12) | He | 0.62 (0.08) | 15.74 (0.17) | -4.24 (0.07) | 7.49 (0.56) | |
| 2059+190..... | 6840 (160) | 7.86 (0.28) | H | 0.51 (0.15) | 13.44 (0.37) | -3.42 (0.15) | 1.33 (0.48) | |
| 2059+247..... | 6070 (130) | 8.17 (0.17) | H | 0.69 (0.11) | 14.36 (0.25) | -3.80 (0.10) | 3.32 (1.12) | |
| 2059+316..... | 10080 (390) | 8.08 (0.18) | He | 0.63 (0.11) | 12.35 (0.26) | -2.87 (0.11) | 0.72 (0.17) | 4 |
| 2105-820..... | 10200 (290) | 8.23 (0.21) | H | 0.75 (0.13) | 12.45 (0.33) | -2.93 (0.13) | 0.81 (0.27) | |
| 2107-216..... | 5830 (140) | 8.40 (0.05) | H | 0.85 (0.03) | 14.93 (0.08) | -4.02 (0.03) | 5.24 (0.23) | |
| 2111+261..... | 8120 (190) | 7.42 (0.19) | H | 0.32 (0.07) | 12.16 (0.26) | -2.88 (0.11) | 0.57 (0.08) | 6 |
| 2136+229..... | 9480 (250) | 7.85 (0.20) | H | 0.52 (0.11) | 12.13 (0.28) | -2.84 (0.12) | 0.58 (0.14) | |
| 2140+207..... | 8860 (300) | 8.07 (0.06) | He | 0.62 (0.04) | 12.75 (0.09) | -3.09 (0.04) | 1.00 (0.07) | 4 |
| 2207+142..... | 7620 (190) | 8.24 (0.16) | H | 0.75 (0.10) | 13.57 (0.24) | -3.45 (0.10) | 1.86 (0.64) | |
| 2246+223..... | 10330 (300) | 8.57 (0.09) | H | 0.97 (0.06) | 12.99 (0.17) | -3.14 (0.07) | 1.56 (0.33) | |

Table 2—Continued

| WD | T_{eff} (K) | $\log g$ | Comp | M/M_{\odot} | M_V | $\log L/L_{\odot}$ | Age ^a (Gyr) | Notes |
|---------------|-------------------------|-------------|------|---------------|--------------|--------------------|---------------------------|-------|
| 2248+293..... | 5580 (110) | 7.53 (0.15) | H | 0.35 (0.06) | 13.94 (0.19) | -3.61 (0.08) | 1.50 (0.21) | 6 |
| 2251-070..... | 4580 (60) | 8.38 (0.05) | He | 0.82 (0.03) | 16.17 (0.08) | -4.43 (0.03) | 7.75 (0.01) | 5 |
| 2253-081..... | 6770 (180) | 8.41 (0.19) | H | 0.86 (0.13) | 14.30 (0.32) | -3.76 (0.12) | 3.75 (0.94) | |
| 2311-068..... | 7980 (240) | 8.27 (0.17) | He | 0.75 (0.11) | 13.40 (0.26) | -3.39 (0.11) | 1.74 (0.58) | 4 |
| 2312-024..... | 6840 (160) | 8.41 (0.22) | He | 0.84 (0.14) | 14.18 (0.34) | -3.75 (0.14) | 3.62 (0.85) | 5 |
| 2316-064..... | 4720 (50) | 8.17 (0.17) | He | 0.68 (0.11) | 15.69 (0.25) | -4.25 (0.10) | 7.30 (0.52) | |
| 2329+267..... | 9400 (240) | 8.02 (0.28) | H | 0.61 (0.16) | 12.40 (0.40) | -2.95 (0.15) | 0.73 (0.27) | |
| 2345-447..... | 5400 (80) | 8.72 (0.07) | He | 1.04 (0.04) | 15.77 (0.13) | -4.38 (0.05) | 6.07 (0.24) | |
| 2347+292..... | 5810 (120) | 7.82 (0.15) | H | 0.48 (0.08) | 14.10 (0.19) | -3.69 (0.08) | 1.89 (0.37) | |
| 2352+401..... | 8260 (260) | 7.99 (0.23) | He | 0.57 (0.13) | 12.88 (0.32) | -3.17 (0.12) | 1.07 (0.32) | 4 |

^aWhite dwarf cooling age only, not including the main sequence lifetime

Note. — (1) Energy distribution better reproduced with pure hydrogen models (yet no H α); (2) Magnetic; (3) C₂H star; (4) DQ star; (5) DZ star; (6) Known or suspected double degenerate binary; (7) ZZ Ceti star; (8) Helium solution adopted despite hydrogen-rich atmosphere (see text).

Fig. 1.— Comparison of temperature (in K) and gas pressure (in dyn cm^{-2}) structures as a function of Rosseland mean optical depth for two models with $T_{\text{eff}} = 6000$ K, $\log g = 8.0$, and $N(\text{H})/N(\text{He}) = 0$. One of these models has its electron density increased artificially by a factor of 1000 (*dotted lines*) with respect to the reference model (*solid lines*).

Fig. 2.— Comparison of the Eddington fluxes (in units of $10^{-5} \text{ ergs cm}^{-2} \text{ s}^{-1} \text{ Hz}^{-1} \text{ ster}^{-1}$) between the two models described in Figure 1.

Fig. 3.— Number of DA and non-DA stars as a function of effective temperature in 1000 K bins for the sample presented in this paper (*solid line*) compared to the parallax subsample of BRL (*dotted line*). The DA/non-DA classification is based on the presence or absence of $\text{H}\alpha$ in the spectrum, and not on the dominant constituent of the atmosphere. These spectral types are based on our own spectroscopic observations.

Fig. 4.— White dwarfs in our sample whose spectra show $\text{H}\alpha$; the spectra already displayed in BRL are not reproduced here. All spectra are normalized to a continuum set to unity, and offset vertically from each other by a factor of 0.3. Equivalent widths decrease from upper left to bottom right. The names of newly identified DA stars are shown in italics.

Fig. 5.— Same as Figure 4 but for our featureless spectra near the $\text{H}\alpha$ region. Spectra are shown in order of right ascension.

Fig. 6.— Our blue spectroscopic observations of DQ stars. Spectra are shown in order of decreasing T_{eff} . All spectra are normalized at 6250 Å and are offset from each other by a factor of 0.5; the spectrum of 1115–029 is blown up by a factor of 2 to make the weak C_2 feature at 5150 Å more obvious. The names of newly identified DQ stars are shown in italics.

Fig. 7.— M_V vs $(V-I)$ color-magnitude diagram for the data set from Table 1. In the two rightmost panels, the data set is split into DA stars (*filled circles*) and non-DA stars (*open circles*), based on the presence or absence of $\text{H}\alpha$. The pure hydrogen and pure helium model sequences are superimposed on the observed data; temperatures are indicated in units of 10^3 K, and $M = 0.4, 0.6, 0.8, 1.0$, and $1.2 M_{\odot}$ from top to bottom. The stars marked in the left panel are discussed in the text.

Fig. 8.— $(B-V, V-K)$ two-color diagram for the data set from Table 1; DA and non-DA stars are represented by filled and open circles, respectively, and the cross indicates the size of the error bars. The objects marked are discussed in the text. The $0.6 M_{\odot}$ pure hydrogen (*solid line*) and pure helium (*dashed line*) model sequences are superimposed on the observed sequences.

Fig. 9.— $(V-I, V-K)$ two-color diagram for the data set from Table 1 (left panel); DA and non-DA stars are represented by filled and open circles, respectively, and the cross indicates the size of the error bars. In the middle and right panels, the data set is divided into DA and non-DA stars, respectively. The objects labeled in the right panel are discussed in the text. The pure hydrogen

(DA panel) and pure helium (non-DA panel) model sequences are superimposed on the observed data (*solid lines*); temperatures are indicated in units of 10^3 K, and $\log g = 7.0, 8.0$, and 9.0 from right to left (DA panel) and from top to bottom (non-DA panel). Also shown in both panels are the mixed hydrogen/helium models with $N(\text{He})/N(\text{H}) = 0.1, 1, 10$, and 100 , from right to left (*dotted* and *dashed lines*), for $\log g = 8.0$. In the right panel, filled and open circles indicate non-DA stars with hydrogen- and helium-rich compositions, respectively. Note the presence of a non-DA gap in the 5000-6000 K region.

Fig. 10.— Fits to the energy distributions of DA stars with pure hydrogen models. Here and in the following Figures, the *BVRI* and *JHK* photometric observations are represented by error bars while the model fluxes are shown as filled circles. In the right panels are shown the observed normalized spectra together with the synthetic line profiles interpolated at the parameters obtained from the energy distribution fits (left panels).

Fig. 11.— Fits to the energy distributions of non-DA stars with pure helium models (*filled circles*). All objects have featureless spectra near the $\text{H}\alpha$ region. G24–9 belongs to this group of peculiar objects whose energy distributions are better reproduced by hydrogen-rich models (shown here as *open circles*).

Fig. 12.— Fits to the energy distributions of white dwarfs with mixed hydrogen and helium atmospheric compositions. The hydrogen-to-helium abundance ratio is determined (or constrained in the case of LHS 290) by fitting the $\text{H}\alpha$ line profile.

Fig. 13.— Fits to the energy distributions of confirmed, or suspected, unresolved double degenerates. In the right panels are shown the observed normalized spectra together with the synthetic line profiles interpolated at the parameters obtained from the energy distribution fits (left panels).

Fig. 14.— Our best fits to two magnetic white dwarfs whose spectrum exhibits Zeeman splitting at $\text{H}\alpha$; all spectra are normalized to a continuum set to unity. The effective temperatures and surface gravities are taken from our fits to the energy distributions. The magnetic parameters are given in each panel. G128–72 has been identified recently by Moran et al. (1998), while GD 175 has been discovered in our survey. For GD 175, the model spectrum shown by the dotted line corresponds to our best fit with a single magnetic DA star, while the thick solid line represents our best fit under the assumption that an additional featureless DC white dwarf contributes equally to the total continuum flux near the $\text{H}\alpha$ region.

Fig. 15.— Our fits at $\text{H}\alpha$ to weakly magnetic, or suspected to be magnetic, DA white dwarfs using non-magnetic pure hydrogen model spectra. All spectra are normalized to a continuum set to unity, and the atmospheric parameters are those obtained from the energy distributions. All objects except LHS 3501 have been observed in spectropolarimetry, but only LHS 1038 and LHS 5064 have shown a Zeeman polarization feature. LHS 3501 is a known magnetic white dwarf with a ~ 500 kG magnetic field Maxted et al. (2000a).

Fig. 16.— A comparison of our best fit to the energy distribution of G227–35 with a pure helium model (*open circles*) at $T_{\text{eff}} = 6280$ K, $\log g = 8.50$, and with a pure hydrogen model (*filled circles*) at $T_{\text{eff}} = 6750$ K, $\log g = 8.64$. Even though the quality of the fit is superior with the pure helium model, G227–35 has most likely a hydrogen-rich atmospheric composition in a strong magnetic field according to Putney & Jordan (1995).

Fig. 17.— A comparison of our best fit to the energy distribution of ESO 439–26 with a pure helium model (*open circles*) at $T_{\text{eff}} = 4490$ K, $\log g = 9.02$, and our best fit using only the V and I bandpasses with a pure hydrogen model (*filled circles*) at $T_{\text{eff}} = 3150$ K, $\log g = 8.29$. Because of the infrared J magnitude, the pure hydrogen solution can be easily ruled out.

Fig. 18.— Our best fits to the energy distributions of G107–70A and B. The combined $\text{H}\alpha$ line profile of both components is compared with the predicted line profile obtained as the sum of the individual model spectra interpolated at the parameters obtained from the fits to the energy distributions, and properly weighted by the respective luminosity.

Fig. 19.— Comparison of effective temperatures and stellar masses determined from the photometric technique used in this analysis (*phot*), and from the spectroscopic technique of fitting simultaneously the Balmer line profiles (*spec*), for 24 DA stars. The dashed line in each panel indicates the 1:1 correspondence. The average uncertainties are shown in each panel as well. The labels correspond to (1) 0011+000, (2) 0326–273, (3) 1606+422, (4) 1655+215, (5) 1716+020, (6) 1824+040, (7) 2329+267, and these objects are discussed in the text. The three vectors in the upper panel indicate the photometric masses obtained under the assumption that two identical white dwarfs contribute to the total flux received at Earth.

Fig. 20.— Our best photometric and spectroscopic fits to LHS 3254 (1655+215), object 4 in Fig. 17, using pure hydrogen models (top panels). The line profiles are normalized to a continuum set to unity and are offset vertically from each other by a factor of 0.2. The discrepancy in $\log g$ (and hence mass) between both techniques can be resolved if some amount of helium is allowed in the atmosphere (bottom panels). From a qualitative point of view, both the pure hydrogen and mixed H/He solutions are indistinguishable.

Fig. 21.— Masses of all white dwarfs in our current trigonometric parallax sample as a function of effective temperature. Not seen here is the hottest DA star in our sample, G19–20 (1716+020), with $T_{\text{eff}} = 13,470$ K and $M = 0.67 M_{\odot}$. Filled and open symbols represent hydrogen-rich and helium-rich atmospheric compositions, respectively, while additional information about the composition of or spectroscopic features seen in some of these objects is provided by the different symbols explained in the legend. Note that there are two C_2H stars which overlap near $T_{\text{eff}} \sim 6200$ K and $M \sim 0.6 M_{\odot}$. The cross in the upper left corner represents the average error in T_{eff} of 200 K and in mass of $0.077 M_{\odot}$.

Fig. 22.— Top panel: Mass distributions for the hydrogen- and helium-rich atmosphere white dwarfs in our parallax sample. The mean mass of the hydrogen-rich subsample is $\langle M \rangle = 0.61 M_{\odot}$

with a dispersion of $\sigma(M) = 0.20 M_{\odot}$, and the corresponding values for the helium-rich subsample are $\langle M \rangle = 0.72 M_{\odot}$ and $\sigma(M) = 0.17 M_{\odot}$. Bottom panel: Mass distributions for hotter DA and DB stars determined from spectroscopic analyses. The mean mass and dispersion for the DA stars are $\langle M \rangle = 0.59 M_{\odot}$, $\sigma = 0.13 M_{\odot}$, and for the DB stars $\langle M \rangle = 0.59 M_{\odot}$, $\sigma = 0.06 M_{\odot}$.

Fig. 23.— Bottom panel: Number of hydrogen-rich (*solid line*) and helium-rich (*dashed line*) stars as a function of effective temperature in 1000 K bins for the results presented in Table 2. Top panel: The corresponding hydrogen- to helium-rich ratio; the error bars represent the Poisson statistics of each bin.

Fig. 24.— Masses of white dwarfs in our trigonometric parallax sample as a function of effective temperature together with the isochrones from the new cooling sequences with C/O core compositions, $q(\text{He}) = 10^{-2}$, and $q(\text{H}) = 10^{-10}$ (*solid lines*). The isochrones are labeled in units of 10^9 years. Also shown are the corresponding isochrones with the main sequence lifetime taken into account (*dotted lines*). The cross in the upper left corner represents the average error in T_{eff} of 200 K and in mass of $0.077 M_{\odot}$.

Fig. 25.— Same as Figure 24 but for cooling sequences with C/O core compositions, $q(\text{He}) = 10^{-2}$, and $q(\text{H}) = 10^{-4}$.

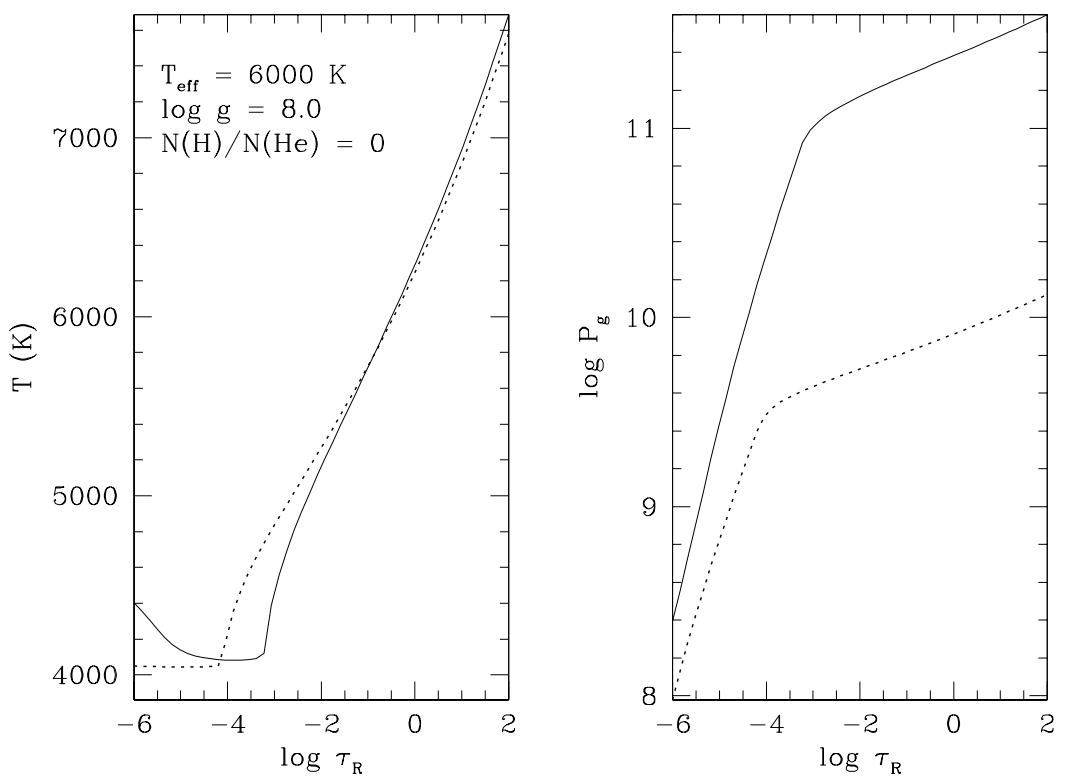


Figure 1

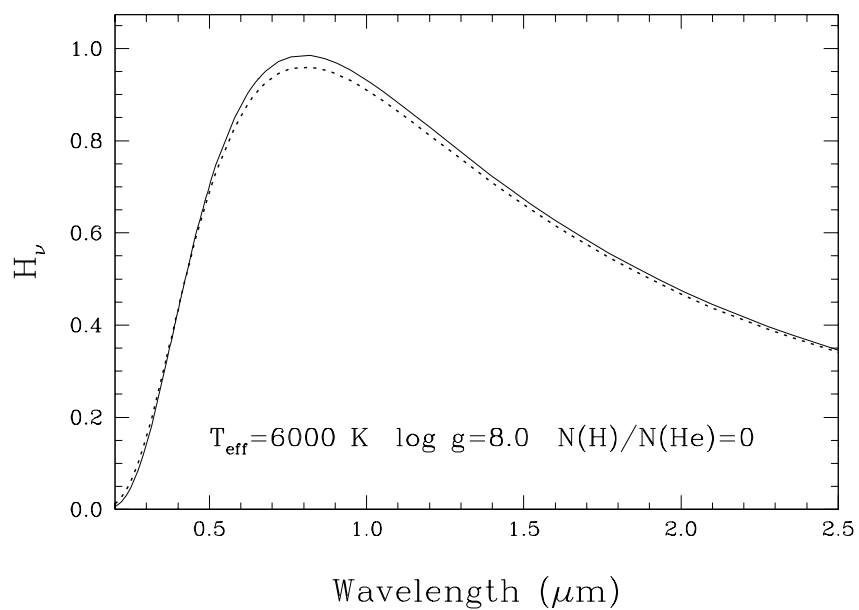


Figure 2

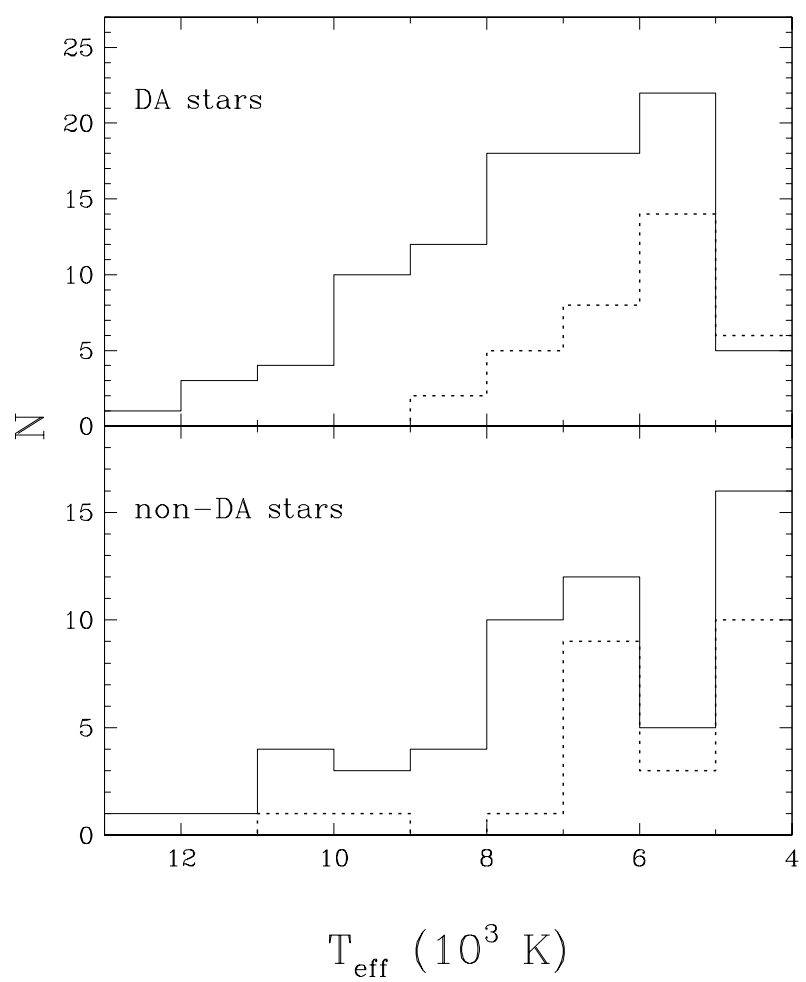


Figure 3

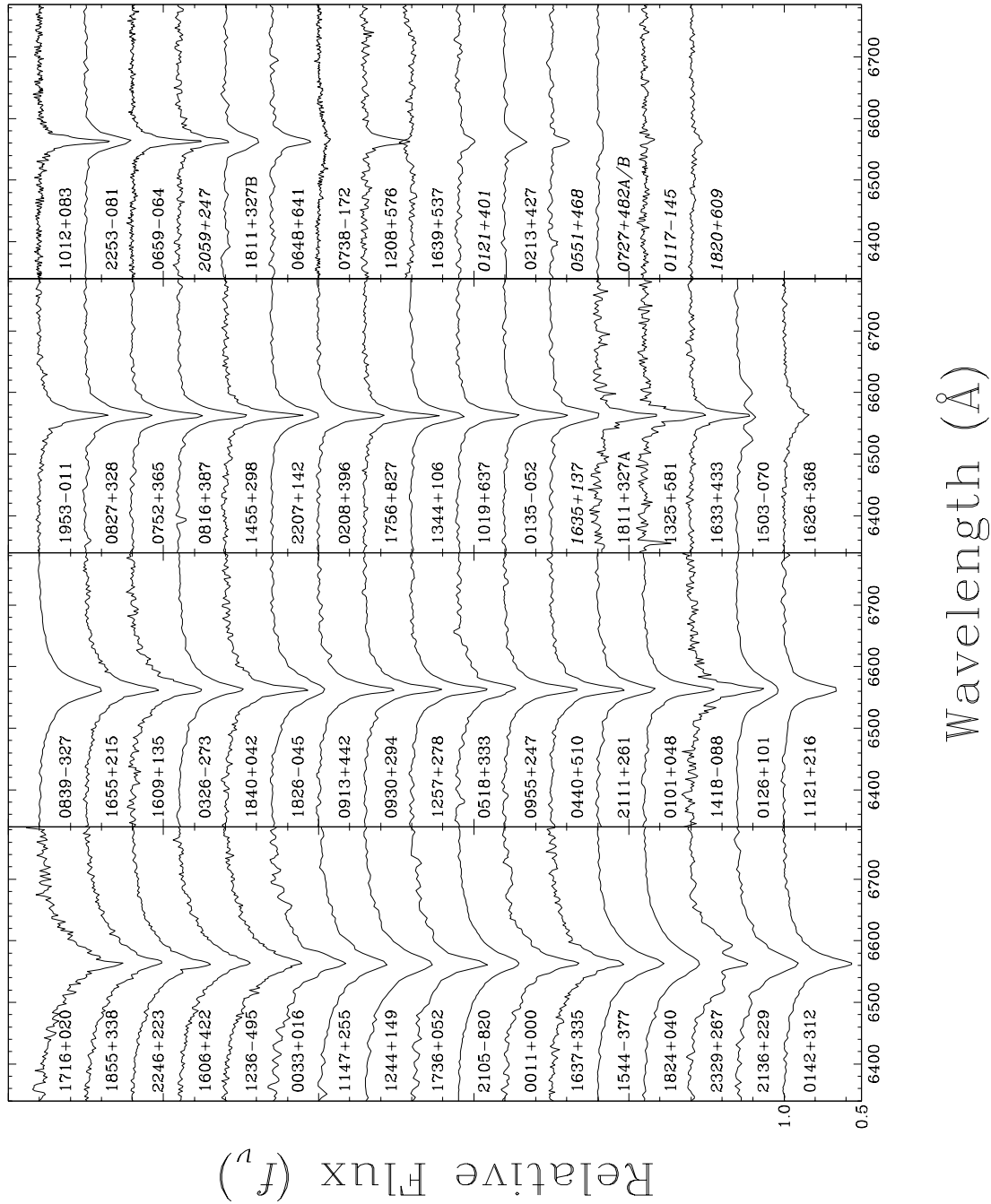


Figure 4

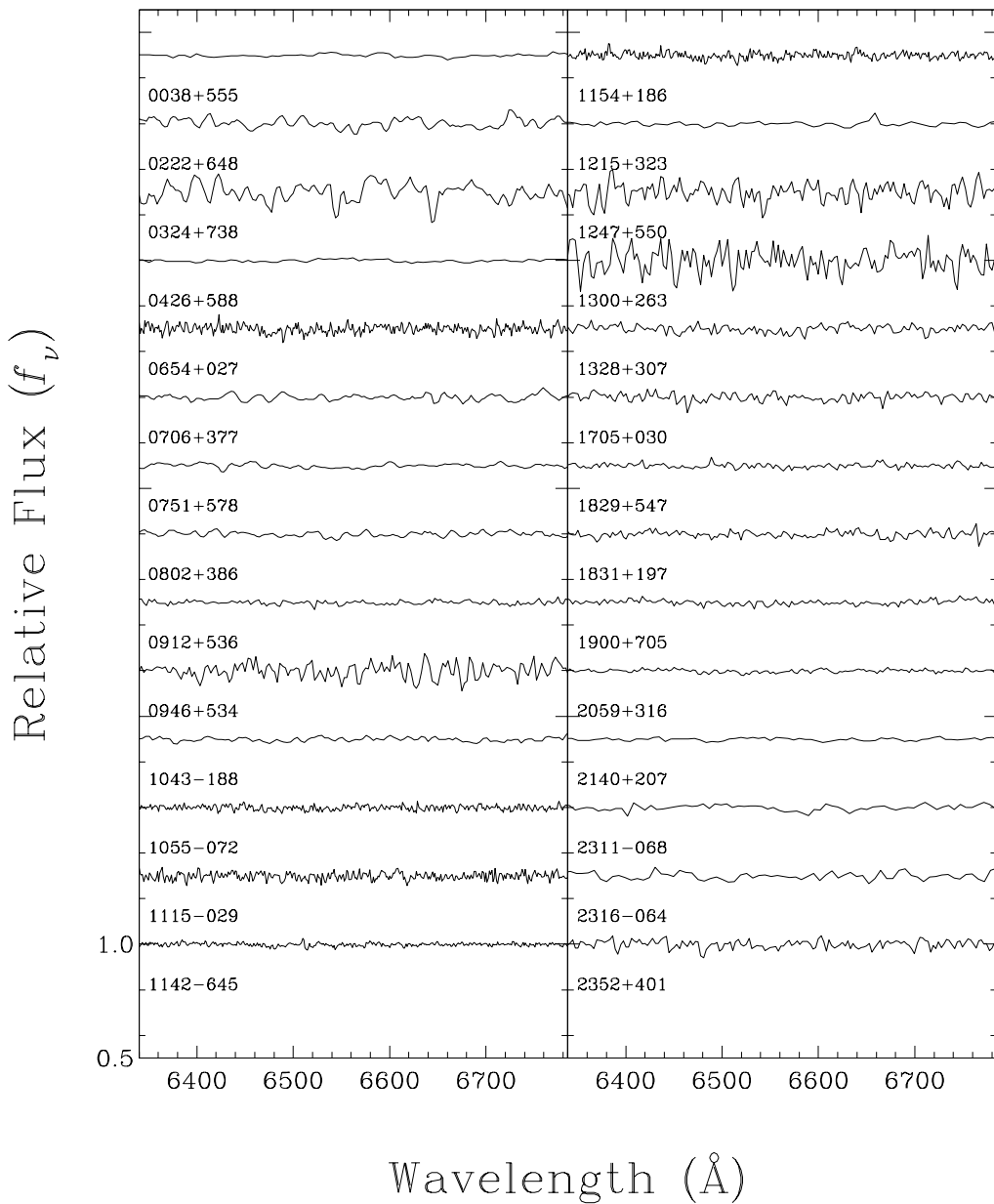


Figure 5

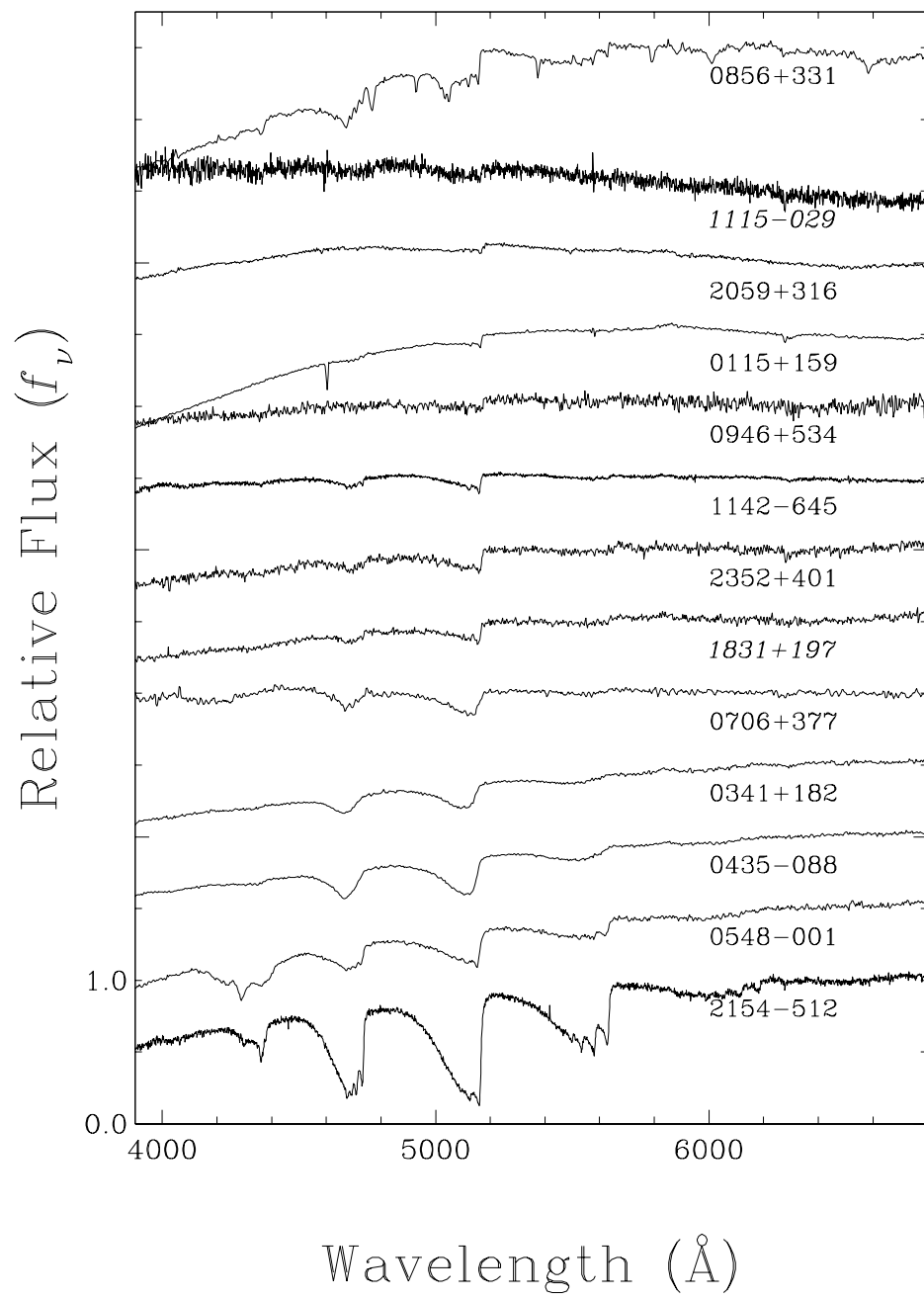


Figure 6

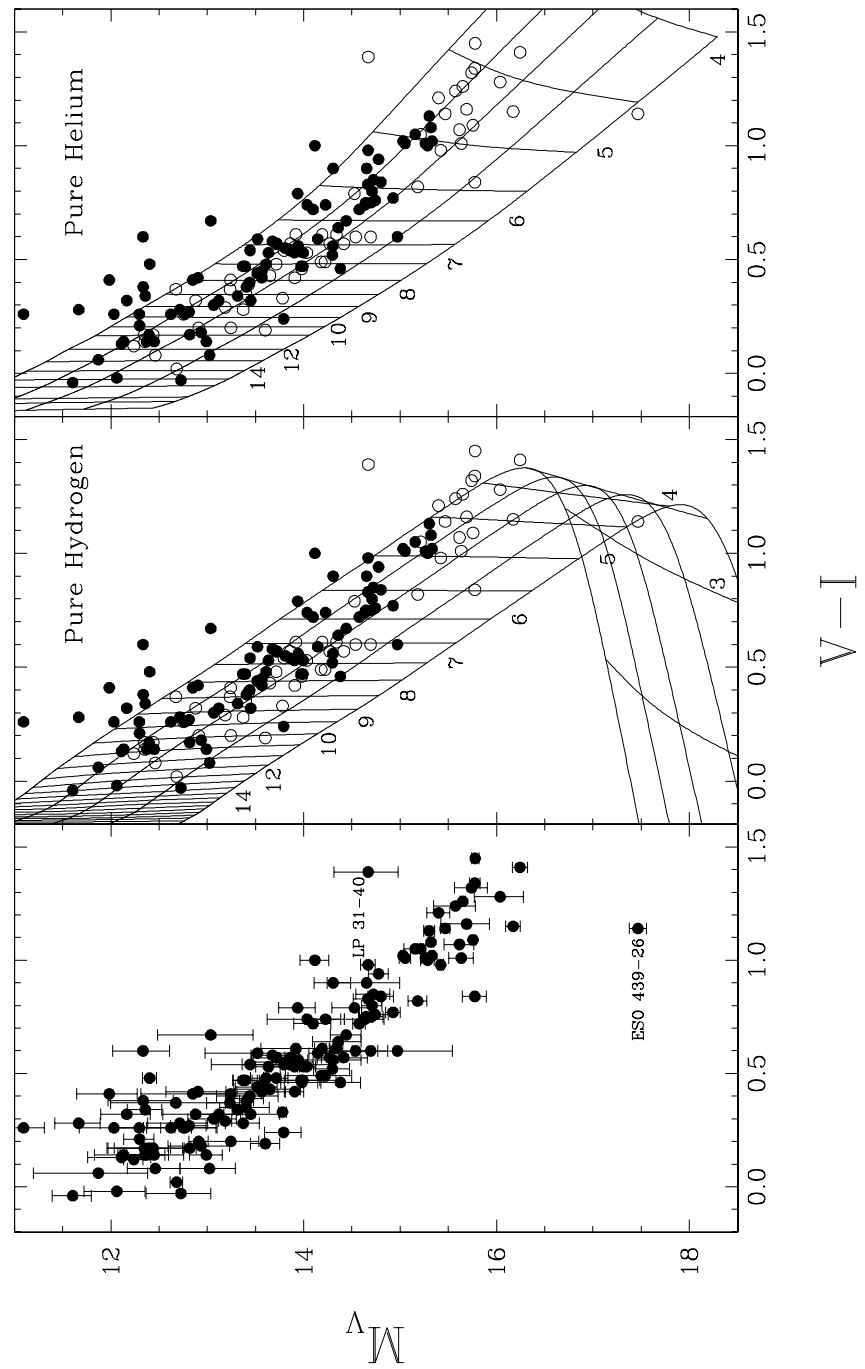


Figure 7

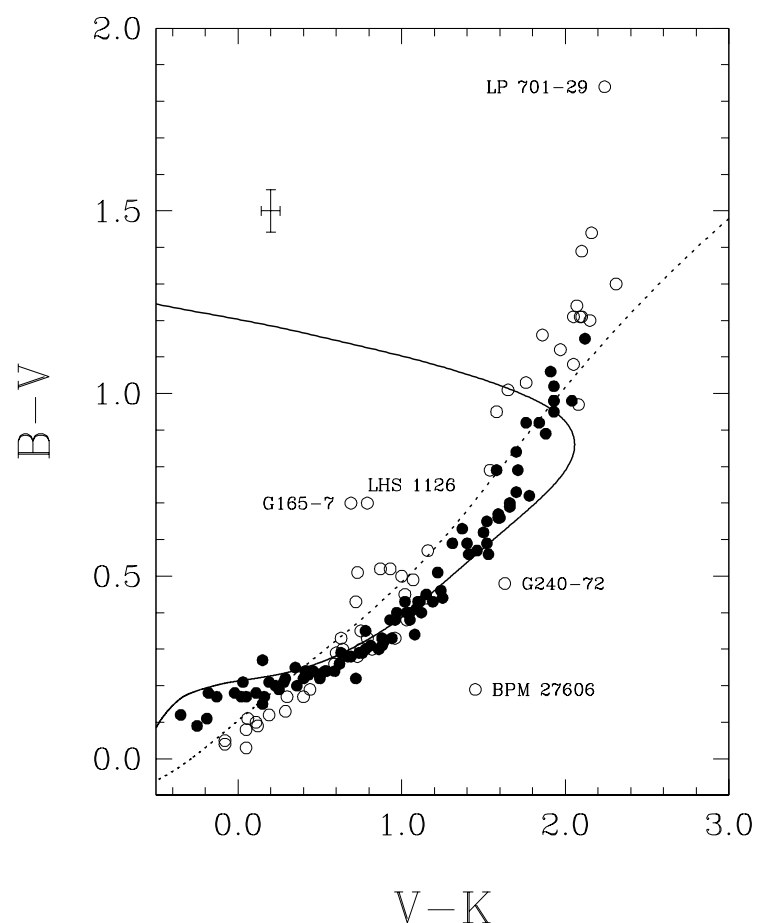


Figure 8

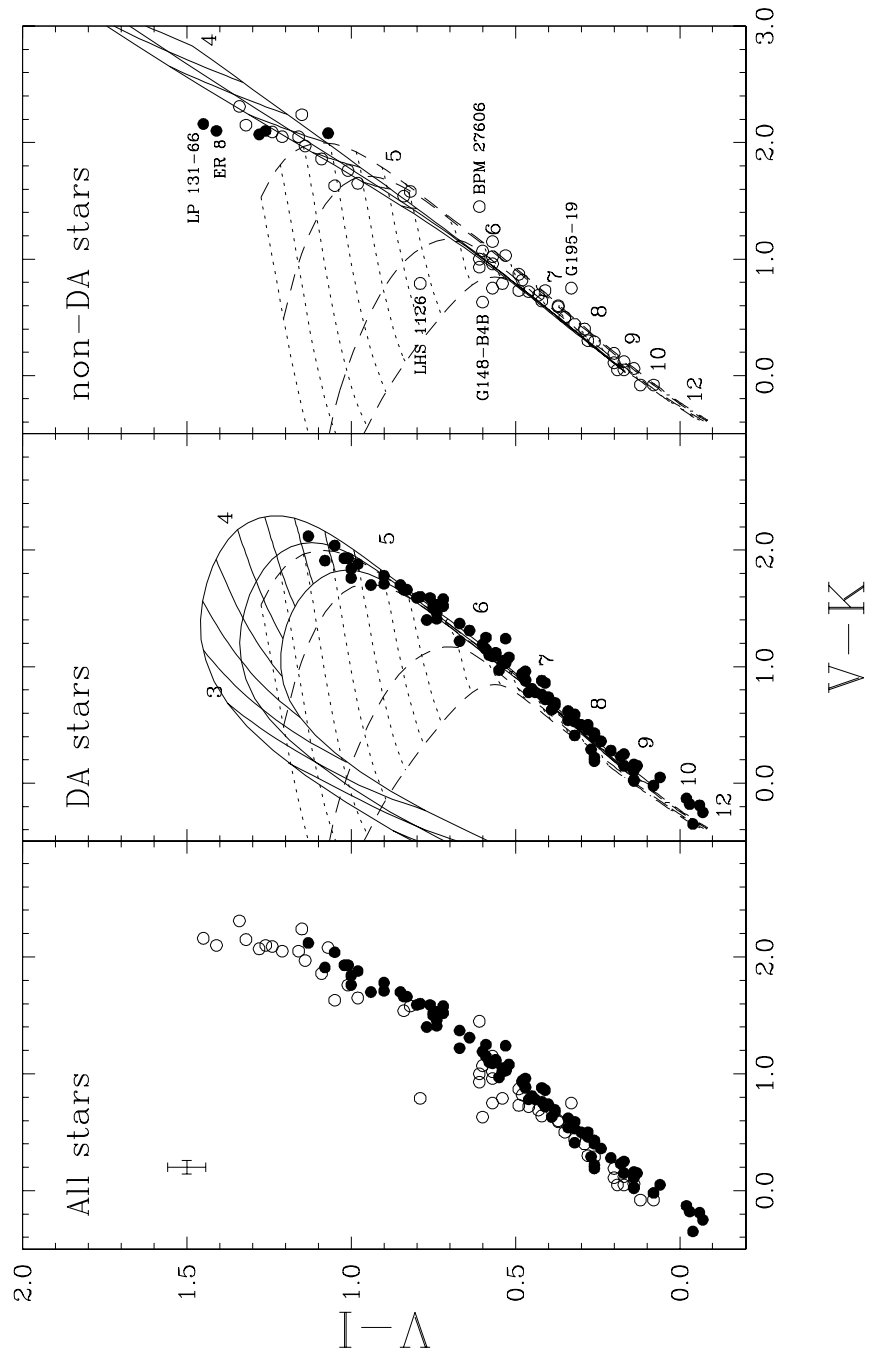


Figure 9

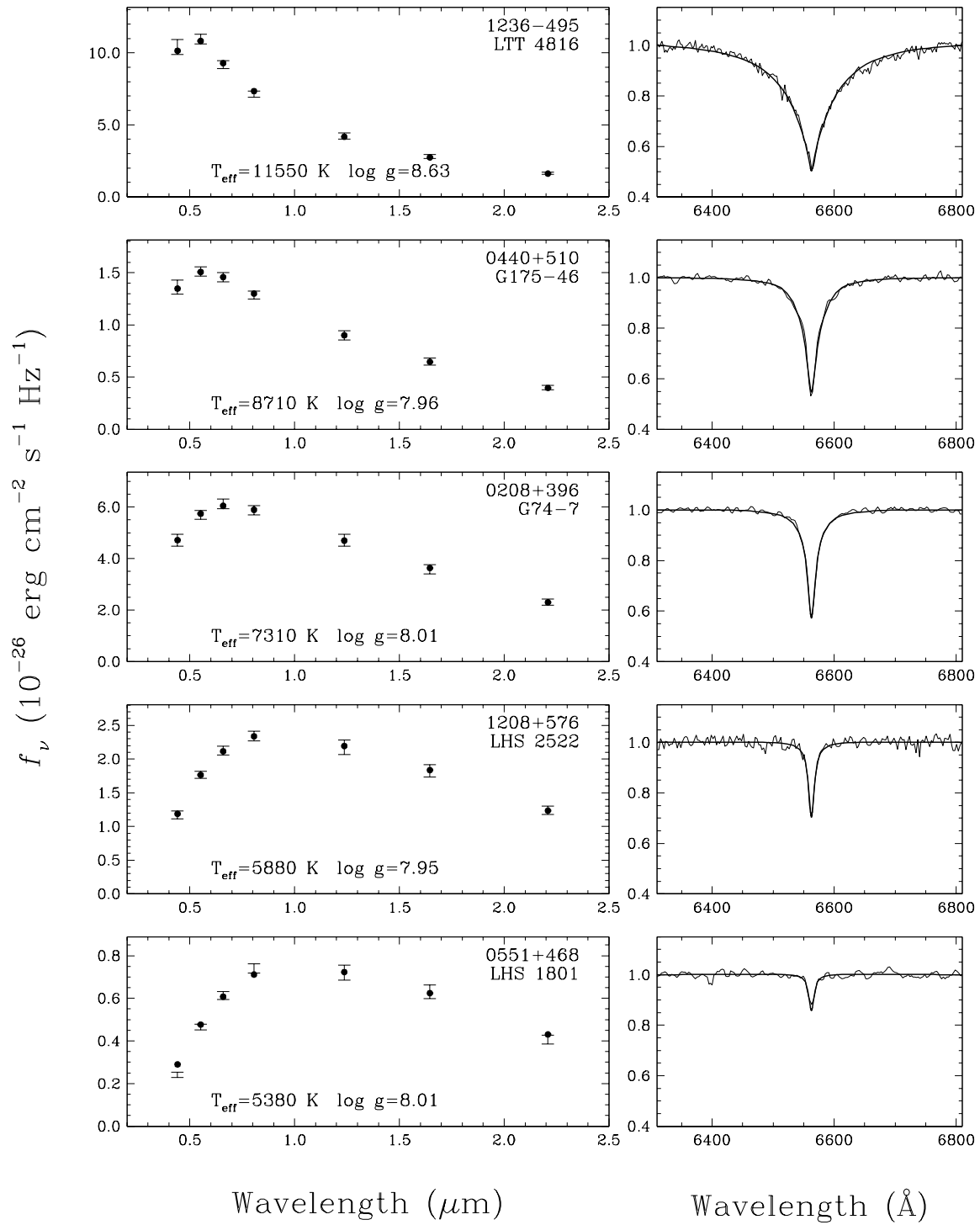


Figure 10

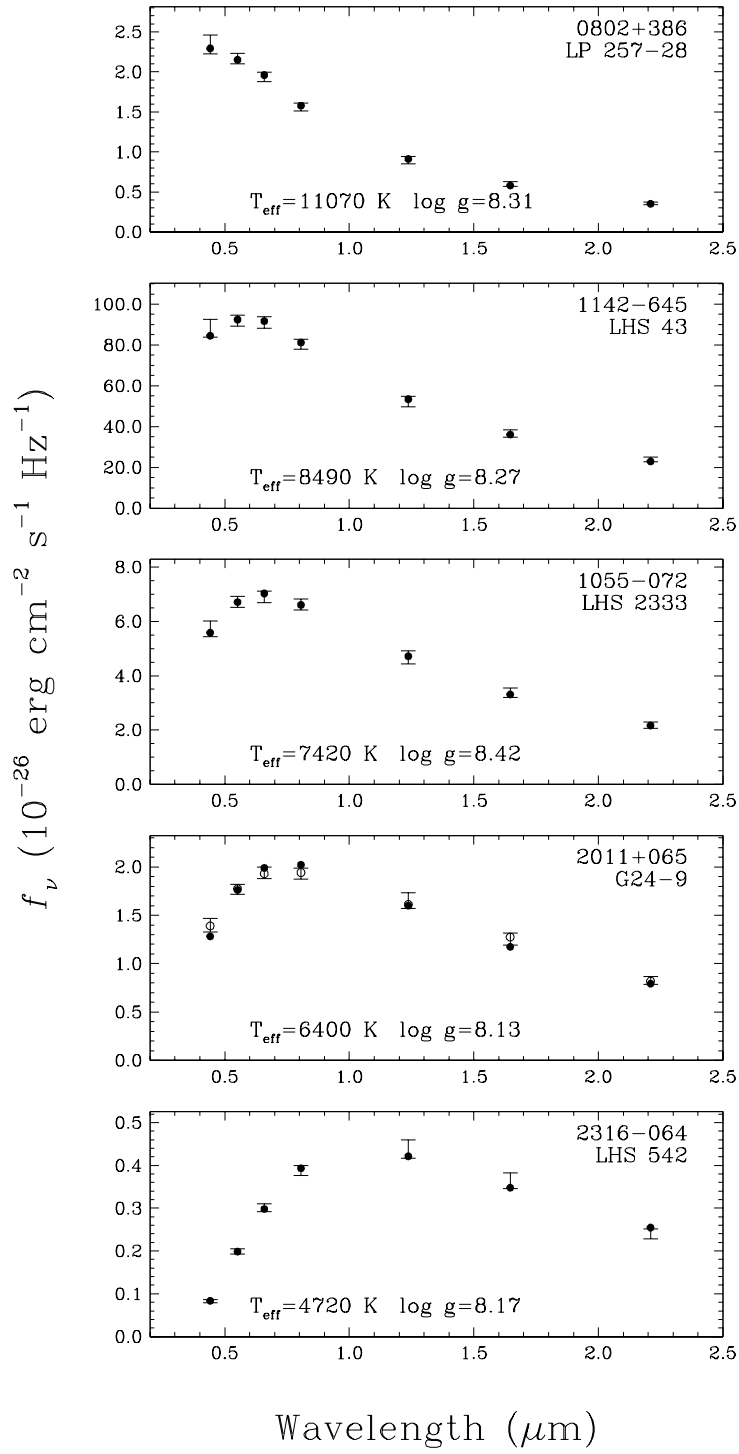


Figure 11

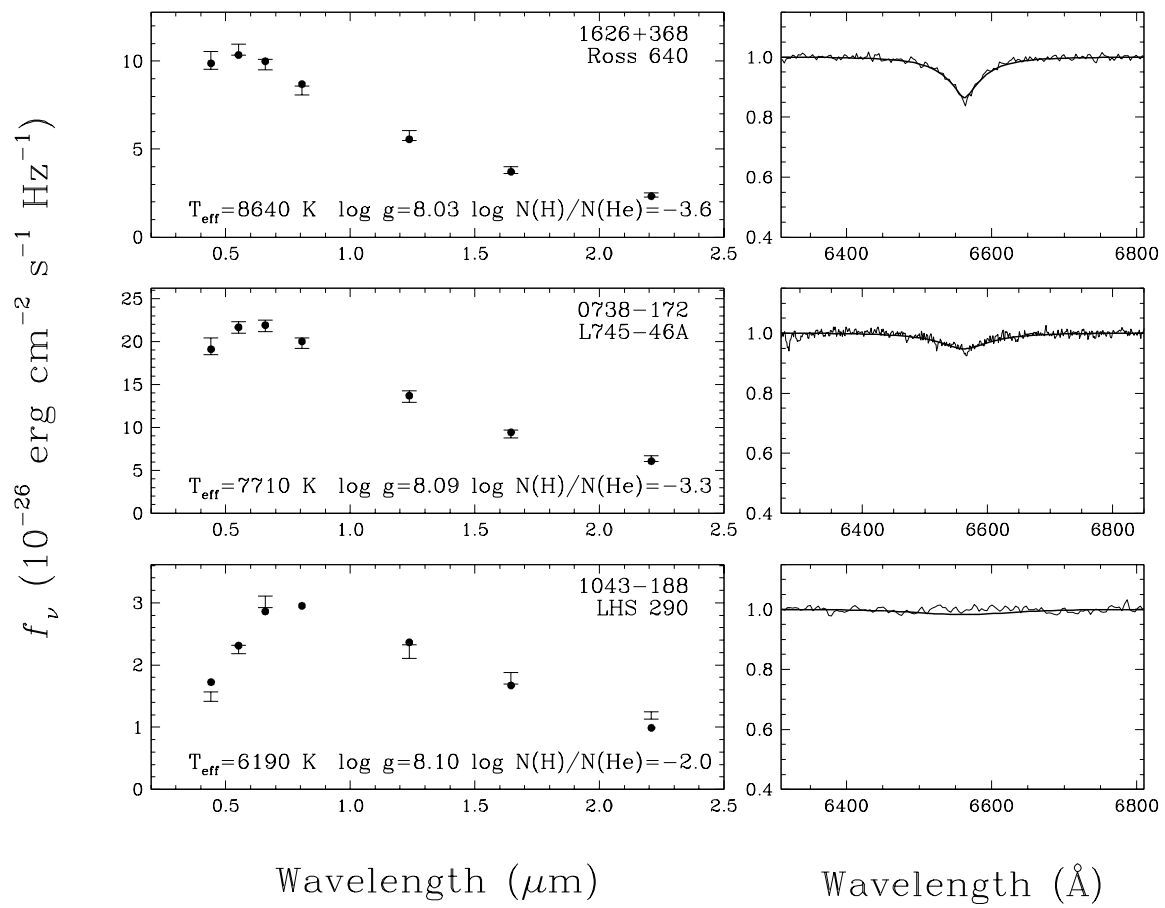


Figure 12

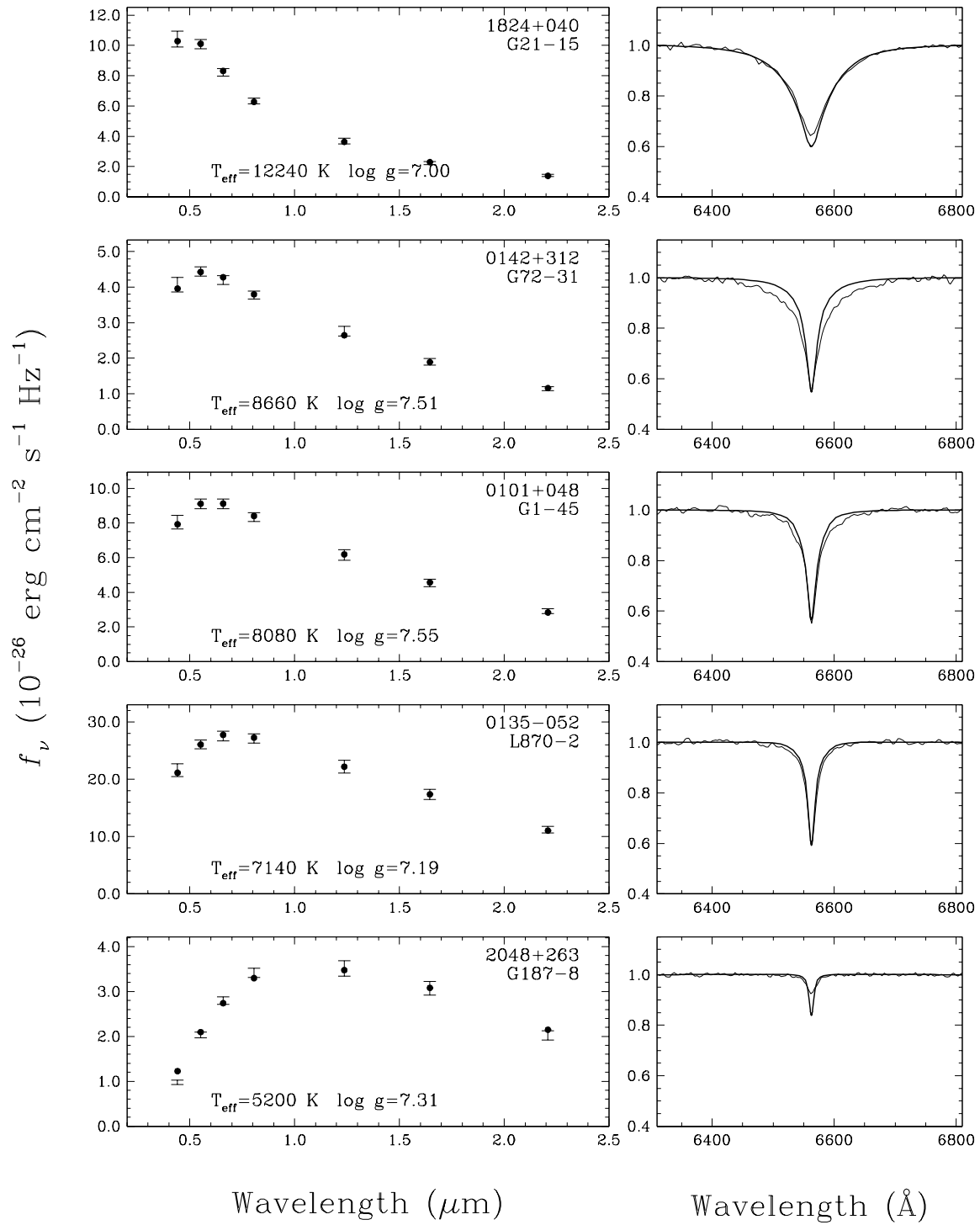


Figure 13

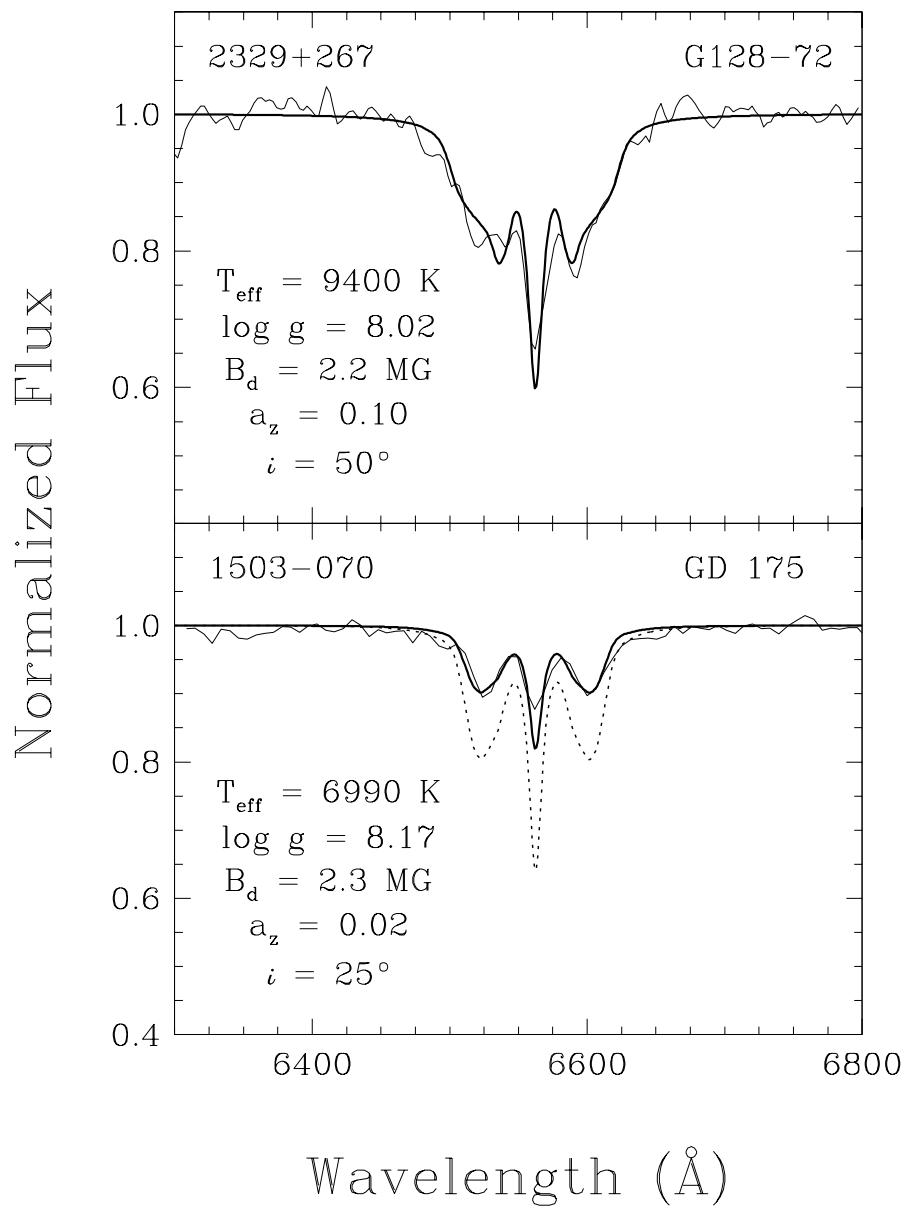


Figure 14

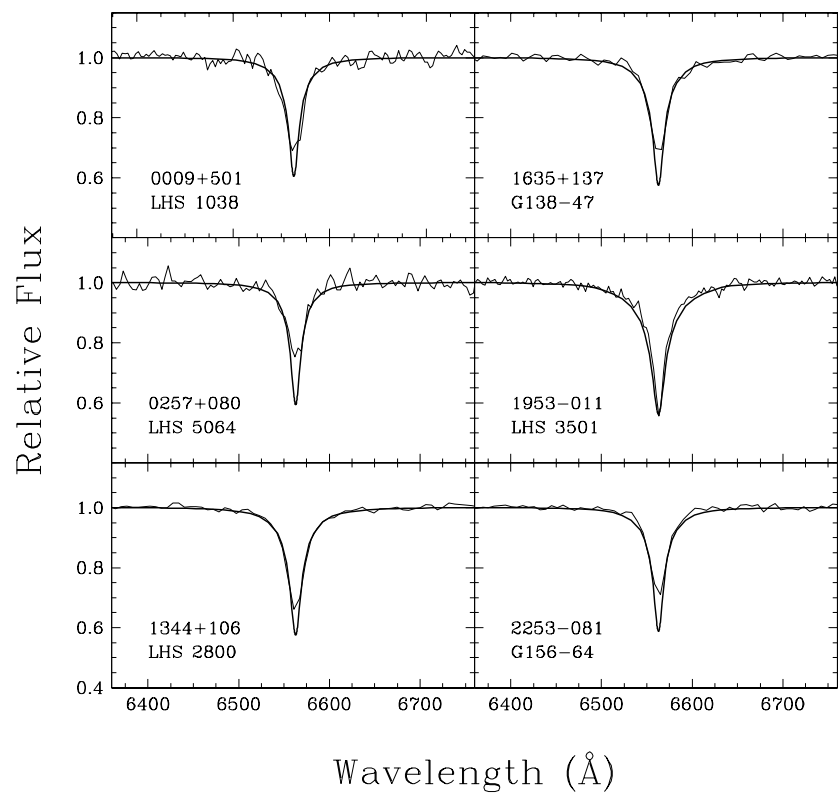


Figure 15

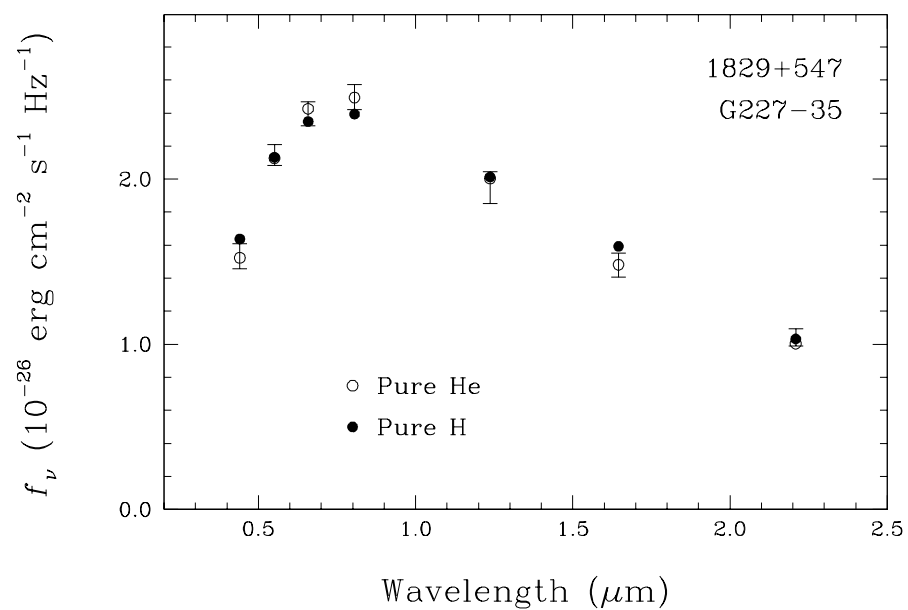


Figure 16

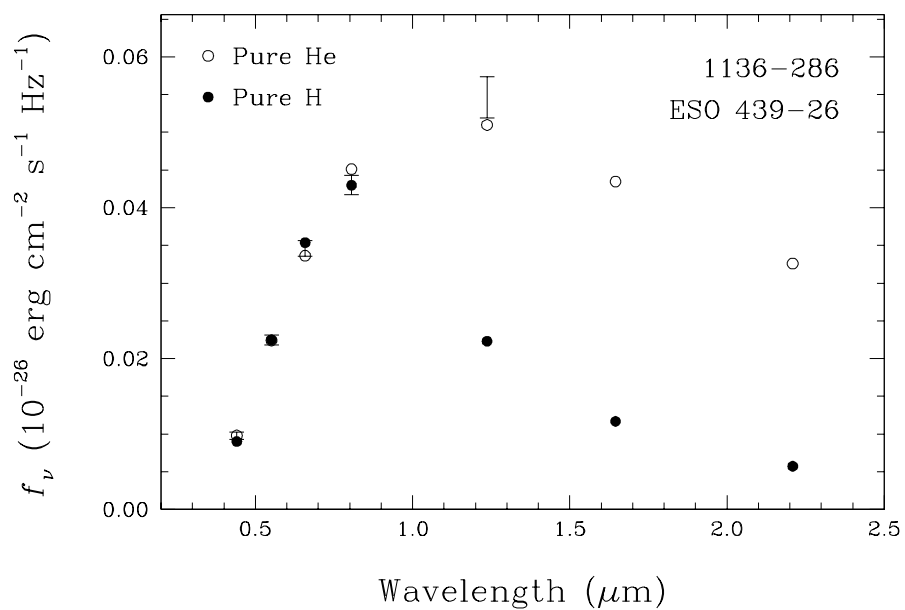


Figure 17

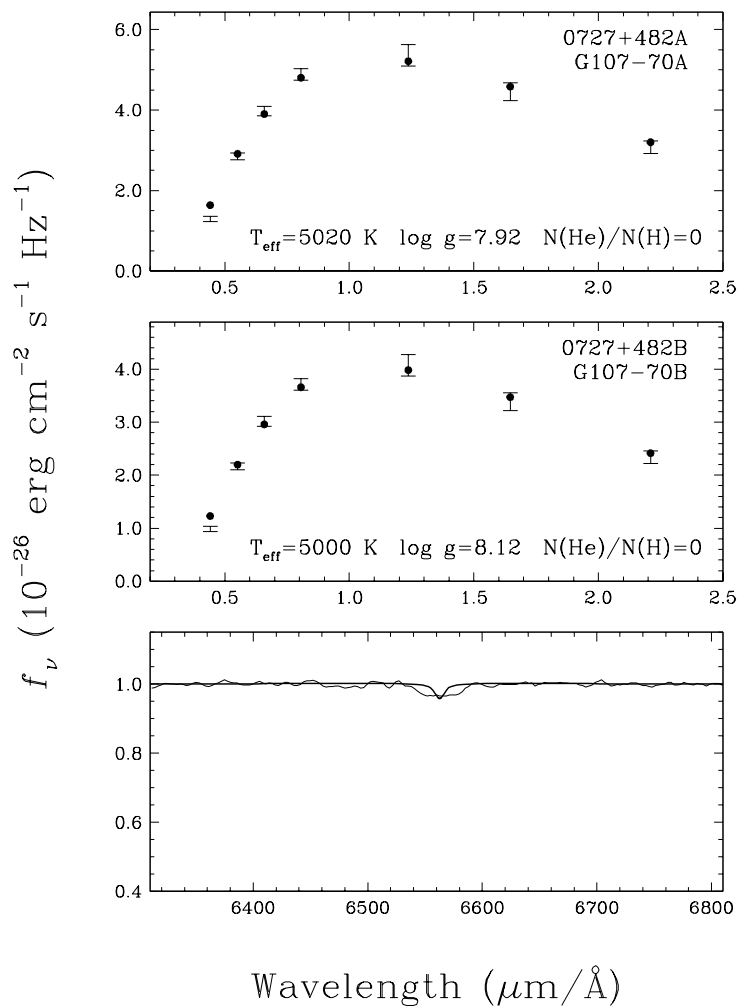


Figure 18

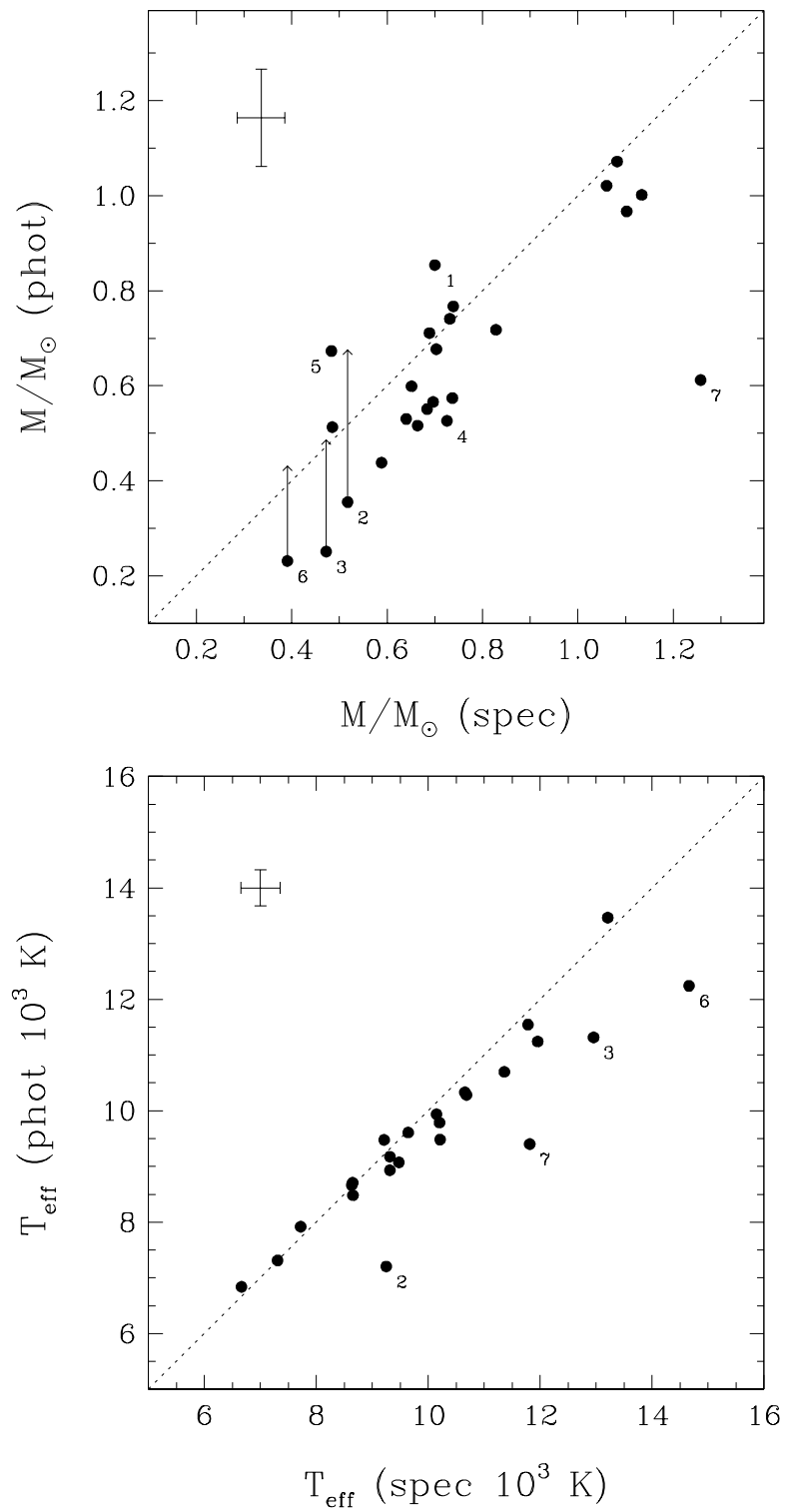


Figure 19

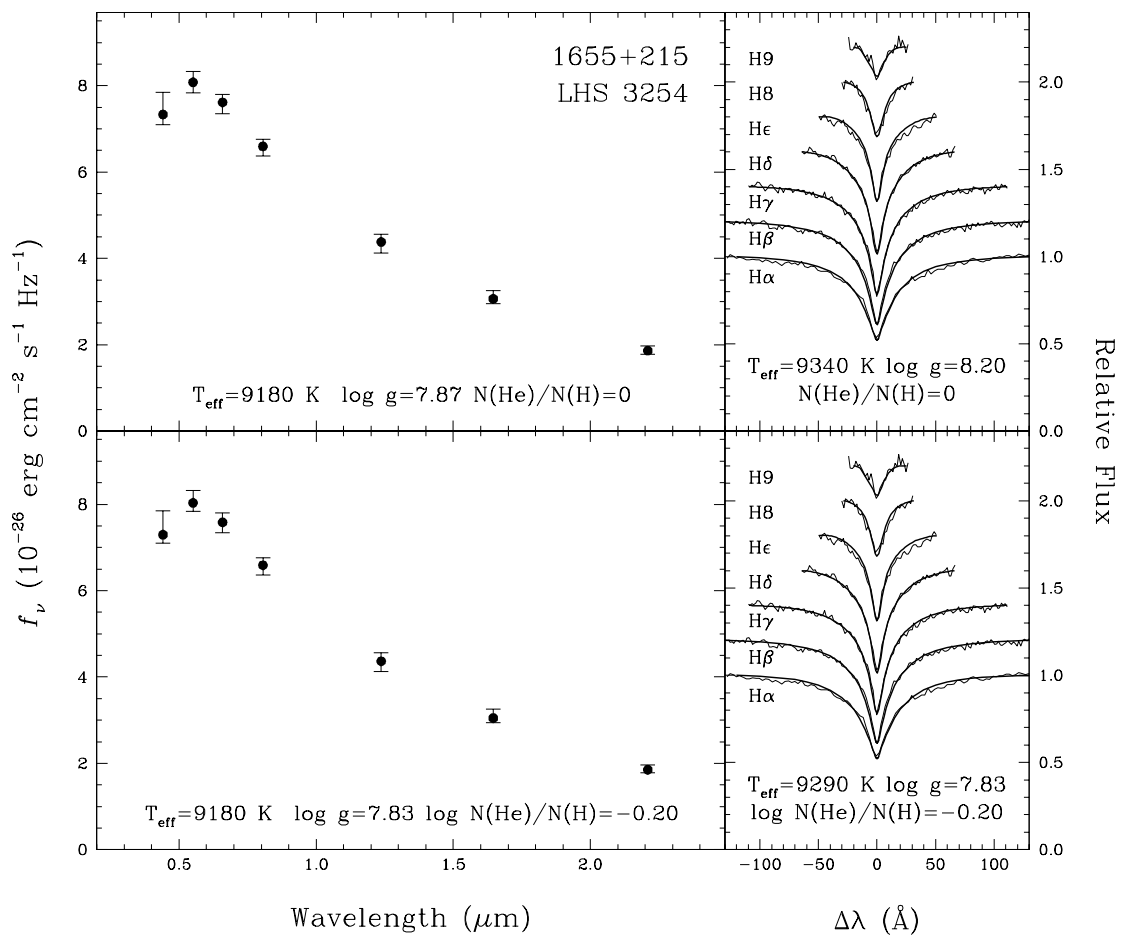


Figure 20

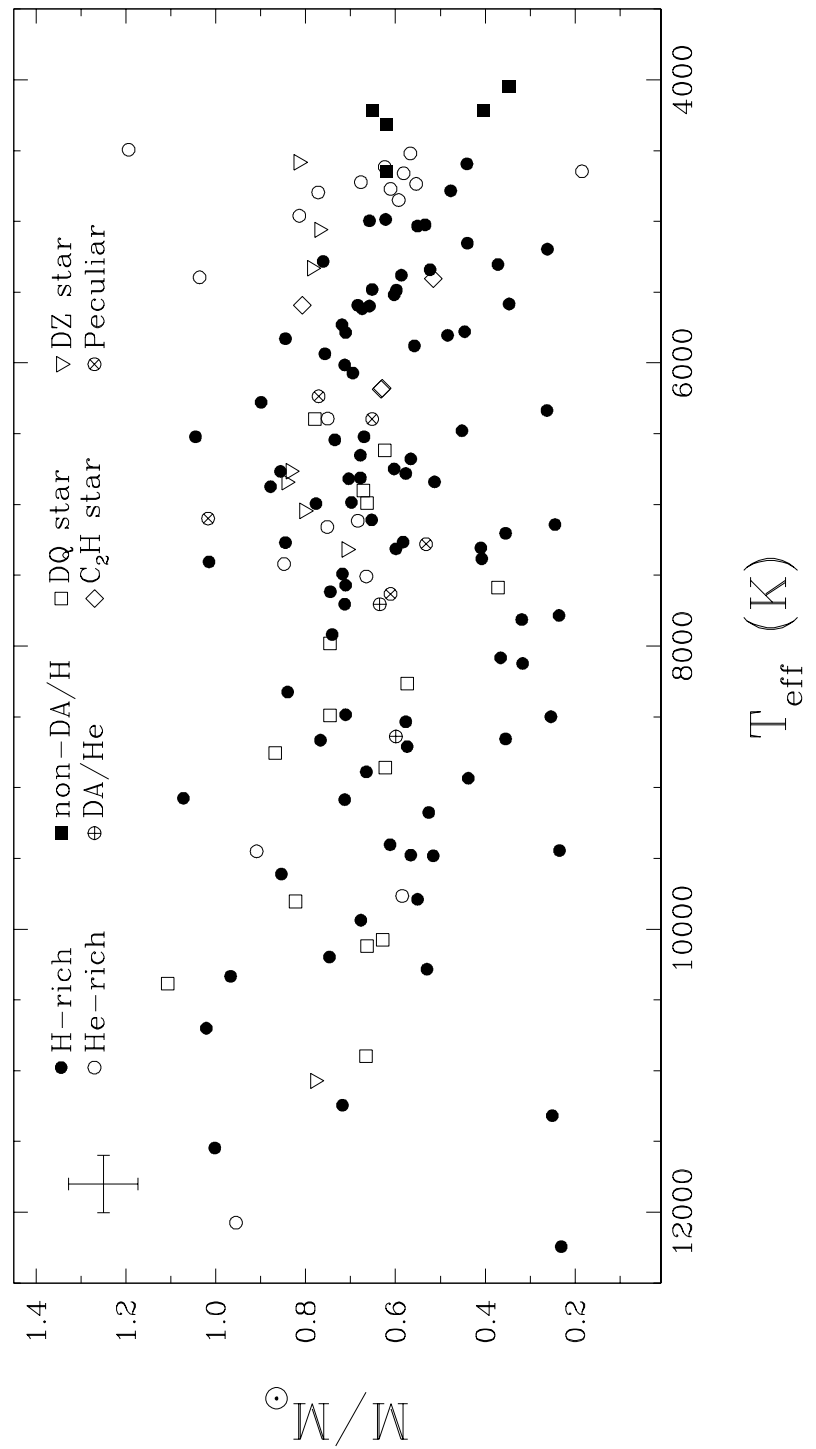


Figure 21

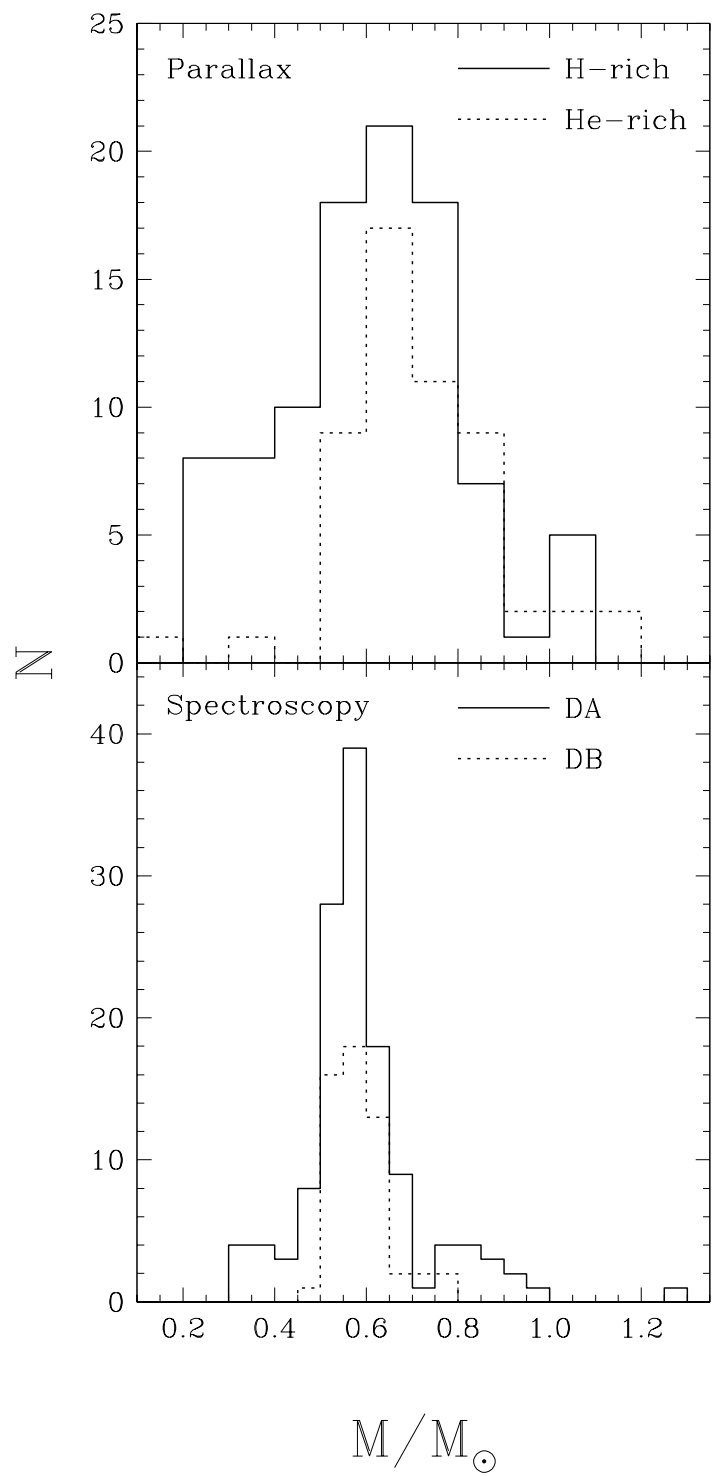


Figure 22

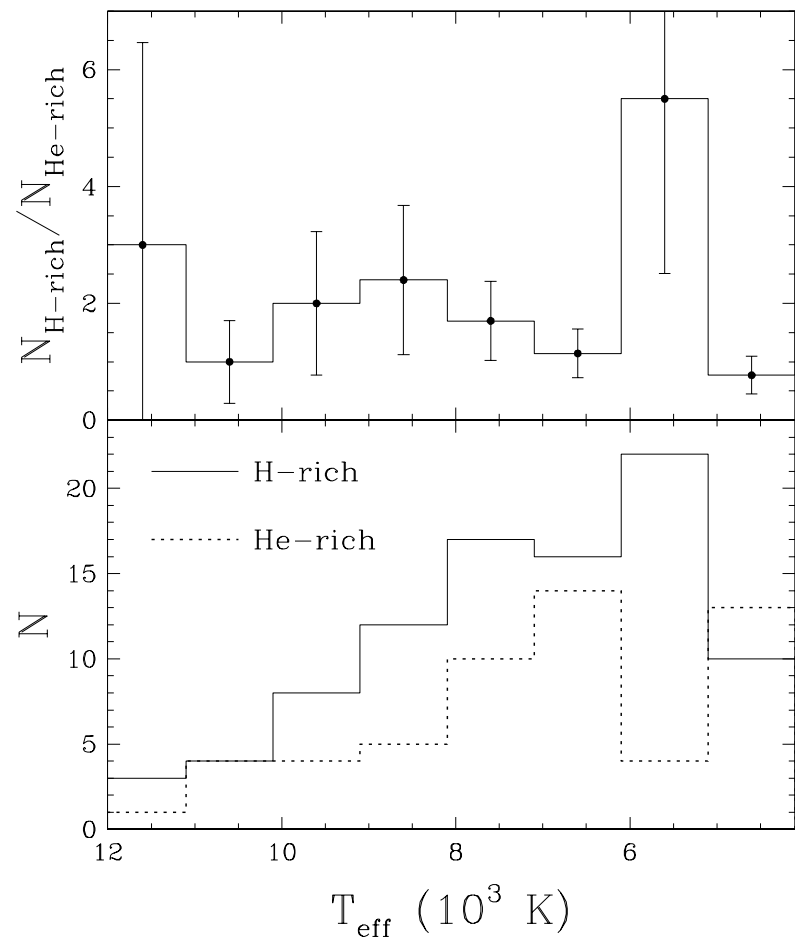


Figure 23

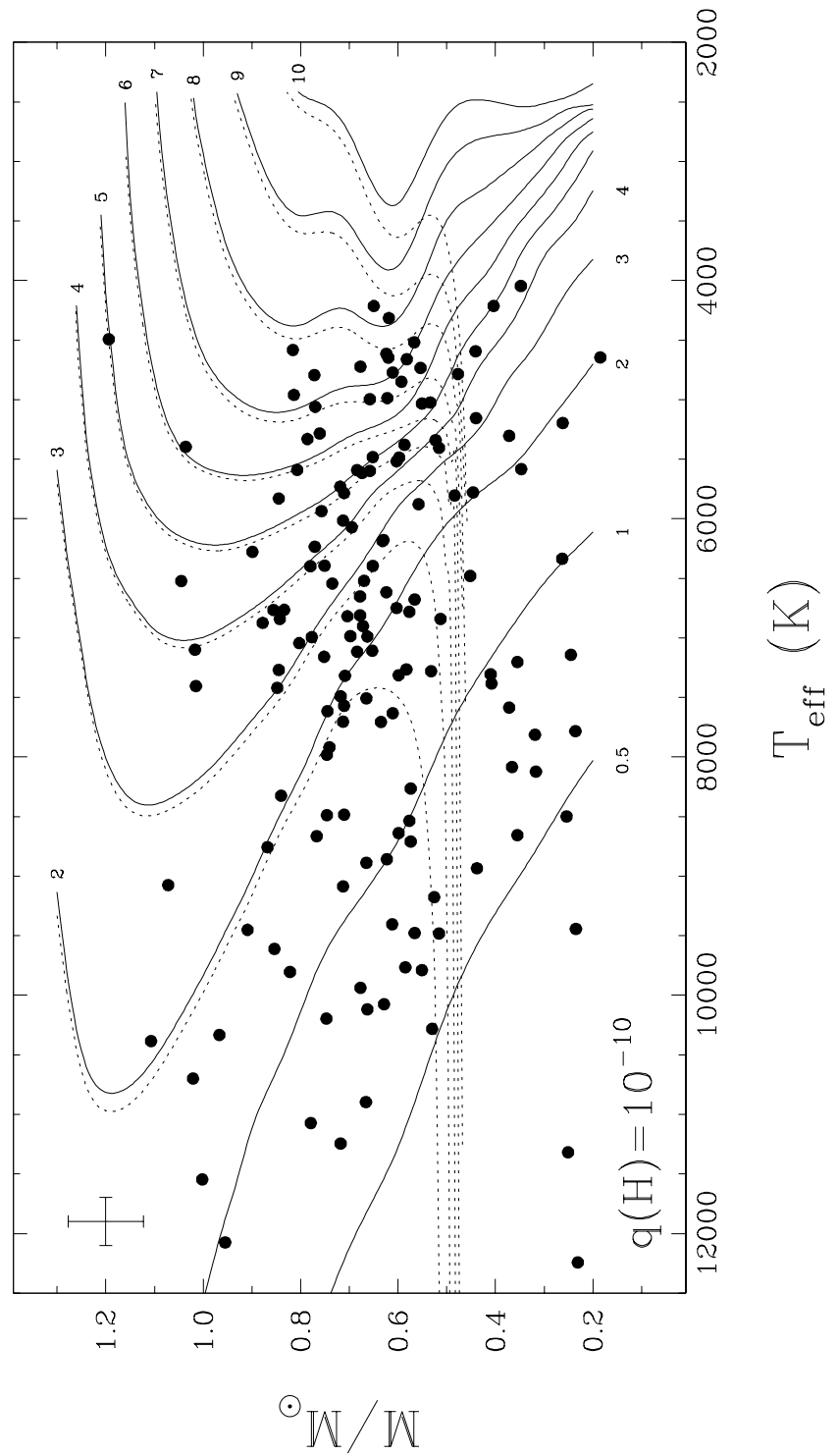


Figure 24

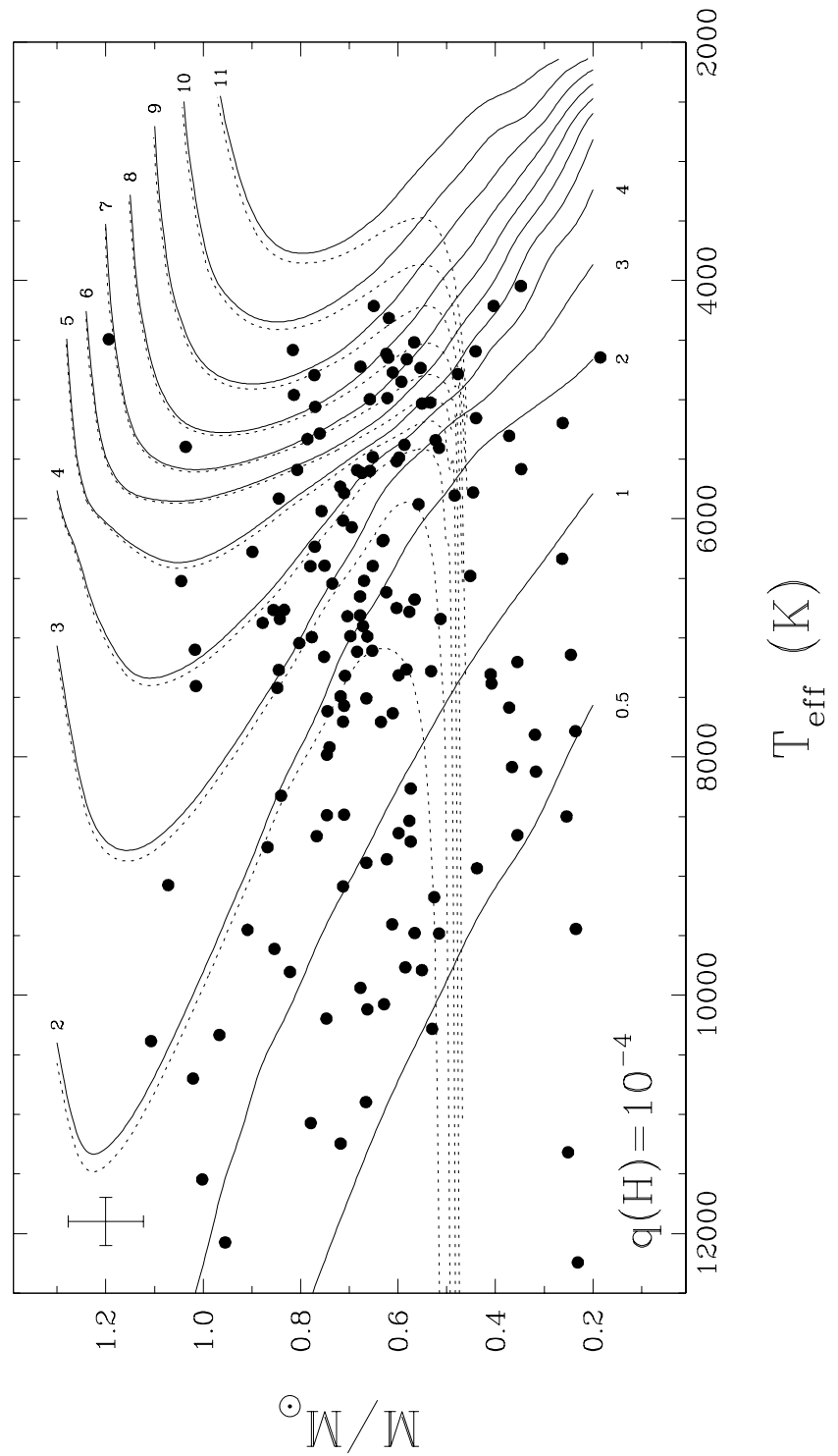


Figure 25